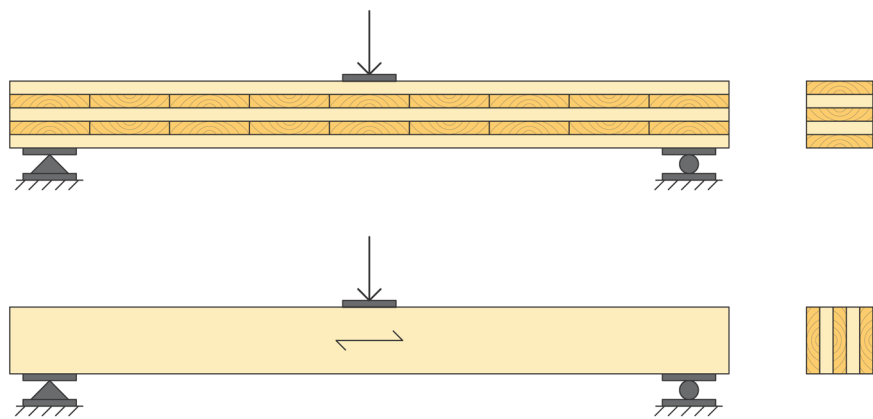




LUND
UNIVERSITY



CHARACTERISATION OF CROSS LAMINATED TIMBER PROPERTIES

EMIL NILSSON

Structural
Mechanics

Master's Dissertation

DEPARTMENT OF CONSTRUCTION SCIENCES
DIVISION OF STRUCTURAL MECHANICS

ISRN LUTVDG/TVSM--21/5250--SE (1-121) | ISSN 0281-6679

MASTER'S DISSERTATION

CHARACTERISATION OF CROSS LAMINATED TIMBER PROPERTIES

EMIL NILSSON

Supervisor: **HENRIK DANIELSSON**, PhD, Division of Structural Mechanics, LTH.

Examiner: Professor **ERIK SERRANO**, Division of Structural Mechanics, LTH.

Copyright © 2021 Division of Structural Mechanics,
Faculty of Engineering LTH, Lund University, Sweden.

Printed by V-huset tryckeri LTH, Lund, Sweden, July 2021 (*PI*).

For information, address:

Division of Structural Mechanics,
Faculty of Engineering LTH, Lund University, Box 118, SE-221 00 Lund, Sweden.

Homepage: www.byggmek.lth.se

Abstract

This project concerns an analysis of a hitherto untested method for determining the modulus of elasticity (MoE) and shear modulus parallel to grain, as well as the rolling shear modulus of cross laminated timber (CLT) through 3-point bending tests. A review of analytical models and methods is included, followed by an evaluation of the effect of the annual ring orientation and shear stress distribution at shear loading of individual board cross-sections. Lastly a validation of the results using 2D and 3D finite element (FE) models are presented.

A total of nine prismatic beams with a square cross section of 100×100 mm were cut centrically from a CLT plate with respect to the longitudinal boards. The beams were cut in two directions with respect to the outermost boards, resulting in two different layups and lengths. Six beams were cut with the outermost board in the longitudinal direction (with a length of 1500 mm), and three beams were cut with the outermost board in the transverse direction (with a length of 900 mm).

Each beam was tested at in-plane loading, and out-of-plane loading for two different spans, respectively, resulting in four tests for each beam and 36 tests in total. By using the test data within the linear-elastic range and performing a linear regression the equivalent stiffness could be evaluated. The results from the in-plane bending tests were used to characterise the MoE and shear modulus parallel to grain by means of Timoshenko theory. The results from the out-of-plane bending tests were used to characterise the rolling shear modulus by means of the Gamma method or Timoshenko theory.

The results were evaluated by comparing the calculated equivalent stiffness of FE-models (with homogenised material properties corresponding to the characterised stiffness properties) to the equivalent stiffness determined experimentally. The results show a promising reliability and validity for the beams with a length of 1500 mm when characterising the stiffness properties using Timoshenko theory, with respect to the shear stiffness being calculated for the gross area of the cross section. Thus, consideration of the shear stress distribution in the transverse boards should be reflected by modification of e.g. the effective area. The rolling shear modulus was characterised in the range of 64–89 MPa for the beams with a length of 1500 mm, with respect to Timoshenko theory, indicating realistic values and that the effect of annual ring pattern is accounted for. The Gamma method, however, resulted in characterised values of the rolling shear moduli that were considered too low with respect to the effect of annual ring pattern.

Keywords: CLT, cross laminated timber, in-plane loading, out-of-plane loading, beam, rolling shear modulus, experimental tests, FE-modelling

Sammanfattning

Det här projektet behandlar en hittills obeprövad metod för att karakterisera elasticitetsmodulen (E-modulen) och skjuvmodulen parallellt med fiberriktningen, samt rullskjuvmodulen för korslimmat trä (KL-trä). Metoden går ut på att testa balkar genom 3-punktsböjprovningar. Arbetet omfattar utvärdering av analytiska modeller och metoder, utvärdering av årsringarnas orientering samt skjuvspänningsfördelningen i enskilda lagertvårsnitt då balkarna belastas i planet. Slutligen presenteras en validering av resultatet genom att jämföra med 2D och 3D finita element (FE) modeller.

Totalt nio prismatiska balkar med ett kvadratisk tvärsnitt på 100×100 mm sågades ut centriskt från en KL-träskiva med avseende på de longitudinella lamellerna. Balkarna sågades i två riktningar med avseende på de yttersta lamellerna, vilket resulterade i två olika uppbyggnader och längder. Detta resulterade i sex balkar med de yttersta lamellerna i balkens längsriktning (med en längd på 1500 mm), och tre balkar med de yttersta lamellerna i balkens tvärriktning (med en längd på 900 mm).

Varje balk belastades både i planet, och ut ur planet för två olika spännvidder, vilket resulterade i fyra provningar per balk, och 36 provningar totalt. Genom att utnyttja resultatet från det linjärelastiska intervallet av mätdatan och sedan utföra en linjär regression kunde den ekvivalenta styvheten för balkarna beräknas. Resultaten från provningarna då balkarna belastades i planet användes för att karakterisera E-modulen och skjuvmodulen parallellt fiberriktningen genom Timoshenko teori. Resultaten från provningarna då balkarna belastades ut ur planet användes för att karakterisera rullskjuvmodulen genom antingen Gammametoden eller Timoshenkoteori.

Slutresultatet utvärderades genom att jämföra den beräknade ekvivalenta styvheten från FE-modellerna (med homogeniserade styvhetsegenskaper motsvarande de karakteriserade styvhetsegenskaperna) med den ekvivalenta styvheten som bestämdes experimentellt. Resultatet visar på en lovande tillförlitlighet och repeterbarhet för balkarna med en längd på 1500 mm då styvhetsegenskaperna bestäms med Timoshenkoteori, och då skjuvstyvheten bestäms med avseende på tvärsnittets bruttoarea. Följaktligen bör hänsyn till skjuvspänningsfördelningen i de tvärgående lamellerna beaktas genom t.ex. den effektiva arean. Rullskjuvmodulen kunde karakteriseras inom intervallet 64–89 MPa för balkarna med en längd på 1500 mm genom Timoshenko teori, vilket indikerar på realistiska värden och att effekten av årsringarnas krökning återspeglas i de karakteriserade värdena. Däremot resulterade användande av Gammametoden i värden på de karakteriserade rullskjuvmodulerna som ansågs vara för låga med hänsyn till inverkan av årsringarnas orientering.

Nyckelord: KL-trä, korslimmat trä, belastning i planet, belastning ut ur planet, balk, rullskjuvmodul, experimentella tester, FE-modellering

Acknowledgements

I would like to thank my supervisor Henrik Danielsson and my examiner Erik Serrano for their unwavering support throughout the project. Their vast knowledge, expertise and interest in the subject has been a source of motivation for me which indubitably changed the project for the better.

I am also grateful towards Södra for providing the cross laminated timber plate from which the beam specimen were cut. I would also like to mention that this project has been conducted in collaboration of Innocrosslam.

I would like to extend my thanks to my friends and neighbours of Vallis for the emotional support that you provided and for the fun times that we shared. I would also like to thank my father for always being there for me.

Lastly, I would like to extend my gratitude toward my mother who passed away last year. You were always my pillar of fortitude, and I know that you would have been proud to see me graduate.

2nd June, 2021

Lund, Sweden

A handwritten signature in black ink, appearing to read 'Emil Nilsson', written over a horizontal line.

Emil Nilsson

Symbols and Notations

Roman

Symbol	Description
L	Longitudinal direction.
T	Tangential direction.
R	Radial direction.
x	Global x -direction of the CLT-plate.
y	Global y -direction of the CLT-plate.
z	Global z -direction of the CLT-plate.
X	Local X -direction of the CLT-beam.
Y	Local Y -direction of the CLT-beam.
Z	Local Z -direction of the CLT-beam.
E	Young's modulus (modulus of elasticity, MoE).
G	Shear modulus (modulus of rigidity).
E_L	Modulus of elasticity parallel to grain.
E_R	Modulus of elasticity perpendicular to grain (R -direction).
E_T	Modulus of elasticity perpendicular to grain (T -direction).
G_{LR}	Shear modulus parallel to grain (LR -plane).
G_{LT}	Shear modulus parallel to grain (LT -plane).
G_{RT}	Rolling shear modulus.
E_0	Modulus of elasticity parallel to grain.
G_0	Shear modulus parallel to grain.
G_R	Rolling shear modulus.
$G_{R,app}$	Apparent rolling shear modulus.
$I_{x,net}$	Net moment of inertia.
$I_{x,net,z}$	Net moment of inertia (in-plane loading).
$I_{x,net,y}$	Net moment of inertia (out-of-plane loading).
$I_{x,gross,z}$	Gross moment of inertia (in-plane loading).
$I_{x,ef}$	Effective moment of inertia (Gamma method).

Roman

Symbol	Description
A_{net}	Net area of the cross section.
A_{gross}	Gross area of the cross section.
i	Layer i of CLT.
a_i	Distance from global centre of gravity of CLT-plate to local centre of gravity of considered layer.
P	Load.
F	Reaction force.
k	Equivalent stiffness.
L	Span length.
w	Deformation (deflection).
u	Translation.
std	Standard deviation.
cov	Coefficient of variation.

Greek

Symbol	Description
ν	Poisson's ratio.
γ_i	Reduction factor (Gamma-factor).
κ	Shear correction factor.
α	Ratio between bending stiffness and effective shear stiffness.
θ	Rotation.
γ	Shear strain.
σ	Stress vector.
ε	Strain vector.
\mathbf{D}	Constitutive matrix.
\mathbf{C}	Compliance matrix.
\mathbf{G}	Transformation matrix.
$\hat{\sigma}$	Global stress vector.
$\hat{\varepsilon}$	Global displacement vector.
$\hat{\mathbf{D}}$	Global constitutive matrix.

Table of Contents

Abstract	I
Sammanfattning	III
Acknowledgements	V
Notations and Symbols	VII
1 Introduction	1
1.1 Context	1
1.2 Aim and objective	3
1.3 Method	4
1.4 Limitations	6
2 Background	7
2.1 Structural scales of wood	7
2.1.1 Macroscopic scale	7
2.2 Linear elasticity	9
2.3 Strength and stiffness properties	11
2.4 Cross laminated timber (CLT)	13
2.4.1 General	13
2.4.2 Strength and stiffness	14
2.4.3 Loading	16
2.5 Analytical methods	18
2.5.1 Gamma method	18
2.5.2 Timoshenko theory	20
2.5.3 Simplified shear correction factor	24
2.5.4 Comparison between analytical methods	24
2.6 Bending stiffness (according to Eurocode)	30
3 Finite element modeling	31
3.1 General	31
3.2 Scope and limitations	32
3.3 Abaqus	33
3.4 Representative beam models	34
3.4.1 2D models	34
3.4.2 3D-models	37
3.5 Convergence study	41
3.6 Preliminary finite element analysis	45
3.6.1 Simple shear model	45
	IX

3.6.2	Shear stress distribution	47
4	Testing and evaluation methods	53
4.1	Specimen preparation	53
4.2	Equipment	55
4.3	Specimen setups	56
4.4	Evaluation methods	59
4.5	Preliminary testing	62
5	Results	67
5.1	Stiffness properties	67
5.1.1	Specimen 1 beams	67
5.1.2	Specimen 2 beams	68
5.1.3	Summary	69
5.2	Finite element models	71
5.2.1	Specimen 1 beams	72
5.2.2	Specimen 2 beams	76
6	Discussion	79
6.1	Test method	79
6.2	Stiffness properties	80
6.2.1	In-plane loading	80
6.2.2	Out-of-plane loading	81
6.3	Validity of results	83
6.3.1	Specimen 1 beams	83
6.3.2	Specimen 2 beams	83
7	Conclusion	85
7.1	Concluding remarks	85
7.2	Further analysis	87
	References	89
	Appendix A Test results	93
A.1	Preliminary tests	93
A.2	Main tests	96
	Appendix B Experimental setups	103
	Appendix C Shear stress distribution	107
C.1	Specimen 1 beam	107
C.2	Specimen 2 beam	110
	Appendix D Matlab code	113
D.1	Script for calculating shear correction factor	113
D.2	Script for performing linear interpolation	116

1 Introduction

1.1 Context

Cross laminated timber (CLT) (see Figure 1.1) is one of the latest of many engineered wood products (EWP) that have been developed in the last 100 years. It was developed in Central Europe about 30 years ago in order to provide an alternative to concrete while also being renewable [1, 2]. Since then, the production of CLT in Europe has increased exponentially due to its many advantages in terms of manufacturing, production, and environmental aspects. During the year 2018 more than one million cubic meter CLT was produced worldwide [1], stating its important role in the timber construction sector.

Despite this fact, the standardization of CLT is still in an early phase and extensive work is currently being done in order to implement regulations and information regarding CLT into standards, as well as revising already established design codes. A big issue to overcome is implementing the results from established research, while also satisfying demands from engineers, industry, and authorities [1]. Recently, the "COST Action FP1402" project [1] was finished as a joint collaboration of researchers around the globe, resulting in a collection of state of the art research on CLT. One of many subjects within this research was "Testing and evaluation". The purpose of this work was to evaluate current methods used to test and verify mechanical properties of CLT. This was done in order to highlight benefits and drawbacks of each method, respectively, as well as pointing out where further development was necessary [1]. Inspired by this work, Erik Serrano sparked the idea that brought upon this Master's degree project, namely the suggestion of an alternative method for determining the stiffness properties of CLT.

The current method used to determine the stiffness properties of CLT according to the current European assessment document (EAD) [3] is to perform a four-point bending

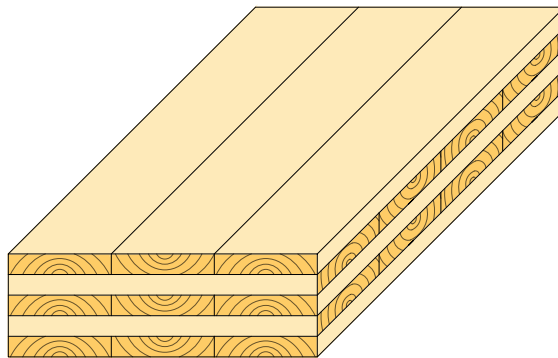


Figure 1.1: Schematic illustration of a cross laminated timber element.

test of a plate. The parallel to grain stiffness is determined by evaluation of test result using the so called Gamma method and an approximation of the rolling shear modulus. The approximation is specified as 50 MPa in [3]. The structure of CLT, where the fibre direction of the laminations is oriented perpendicular to the fibre direction of each adjacent layer, results in the rolling shear modulus impacting the stiffness and load bearing properties. The Gamma method enables analysis of CLT using conventional Bernoulli-Euler beam theory, since shear deformations are taken into account by using an effective moment of inertia with reduced stiffness contribution from the longitudinal layers by weighted Gamma-factors. The Gamma-factors depend on the thickness of the constituent layers, the modulus of elasticity (MoE) parallel to grain, the rolling shear modulus, the span and boundary conditions of the beam. The rolling shear modulus is typically many times lower than the longitudinal shear modulus and displays the same uncertainty when it is measured as other material properties for timber. Inaccurate assumptions of the rolling shear modulus could lead to large deviations when determining other stiffness properties using the above mentioned methodology.

In the proposed alternative method two consecutive three-point bending tests are conducted on a CLT-beam for different span. The MoE parallel to grain, the longitudinal shear modulus and the rolling shear modulus are then characterised by rotating the cross section 90° about its longitudinal axis between the two tests. This is further described in Section 1.3.

1.2 Aim and objective

This project serves to analyse the possibility of using three-point bending tests to determine the MoE and shear modulus parallel to the fibre direction and the rolling shear modulus for the laminations of the CLT element. Given that it is a hitherto untested method, focus was put on evaluating the reliability, i.e. if the results can be reproduced when repeated under the same conditions, and the validity, i.e. how well the results measure the intended parameters. The reliability was based on the spread in the results from the experimental tests. The validity was evaluated by using data from experimental tests together with analytical models and then comparing the results with 2D and 3D finite element (FE) models. Out of the three determined stiffness properties, the main focus was put on evaluating the validity of the rolling shear modulus, and what main parameters that would affect the outcome.

The following sub-goals were defined to fulfil this purpose:

- Define suitable loading conditions and specimen geometry for the suggested test method.
- Define suitable methods to apply the analytical models, with respect to the Gamma method and Timoshenko theory.
- Create suitable FE-models corresponding to the specimen tested in laboratory.
- Study the effect of different material and geometry parameters when determining the stiffness properties with the alternative method. This is done by using results from experimental tests, analytical models and FE-models.

1.3 Method

The project can be divided into four parts. The first part consisted of a literature study, where the main goal was to establish knowledge about wood in general, cross laminated timber, analytical models (Gamma method and Timoshenko theory) and how suitable FE-models could be established. The study was done with respect to CLT as a beam. As CLT is traditionally used as wall or floor elements, load cases and geometrical definitions were uniquely defined to serve the purpose of this project. Preliminary calculations in order to define suitable loading conditions and geometry for the suggested test method were conducted. Lastly, a study of how the annual ring orientation affects the measured rolling shear modulus was conducted numerically in order to gain a better understanding and to account for this later in the FE-models.

The second part consisted of experimental tests using the suggested method, see Figure 1.2. Nine beams were cut out of a CLT plate. Two consecutive 3-point bending tests corresponding to two different spans were conducted for each beam, respectively. Further, each beam was loaded both in-plane and out-of-plane (by rotating the beam 90° about its longitudinal axis), resulting in 4 tests for each beam, and 36 tests in total. The results from the bending tests were obtained as force-deformation data. By performing a linear regression on the linear part of the resulting curve the equivalent stiffness k could be determined. By use of Timoshenko theory and the Gamma method, the MoE and shear modulus parallel to grain to grain E_0 and G_0 , as well as the rolling shear modulus G_R were determined for each beam. E_0 and G_0 were determined from the in-plane bending tests. Similarly, G_R was determined from the out-of-plane bending tests. By use of the previously determined stiffness properties, G_R could be determined by use of either the Gamma method or Timoshenko theory.

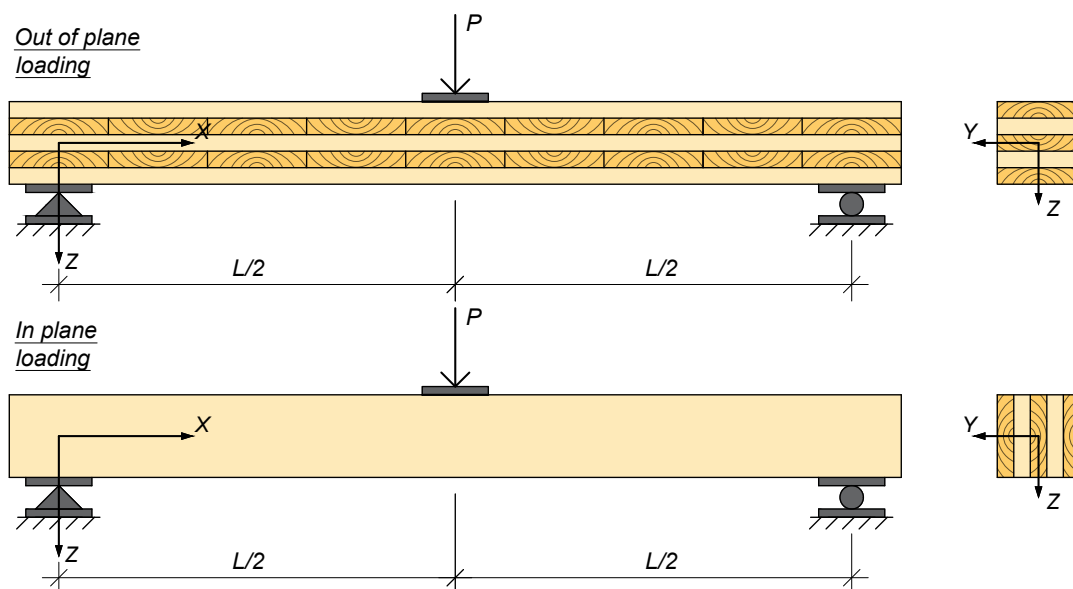


Figure 1.2: Test arrangement for measuring stiffness properties according to alternative method.

The third part consisted of FE-analyses where several models corresponding to the tested beam specimen were established. The stiffness properties calculated analytically from the test data were used in the models. Subsequently the validity of the stiffness properties was studied by comparing the equivalent stiffnesses from the test data and FE-models, respectively. A good correlation would indicate that the stiffness properties were representative values for the constituent boards of the tested beams. Furthermore, the shear stress distribution was studied for beams loaded in-plane by means of FE-models, as it seemed to have a significant effect on the correlation of the results mentioned above. This was done to investigate how the shear stress distribution could be accurately represented in analytical beam models (Timoshenko theory). Two suggestions were considered in this project: representing the shear stress distribution by use of the gross area, or use of the net area signifying only the longitudinal boards.

The fourth part consisted of evaluating and comparing the results from the experimental tests and analytical models with the results from the FE-models.

1.4 Limitations

The following limitations apply for this dissertation:

- The constituent boards of the CLT are assumed to be homogeneous and of equal properties as the other boards oriented in the same direction.
- Only symmetrical layups with the same layer thickness throughout the cross section are analysed in this project.
- The CLT is assumed to consist of clear wood boards only, meaning that potential defects (such as knots) are not explicitly considered.
- For analytical beam models, bending stresses are assumed to only occur in the longitudinal layers when the CLT is exposed to bending.
- The annual rings are assumed as a perfectly cylindrical pattern expanding from the pith and outwards.
- Climate effects such as moisture or temperature are not considered.
- Duration of load (DOL) effects are not considered.

2 Background

2.1 Structural scales of wood

Wood is a biologically engineered product, that has been designed by nature for millions of years to best suit the needs of the tree itself. The stem and branches are optimally designed to resist gravity and wind loads which mainly create stresses in the direction parallel to the stem. Thus, the wood fibres have been adapted to provide maximum strength in this direction, whereas the strength in the directions perpendicular to the stem are quite low in comparison [4].

Wood is a complex material when it comes to its internal structure. It is anisotropic meaning that the physical properties differ in different directions within the material. The complexity of the material is augmented by the fact that anisotropy can be recognized at different scales of material structure [5].

Four orders of structural variation can be recognized, namely: macroscopic, microscopic, ultrastructural, and molecular [6]. This dissertation will only incorporate modelling on the macroscopic level and emphasis will be put on how modelling can be performed at that level. Everything beneath the macroscopic level will be regarded as the microscopic level for simplification and will not be considered in this dissertation.

2.1.1 Macroscopic scale

When a tree is cut and the cross section is analysed, the macroscopic structure of the wood can be seen clearly, see Figure 2.1. At the center of the stem is the pith from which the growth of the tree can be traced, radiating outwards in a cylindrical pattern. The growth-pattern is made up of annual increments alternating between lighter and darker rings, so called annual rings. One annual ring is made up of earlywood and latewood. Earlywood is formed when water supply is high and thus typically is lighter due to its larger cell cavities. Latewood is formed when water supply is lower and is darker and more dense. Resulting, the growth rings entail a variation of mechanical properties, e.g. density or MoE parallel to grain, over the cross section [4]. When using models to replicate the structural behaviour of timber elements on the macroscopic scale, normally homogenized mean values of the strength and stiffness properties are used as an approximation.

Tracing the growth of the tree on the macro scale, three principal directions can be found: the longitudinal direction (L), the radial direction (R) and the tangential direction (T), see Figure 2.1. The R- and T-directions are defined from the growth ring orientation and the L-direction is defined aligned the direction of the wood fibres. The L-direction does not necessarily align perfectly with the longitudinal direction of the stem, due to occurrence of spiral growth [7].

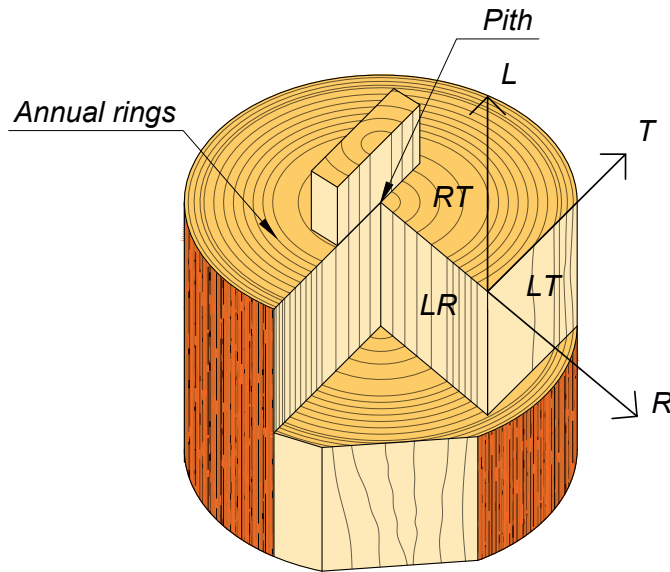


Figure 2.1: Cross section of a log where the annual rings are clearly visible. Main directions L, R, T, and planes LR, LT and RT are defined accordingly.

The macro scale is commonly used to perform stress analysis of wood. For a 2D plane strain or stress analysis wood is in the LR- and LT-planes commonly modelled as a homogeneous and transversely isotropic material, while in the RT-plane it may involve consideration of the cylindrical growth ring pattern [8]. The cylindrical growth pattern is of great importance in this project and will later be proven to have a big impact on the shear stiffness of CLT.

Imperfections such as knots, resin pockets, medullary rays, cracks, compression wood etc. are developed during the growth of the tree and could have a large impact on the strength of wood when it is considered on the macro scale [4]. Explicit modelling of such defects can be done, but is not included in the scope of this work. In modelling, the material will instead be treated as *clear wood*, meaning that no such defects are present. For the sake of clarity, wood that has been processed to fit construction purposes, and that contains defects, will further on be denominated as timber. The terminology "wood" will be used as a more broad and general term. Clear wood has different mechanical properties as opposed to timber, which is mentioned further in Section 2.3.

Further studying Figure 2.1, the variation of the material principal directions (LRT) in a board can be seen schematically. The variation depends on the sawing pattern of the board, i.e. the geometrical size and orientation of the board cut-out, as well as distance to the pith. The annual ring pattern affect the overall strength and stiffness of the board, as well as its drying properties. The effect of annual ring pattern is shown to have great impact on the rolling shear stiffness of individual board cross sections and is further discussed in Section 3.6.1.

2.2 Linear elasticity

When considering linear elastic materials in three dimensions, Hooke's generalized law may be applied. Through the following restrictions the application of Hooke's law to wood composites is simplified in this dissertation:

- Only small strains are considered.
- There is no variation in material parameters due to e.g. temperature variation, moisture content or loading rate.

For orthotropic materials such as wood, where the three main directions are the longitudinal, radial, and tangential direction the linear relation between the stress and the strain in local coordinates can be expressed as

$$\boldsymbol{\sigma} = \mathbf{D}\boldsymbol{\varepsilon} \quad (2.1)$$

or as the inverse relation

$$\boldsymbol{\varepsilon} = \mathbf{D}^{-1}\boldsymbol{\sigma} = \mathbf{C}\boldsymbol{\sigma} \quad (2.2)$$

where $\boldsymbol{\sigma}$ is the stress vector, $\boldsymbol{\varepsilon}$ is the (elastic) strain vector given by

$$\boldsymbol{\sigma} = [\sigma_{LL} \quad \sigma_{RR} \quad \sigma_{TT} \quad \tau_{LR} \quad \tau_{LT} \quad \tau_{RT}]^T \quad (2.3)$$

$$\boldsymbol{\varepsilon} = [\varepsilon_{LL} \quad \varepsilon_{RR} \quad \varepsilon_{TT} \quad \gamma_{LR} \quad \gamma_{LT} \quad \gamma_{RT}]^T \quad (2.4)$$

and \mathbf{C} is the compliance matrix according to

$$\mathbf{C} = \begin{bmatrix} \frac{1}{E_L} & -\frac{\nu_{RL}}{E_R} & -\frac{\nu_{TL}}{E_T} & 0 & 0 & 0 \\ -\frac{\nu_{LR}}{E_L} & \frac{1}{E_R} & -\frac{\nu_{TR}}{E_T} & 0 & 0 & 0 \\ -\frac{\nu_{LT}}{E_L} & -\frac{\nu_{RT}}{E_R} & -\frac{1}{E_T} & 0 & 0 & 0 \\ 0 & 0 & 0 & \frac{1}{G_{LR}} & 0 & 0 \\ 0 & 0 & 0 & 0 & \frac{1}{G_{LT}} & 0 \\ 0 & 0 & 0 & 0 & 0 & \frac{1}{G_{RT}} \end{bmatrix} \quad (2.5)$$

The constitutive matrices, \mathbf{C} and \mathbf{D} , contains the elasticity coefficients: three moduli of elasticity, E_L , E_R , E_T , three moduli of shear, G_{LR} , G_{LT} , G_{RT} and six Poisson's ratios, ν_{LR} , ν_{LT} , ν_{RL} , ν_{RT} , ν_{TL} and ν_{TR} . The index of the moduli of elasticity and shear denote what direction or plane the stiffness is regarding. For uniaxial loading the first index of the Poisson's ratio denote the loading direction and the second index denote the strain direction [7]. Due to linear elasticity being considered the following relations hold

$$\frac{\nu_{RL}}{E_R} = \frac{\nu_{LR}}{E_L}, \quad \frac{\nu_{TL}}{E_T} = \frac{\nu_{LT}}{E_L}, \quad \frac{\nu_{TR}}{E_T} = \frac{\nu_{RT}}{E_R} \quad (2.6)$$

which results in symmetrical \mathbf{C} and \mathbf{D} matrices.

Generally for wood the local coordinate system does not coincide with the global coordinate system and a relation between the two has to be established. This can be expressed the direction cosines between the respective coordinate axes of the two coordinate systems, a_{local}^{global} . The transformations may be written as

$$\hat{\boldsymbol{\sigma}} = \mathbf{G}^T \boldsymbol{\sigma} \quad (2.7)$$

$$\boldsymbol{\varepsilon} = \mathbf{G} \hat{\boldsymbol{\varepsilon}} \quad (2.8)$$

$$\hat{\mathbf{D}} = \mathbf{G}^T \mathbf{D} \mathbf{G} \quad (2.9)$$

where $\hat{\boldsymbol{\sigma}}$, $\hat{\boldsymbol{\varepsilon}}$ and $\hat{\mathbf{D}}$ are the stress respective strain vector and the constitutive matrix with reference to global coordinates and \mathbf{G} is the transformation matrix between local and global coordinate systems [7] given by

$$\mathbf{G} = \begin{bmatrix} a_L^x a_L^x & a_L^y a_L^y & a_L^z a_L^z & a_L^x a_L^y & a_L^z a_L^x & a_L^y a_L^z \\ a_R^x a_R^x & a_R^y a_R^y & a_R^z a_R^z & a_R^x a_R^y & a_R^z a_R^x & a_R^y a_R^z \\ a_T^x a_T^x & a_T^y a_T^y & a_T^z a_T^z & a_T^x a_T^y & a_T^z a_T^x & a_T^y a_T^z \\ 2a_L^x a_R^x & 2a_L^y a_R^y & 2a_L^z a_R^z & a_L^x a_R^y + a_L^y a_R^x & a_L^z a_R^x + a_L^x a_R^z & a_L^y a_R^z + a_L^z a_R^y \\ 2a_T^x a_L^x & 2a_T^y a_L^y & 2a_T^z a_L^z & a_T^x a_L^y + a_T^y a_L^x & a_T^z a_L^x + a_T^x a_L^z & a_T^y a_L^z + a_T^z a_L^y \\ 2a_R^x a_T^x & 2a_R^y a_T^y & 2a_R^z a_T^z & a_R^x a_T^y + a_R^y a_T^x & a_R^z a_T^x + a_R^x a_T^z & a_R^y a_T^z + a_R^z a_T^y \end{bmatrix} \quad (2.10)$$

For the two-dimensional case, where the stresses in the out-of-plane direction are very small or negligible, *plane stress* conditions can be applied meaning that only in-plane stresses exist. Thus, Hooke's generalized law in the local coordinate system reduces to

$$\boldsymbol{\sigma} = \mathbf{D} \boldsymbol{\varepsilon} \quad (2.11)$$

$$\boldsymbol{\varepsilon} = \mathbf{D}^{-1} \boldsymbol{\sigma} = \mathbf{C} \boldsymbol{\sigma} \quad (2.12)$$

$$\boldsymbol{\sigma} = [\sigma_{ii} \quad \sigma_{jj} \quad \tau_{ij}]^T \quad (2.13)$$

$$\boldsymbol{\varepsilon} = [\varepsilon_{ii} \quad \varepsilon_{jj} \quad \gamma_{ij}]^T \quad (2.14)$$

$$\mathbf{C} = \begin{bmatrix} \frac{1}{E_i} & -\frac{\nu_{ji}}{E_j} & 0 \\ -\frac{\nu_{ij}}{E_i} & \frac{1}{E_j} & 0 \\ 0 & 0 & \frac{1}{G_{ij}} \end{bmatrix} \quad (2.15)$$

where the indexes i and j denote the local ij -coordinate system of the constituent boards that comprise the CLT-beam.

2.3 Strength and stiffness properties

This section presents information about strength and stiffness properties of wood, whereas Section 2.4.2 will focus more on strength and stiffness regarding CLT. The presentation given hereafter is based on [2] and [4] where no other reference is given.

Norway spruce (*Picea abies*) and Scots pine (*Pinus sylvestris*) are the most commonly used wood species for structural purposes in Sweden and fall into the category of conifers. Wood produced from conifers is usually referred to as *softwood*. The analyses, experiments and discussions in this dissertation will only relate to spruce which is a softwood. However, due to the similar cell structure of conifers, the results are probably applicable to other softwoods as well [7].

The strength and stiffness properties of wood are in general affected by geometry, environmental conditions, load conditions and duration and defects. These properties may vary spatially in both the plane of the cross section and also in the longitudinal direction of the wooden board. For a clear wood specimen, the density and MoE tend to increase from the pith and outwards. This increase of the MoE in particular can be significant, where it is stated to be about a factor 2 from the pith and outwards in [4]. When conducting bending tests the largest stresses occur at the edges of the board. Thus, the measured MoE will mainly be governed by the stiffness of these areas. Segments of clear wood are often found in timber. Therefore clear wood properties such as density and annual ring width influence the MoE when conducting bending tests.

However, for a timber specimen, defects such as knots, compression wood, slope of grain, decay, bark pockets and resin pockets could heavily affect both the stiffness and strength of the timber. A bending test measuring the MoE for timber is hence also influenced by knots, slope of grain, and even compression wood and spiral wood if they are severe. Of all the above mentioned defects, knots have the most influential effect on the strength and stiffness of timber based on frequency of occurrence and impact. The strength is mostly affected by knots where there is tension, whereas the effect on the stiffness is caused by the slope of grain surrounding the knot.

Usually when loaded, failure of timber will occur where the timber has its weakest link, and where the stress exceeds the local critical stress. As a larger geometry also entails a higher probability of defects, the strength could be negatively influenced by an increase in stressed volume. This increase is generally interconnected to the length of the tested beam, whereas increases of width and thickness have a smaller impact in comparison. This phenomenon is called the size effect and is usually included in design with a correction factor. In modelling it can be included by e.g. probabilistic theories such as Weibull theory. However, it is not included in the scope of this project.

Strength and stiffness properties for different softwoods are shown in Tables 2.1 and 2.2, respectively. The strength properties in Table 2.1 given for Norway spruce and Spruce correspond to clear wood specimen, whereas the properties given for C24 timber are characteristic values. The indices in Table 2.1 are defined as follows: t denotes tension, c denotes compression and v denotes shear.

Table 2.1: Material strength properties for different softwoods in MPa from the compilation in [8].

Species	f_{Lt}	f_{Lc}	f_{Rt}	f_{Rc}	f_{Tt}	f_{Tc}	f_{vLR}	f_{vLT}	f_{vRT}
Norway spruce	63	29	4.9	3.6	2.8	3.8	6.1	4.4	1.6
Spruce	75	50	4.9	7.0			8.6		
Timber, C24	14	21	0.4	2.5	0.4	2.5	4.0	4.0	

Table 2.2: Stiffness parameters for Norway spruce at 12 % moisture content [7].

Parameter	Measurements
E_L , MPa	13500 – 16700
E_R , MPa	700 – 900
E_T , MPa	400 – 650
G_{LR} , MPa	620 – 720
G_{LT} , MPa	500 – 850
G_{RT} , MPa	29.0 – 39.0
ν_{RL}	0.018 – 0.030
ν_{TL}	0.013 – 0.021
ν_{TR}	0.24 – 0.33

As can be seen in Table 2.2 the stiffness parallel to grain E_L is by far the greatest. The stiffnesses perpendicular to grain E_R and E_T are of similar magnitude, although E_R is in general greater than E_T . One thing to note is the small shear stiffness G_{RT} , a typical property of softwoods [8]. G_{RT} is also known as the *rolling shear* stiffness and is further discussed in Section 2.4.

2.4 Cross laminated timber (CLT)

2.4.1 General

CLT is an engineered wood product (EWP) that comprises at least three cross-wise arranged strength graded board layers [9] with individual thicknesses of 20 – 60 mm [2]. The compound structure is usually created by face gluing, i.e. applying adhesive bonding in between the perpendicular layers. The intermediate layers can be manufactured with or without a gap between each adjacent board. In the case without a gap the boards can either be edge glued, i.e. with adhesive bonding in between the adjacent boards, or non-edge glued. CLT sections are normally comprised of finger jointed timber boards.

The structure of CLT is normally symmetrical and built up of either 3, 5 or 7 layers [2, 9]. For defining the numbering and *global* (xyz) axes of the CLT plate it is referred to [10], see Figure 2.2.

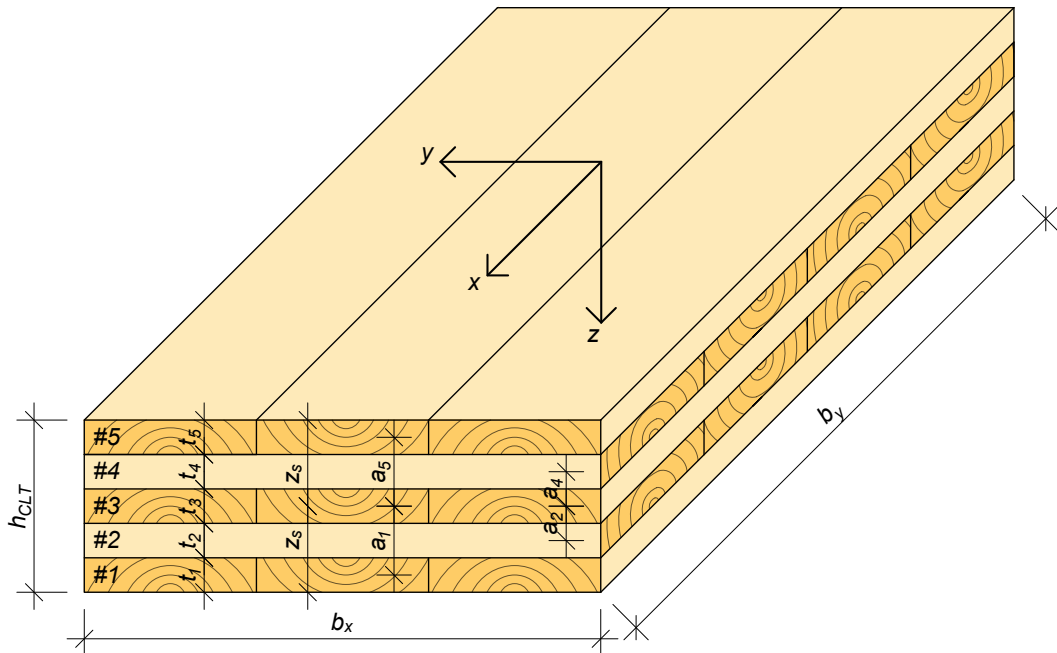


Figure 2.2: Definition of numbering and axes for a CLT cross section.

The following designations for the global directions are stated in [2]:

- the x -axis is parallel with the grain of the outermost layer of the boards.
- the y -axis is perpendicular to the grain of the outermost layer of the boards, and in the plane of the CLT.
- the z -axis is perpendicular to the xy -plane.
- 0 represents local axes for boards or layers, parallel with the grain.
- 90 represents local axes for boards or layers, perpendicular to the grain, and in the plane of the board or layer.

- 090 represents the local plane with a direction of 0 and 90, e.g. longitudinal shear.
- 9090 represents the local plane with a direction of 90 and 90, e.g. rolling shear.

The indices and positive directions of forces and stresses are also defined according to [10], and illustrated in Figure 2.3.

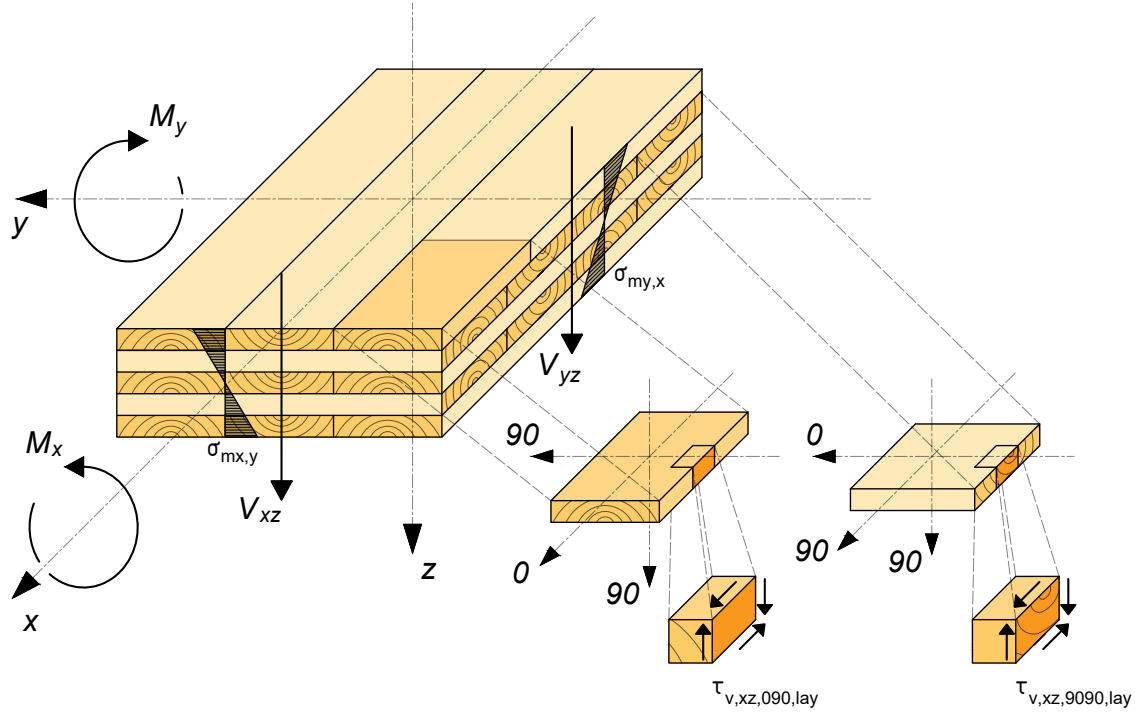


Figure 2.3: Definitions of indices as specified in SS-EN-16351.

Furthermore, the stiffness properties are assumed to be homogeneous and the same for all layers, and are denoted as:

$E_{0,xlay,mean} = E_0$ is the mean modulus of elasticity for a layer parallel with the grain in the x -direction.

$E_{0,ylay,mean} = E_0$ is the mean modulus of elasticity for a layer parallel with the grain in the y -direction.

$G_{090,xlay,mean} = G_0$ is the mean shear modulus along the x -axis.

$G_{090,ylay,mean} = G_0$ is the mean shear modulus along the y -axis.

$G_{9090,xlay,mean} = G_R$ is the mean rolling shear modulus in the plane where both axes are perpendicular to grain.

2.4.2 Strength and stiffness

The structure of CLT, where every other layer is oriented transversely, and each layer consists of structurally graded timber boards, evens out the variability and property differences of wood mentioned in Section 2.3. CLT elements have a greater characteristic strength and less variability when compared to the timber boards of which

it is comprised of [2]. The risk of the weakest cross sections coinciding in the same direction of the CLT is small. This is referred to as the *system effect* and also includes the increase in strength from the interaction between multiple boards. This is similar to what is referred to as the laminating effect of glulam [4], which can be explained as the compound effect of three different phenomena:

1. Due to inhomogeneities and defects a single board exposed to bending may exhibit a certain deformation pattern. If the same board is constrained in a CLT beam exposed to bending it would most certainly exhibit another deformation pattern. This is called effect of test procedure.
2. The smearing of defects mentioned above, also referred to as the *dispersion effect*.
3. Stresses tend to distribute to areas of high stiffness. Thus areas of low stiffness or areas that contains knots will be reinforced by adjacent boards, when contained in CLT.

However, the impact of the dispersion effect may be questioned for CLT containing boards with thicknesses of 20 - 50 mm, as knots fit into the same order of magnitude. A significant impact would likely be attained from the dispersion effect for EWP comprised of thinner boards [4].

In bending, it is often the tensile strength of the outermost layers and the rolling shear strength of the transverse layers that are governing. In design, it is often the characteristic 5-percentile values of the strength parameters that are used, whereas for stiffness parameters it is often the mean values that are used. When compared to other timber slab products, such as stress laminated timber decks, CLT has a lower bending strength in the main direction in comparison. However, the transverse bending strength is substantially higher.

The stiffness of finger joints is very high and often comparable to that of a clear wood specimen. However, depending on the location of the finger joint the strength of CLT could be heavily affected. A finger joint located in a bottom longitudinal layer exerted to tensile stresses could lead to an early fracture. Furthermore, the adhesives that are used today are usually extremely brittle, and will likely exhibit the same mechanical properties as the wood itself.

A characteristic feature of CLT and some other timber composites is the *apparent stiffness*. The apparent stiffness of CLT can be seen as the global stiffness, resulting from the conjoint stiffness of the constituent boards in a particular direction or plane. Given the significant impact of the rolling shear stiffness on CLT, the choice was made to focus on the parameters affecting the rolling shear modulus G_R , and the so called apparent rolling shear modulus $G_{R,app}$. In a report published by Aicher and Dill-Langer [11] it is shown that the rolling shear modulus of CLT is not an intrinsic material property but rather an apparent shear stiffness "smeared" over the structural element. The geometry, principal direction stiffnesses and distinctively the annual ring orientation are shown to affect the apparent shear modulus of CLT. This is further investigated within this project in Section 3.6.1 by means of the Finite element method.

2.4.3 Loading

The plate can be seen as an orthotropic panel that can be exposed to two kinds of loading: *in-plane* loading and *out-of-plane* loading. The type of loading is defined based on the loading direction according to Figure 2.4. In-plane loading is defined as loading in the xy -plane in Figure 2.4. Normally, this type of loading is occurring for wall elements loaded by axial forces. Out-of-plane loading is defined as loading perpendicular to the xy -plane in Figure 2.4. Normally, this type of loading is occurring for floor elements loaded by forces acting perpendicular to the plane of the CLT.

As the purpose of this dissertation is to examine *beam specimens* cut out from a CLT plate, some further definitions are needed in order to avoid discrepancies when applying the above mentioned load cases to a beam, see Figure 2.4. Note that the global CLT coordinate system is denoted with lowercase xyz , whereas the beam coordinate system is denoted with capital XYZ .

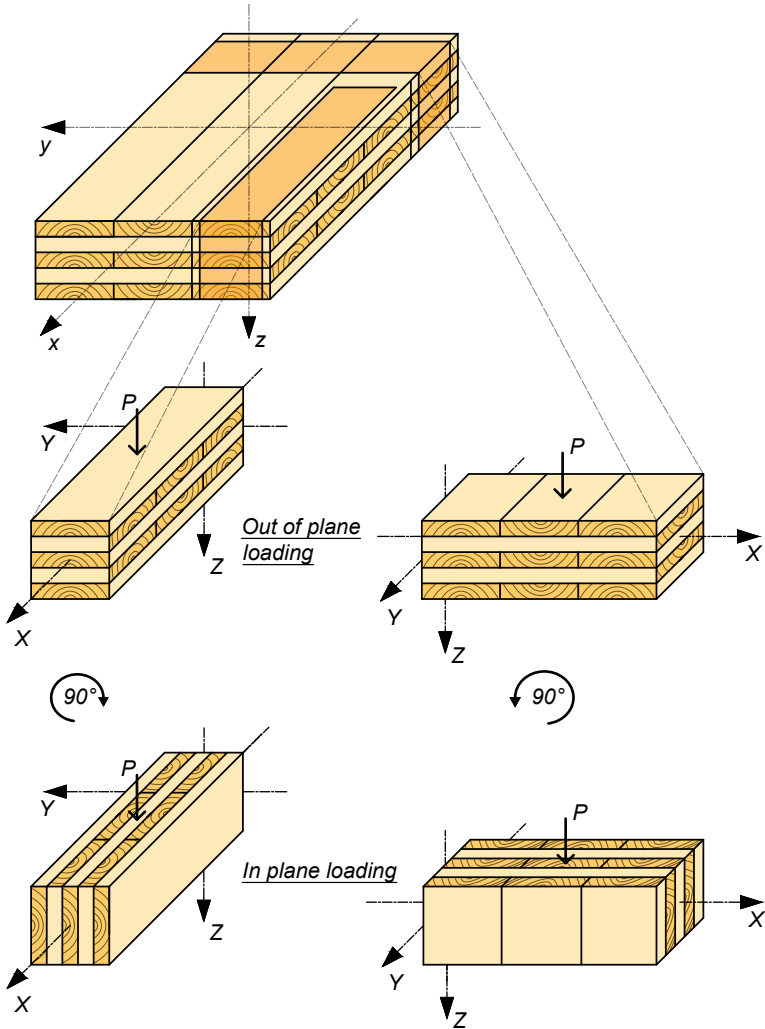


Figure 2.4: Definitions of loading and coordinate systems of beam cut out of a CLT plate.

When considering a three dimensional CLT-beam as a one dimensional beam according to beam theory, certain assumptions and approximations have to be made with respect to the different load cases shown in Figure 2.4.

Out-of-plane loading gives rise to the largest bending stresses in the boards with the fibres parallel to the stressed direction, due to the MoE of wood parallel to grain being approximately 20 times larger than the MoE perpendicular to grain [9]. Thus, a commonly used approximation is to assume that the MoE perpendicular to grain is negligible, and that no bending stresses are transferred through the transverse layers. This assumption is also motivated by the fact that the transverse boards normally are not edge glued, meaning that transfer of bending stresses cannot occur between two adjacent boards. Worth noting here is that for beams where the outermost layer is oriented in the transverse direction it can be assumed that no bending stresses nor shear stresses occur in these layers. Thus, the outermost layers can be disregarded from when calculating the moment of inertia, and the beam can be viewed upon as containing only three constituent layers.

In-plane loading will also give rise to the largest bending stresses in the boards with the fibres parallel to the stressed direction. This is due to the approximation that the transverse boards are rigidly connected to the longitudinal boards, and that the MoE perpendicular to grain is negligible. Thus, a commonly used approximation is to disregard the contribution from the transverse boards when calculating the bending stiffness. Based on the assumption of zero bending stresses in the transverse layers the resulting shear stresses should also be zero in these layers, whereas the contribution of these layers towards the stiffness should not be included. This was initially assumed within this project, however, by means of FE-models it was shown that a considerable portion of the shear stresses are transferred through the transverse layers for in-plane loading. This is further elaborated in Section 3.6.2.

A key aspect deriving from the structure of CLT when it is exposed to out-of-plane loading is rolling shear. Rolling shear occurs when the transverse boards are subjected to shear stresses in the RT-plane, caused by a non-uniform bending moment [9]. This causes the fibres to “roll” on top of each other. Rolling shear stiffness and strength are several times lower than the other stiffness and strength parameters, see Tables 2.1 and 2.2, and thus play a significant role when determining the ultimate strength and deformations of CLT. The ultimate strength of CLT is verified by comparing the maximum stress towards the strength property of the individual constituent board. The distribution of bending and shear stresses for the above mentioned load cases are shown schematically in Figure 2.5.

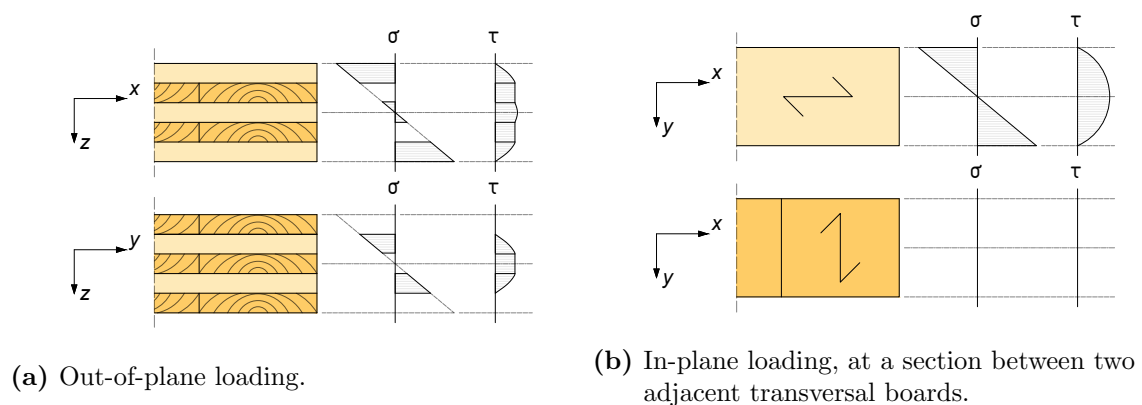


Figure 2.5: Bending and shear stresses for symmetrical CLT layups based on initial assumptions. Rolling shear occurs in transverse layers exposed to shear stress.

2.5 Analytical methods

For a clear main load direction, CLT can normally be treated like a beam, and beam theory can be applied [2]. Generally, the out-of-plane stresses for a one-dimensional beam model loaded perpendicular to its longitudinal plane are assumed as zero. This is due to that Poisson's ratio is assumed as zero and that no transverse contraction occur. Thus, the only non-zero stresses in the beam are σ_X , τ_{XY} and τ_{XZ} , where it is referred to Figure 2.6 for definition of directions. As pointed out in Section 2.4.3 the rolling shear stiffness of CLT is significantly lower than other stiffness parameters, meaning that shear strains make up a large portion of the total strains for CLT. The analytical models described in this section (The Gamma method and Timoshenko theory) represent two methods of accounting for shear strains when evaluating the stiffness of CLT. The Gamma method can only be applied for out-of-plane loading, whereas Timoshenko theory can be applied for both in-plane and out-of-plane loading, respectively.

2.5.1 Gamma method

The Gamma method is derived from the method described in Eurocode 5, Annex B [12], where the transverse layers of the cross section are seen as flexibly connected to the longitudinal layers by mechanical fasteners. The slip between two longitudinal layers correspond to the rolling shear strains in the transverse layer. The Gamma method is based on a number of assumptions that were not evaluated within this project. For information regarding these assumptions, it is referred to [12].

The Gamma method accounts for shear strains in the transverse layers by replacing the net moment of inertia $I_{x,net}$ when calculating the *bending stiffness* $EI_{x,net}$, with an effective moment of inertia $I_{x,ef}$. The effective moment of inertia is calculated by reducing the "Steiner"-terms of the longitudinal boards by means of weighted *Gamma*-factors. The Gamma-factors depend on the thickness of the constituent layers, the MoE parallel to grain, the rolling shear modulus, the span and boundary conditions of the beam [2]. In this project, only prismatic beams containing boards with equal thickness and stiffness properties in all layers are considered. Thus, the expressions for the Gamma-factors can be simplified. For a 5-layer CLT beam meeting the aforementioned criteria $I_{x,ef}$ can be calculated as

$$I_{x,ef} = \frac{b_x t_1^3}{12} + \gamma_1 b_x t_1 a_1^2 + \frac{b_x t_3^3}{12} + \frac{b_x t_5^3}{12} + \gamma_5 b_x t_5 a_5^2 = b_x \left(\frac{3 \cdot t_1^3}{12} + 2 \cdot \gamma_1 t_1 a_1^2 \right) \quad (2.16)$$

where

- a_i is the distance from the global centre of gravity (CoG) to the local CoG for the constituent longitudinal boards i , see Figure 2.2.
- γ_i is the reduction factor (denoted Gamma-factor), see Figure 2.2.
- b_x is the width of the beam. In this project $b_x = 100$ mm.

Furthermore, if the considered 5-layer CLT-beam has the outermost layers oriented in the longitudinal direction the parameters a_i and γ_i will be identical for these layers

and can be calculated as

$$a_1 = \frac{t_1}{2} + t_2 + \frac{t_3}{2}, \quad (a_1 = a_5) \quad (2.17)$$

$$\gamma_1 = \frac{1}{1 + \frac{\pi^2 E_0 t_1}{l_{ref}^2} \frac{t_2}{G_R}}, \quad (\gamma_1 = \gamma_5) \quad (2.18)$$

where

l_{ref} is the reference length based on support conditions.

For simply supported conditions used in this project $l_{ref} = L$.

If the the outermost layers of the considered 5-layer CLT-beam are oriented in the transverse direction, the beam can instead be seen as an equivalent 3-layer beam (consisting of the innermost layers of the original 5-layer beam), based on the assumptions made in Section 2.4.3. According to [2] the approach for a 3-layer beam is to reduce the stiffness contribution of the second longitudinal layer, counting from the bottom and up according to Figure 2.2). For a 3-layer CLT beam meeting the aforementioned criteria $I_{x,ef}$ can be calculated as

$$I_{x,ef} = \frac{b_x t_1^3}{12} + b_x t_1 a_1^2 + \frac{b_x t_3^3}{12} + \gamma_3 b_x t_3 a_3^2 = b_x \left(\frac{2 \cdot t_1^3}{12} + (1 + \gamma_3) t_1 a_1^2 \right) \quad (2.19)$$

Consequently, the parameters a_i and γ_i can be calculated as

$$a_1 = \frac{t_1}{2} + \frac{t_2}{2}, \quad (a_1 = a_3) \quad (2.20)$$

$$\gamma_1 = 1 \quad (2.21)$$

$$\gamma_3 = \frac{1}{1 + \frac{\pi^2 E_0 t_3}{l_{ref}^2} \frac{t_2}{G_R}} \quad (2.22)$$

The Gamma method is used in conjunction with Bernoulli Euler theory (BE-theory). BE-theory is based on the fundamental assumption that plane sections remain plane and normal to the beam axis throughout deformation, i.e. that the rotation of the cross section θ equals the slope of the beam w' , see Figure 2.6. As this means that shear strains are not taken into consideration, the only non-zero strain is the normal strain ε_X . Contradictory to this statement, as stresses are normally derived from strains, it does not mean that shear stresses do not exist in the beam. The shear stresses are derived from equilibrium. As pointed out above, the contributions from the shear strains to the total beam deflection are accounted for by replacing the conventional term of the bending stiffness $EI_{x,net}$ with the effective bending stiffness $EI_{x,ef}$.

For a simply supported beam, loaded by a load P at $X = L/2$ (see Figure 2.6), the following equation can be derived for the deformation w according to BE-theory

$$w(X) = \frac{P}{12 \cdot EI_{x,net}} X^3 - \frac{PL^2}{16 \cdot EI_{x,net}} X \quad (2.23)$$

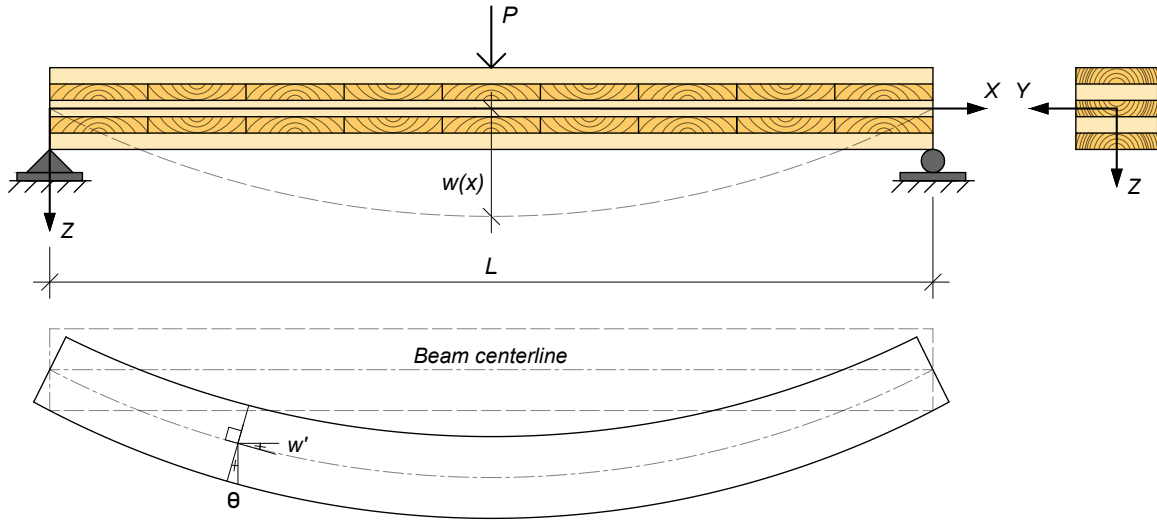


Figure 2.6: Beam-model according to Bernoulli-Euler theory, where out-of-plane loading of CLT is considered.

where

- X is the considered position along the length of the beam L in the interval of $[0 \leq X \leq L/2]$.
- $I_{x,net}$ is the net moment of inertia.
- E is the MoE in the parallel to grain direction $E = E_0$.

Finally, by substituting the bending stiffness using either Equation 2.16 or 2.19 (depending on the layup of the beam), Equation 2.23 can be rewritten as

$$w(X) = \frac{P}{12 \cdot EI_{x,ef}} X^3 - \frac{PL^2}{16 \cdot EI_{x,ef}} X \quad (2.24)$$

2.5.2 Timoshenko theory

Similar to BE-theory, Timoshenko theory assumes that plane sections remain-plane during deformation. However, the cross section does not need to remain perpendicular to the beam axis during deformation, i.e. the rotation of the beam is instead an independent variable θ , see Figure 2.7. The shear strains can be derived from the difference between rotation and the slope of the beam ($\theta - w'$). For a simply supported CLT beam, loaded by a load P at $X = L/2$ (see Figure 2.6), the following equation can be derived for the deformation w according to Timoshenko theory

$$w(X) = \frac{P}{12 \cdot EI_{x,net}} X^3 + \frac{P}{EI_{x,net}} \left(-\frac{L^2}{16} + \frac{\alpha}{2} \right) X \quad (2.25)$$

where

- X is the considered position along the length of the beam L in the interval of $[0 \leq X \leq L/2]$.
- $I_{x,net}$ is the net moment of inertia.

The parameter α is calculated as

$$\alpha = \frac{EI_{x,net}}{\sum_{i=1}^n G_i A_i \kappa} \quad (2.26)$$

where

- n denotes the total number of layers in beam
- A_i is the area of the considered layer i .
- G_i is the shear stiffness of the considered layer i .
- κ is the shear correction factor, calculated with Equation 2.27.

The term $GA\kappa$ is in this project denoted as *effective shear stiffness*. The bending stiffness $EI_{x,net}$ signifies the resistance of the beam toward bending, where the moment of inertia $I_{x,net}$ is calculated for the layers transferring bending stresses. Similarly the effective shear stiffness is a measure of the combined resistance of the constituent layers toward shear deformations. The area A should correspond to the cross sectional area transferring the shear stresses when the beam is exposed to loading. The area assumed to be transferring the shear stresses is denoted "*effective area*" in this project. For out-of-plane loading the effective area is defined as the area enclosed by (and including) the outermost longitudinal layers of the beam. For in-plane loading the effective area is harder to define, as the shear stress distribution in the transverse layers was

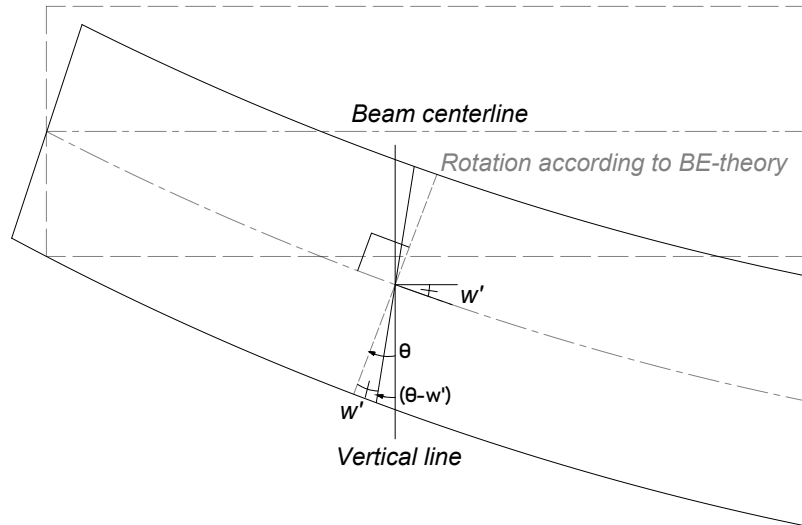


Figure 2.7: Shear strains according to Timoshenko theory for a beam model in accordance with Figure 2.6.

shown to vary in the longitudinal direction of the beam. This is further elaborated in Section 3.6.2, whereas two areas will be defined here. The area consisting only of the longitudinal layers, denoted net area A_{net} , and the area of the entire cross section, denoted gross area A_{gross} .

The correction factor κ accounts for that the stiffness is being overestimated due to the assumption that plane sections remain-plane. The correction factor depend partly on the geometrical shape and is for rectangular and homogeneous cross sections where the transverse contraction is negligible equal to 5/6. It was assumed in Section 2.4 that CLT beams loaded in-plane can be regarded as rectangular cross sections where only the longitudinal boards contribute to the bending stiffness. Thus, $\kappa = 5/6$ is a consistent approximation.

For CLT loaded out-of-plane the expression for κ becomes more complex as the stiffness and geometry of each constituent board is accounted for according to [2]

$$\kappa = \frac{(\sum (EI + EAa^2))^2}{\sum G_i b t_i \cdot \int_h \frac{S^2(z) E^2(z)}{G(z) b(z)} dz} \quad (2.27)$$

The expression on the right hand side of the denominator in Equation 2.27 contains a double integral involving the static moment $S(z)$.

$$\int_h \frac{[E(z) \cdot S(z)]^2}{G(z) \cdot b} dz = \int_h \frac{[E(z) \cdot \int A \cdot z dz]^2}{G(z) \cdot b} dz \quad (2.28)$$

The double integral in Equation 2.28 can be determined layer by layer using polynomials and then summed [13]. Equation 2.29 illustrates this process for one layer considered

$$\begin{aligned} \int_{z_{i,o}}^{z_{i,u}} [E \cdot S]^2 dz &= \frac{E_i^2 b^2}{60} (3 \cdot z_{i,u}^5 - 10 \cdot z_{i,o}^2 z_{i,u}^3 + 15 \cdot z_{i,o}^4 z_{i,u} - 8 \cdot z_{i,o}^5) + \\ &+ [E \cdot S]_i \frac{b \cdot E_i}{60} (20 \cdot z_{i,u}^3 - 60 \cdot z_{i,o}^2 z_{i,u} + 40 \cdot z_{i,o}^3) + \\ &+ [E \cdot S]_i^2 (z_{i,u} - z_{i,o}) \end{aligned} \quad (2.29)$$

where

- $z_{i,o}$ is the z -coordinate from the upper edge of the considered layer to the global CoG.
- $z_{i,u}$ is the z -coordinate from the lower edge of the considered layer to the global CoG
- E_i is the MoE in the stressed direction.

The index i denotes the currently considered layer of the CLT plate. Only the MoE parallel to grain E_0 was considered in this project, and the MoE perpendicular to grain E_{90} was assumed as zero for beam modelling approaches. The term containing the statical moment $[E \cdot S]_i$ is calculated by summing the distances from the upper

and lower edge, respectively, to the global centre of gravity. The summation is done for layer k starting from either the upper edge to the currently considered layer i . As the static moment is considered, only $n - 1$ layers have to be calculated.

$$[E \cdot S]_i = \sum_{i=1}^{n-1} [E \cdot S]_{z_{i,o}}^{z_{i,u}} \quad (2.30)$$

In Equation 2.30 the contribution of each individual layer k is given as

$$[E \cdot S]_{z_{i,o}}^{z_{i,u}} = E_i b \cdot \left(\frac{z_{i,u}^2}{2} - \frac{z_{i,o}^2}{2} \right) \quad (2.31)$$

The process of solving κ described by Equations 2.27-2.31 is done numerically by the means of a *MATLAB*-script, see Appendix D. The script was originally created by doctoral student Gustaf Larsson (et al.), and later modified by senior lecturer Henrik Danielsson, from whom it was received from.

For in-plane loading the bending stiffness is calculated with respect to bending around the global z -axis of the CLT-beam (see Figure 2.5), where the corresponding moment of inertia is denoted $I_{x,net,z}$. The effective shear stiffness is calculated with respect to the shear modulus parallel to grain G_0 , the effective area A and the assumption of $\kappa = 5/6$. Consequently using Equation 2.26 the parameter α can be expressed as

$$\alpha = \frac{6 \cdot EI_{x,net,z}}{5 \cdot G_0 A} \quad (2.32)$$

For out-of-plane loading the bending stiffness is calculated with respect to bending around the global y -axis of the CLT-beam (see Figure 2.5), where the corresponding moment of inertia is denoted $I_{x,net,y}$. The effective shear stiffness is calculated with respect to the shear moduli of the constituent boards considered, the effective area A and the assumption of $\kappa = 5/6$. Depending on the layup the parameter α will differ. For a 5-layer beam, with equal thickness of all boards and the same stiffness properties for boards oriented in the same direction, the parameter α can be expressed as

$$\alpha = \frac{EI_{x,net,y}}{b_x t (2 \cdot G_R + 3 \cdot G_0) \kappa} \quad (2.33)$$

where

- t is the layer thickness. In this project $t = 20$ mm.
- b_x is the width of the beam. In this project $b_x = 100$ mm.

For a 3-layer beam, with equal thickness of all boards and same the stiffness properties for boards oriented in the same direction, the parameter α can be expressed as

$$\alpha = \frac{EI_{x,net,y}}{b_x t (G_R + 2 \cdot G_0) \kappa} \quad (2.34)$$

2.5.3 Simplified shear correction factor

The shear correction factor κ involves complicated equations and even the alternative method according to Equation 2.29 proves rather complex. Approximate values for the shear correction factor have been suggested by Jöbstl and are given in [13]. The values are representative for symmetrical layups with equal layer thicknesses and a shear moduli ratio of $G_{9090}/G_0 = 1/10$. The suggested values are for three layers $\kappa = 0.21$ and for five layers $\kappa = 0.24$. By using Equations 2.27–2.31 and iterating for different values of G_R the relation between κ and G_R can be illustrated. This is done for two symmetrical CLT beams with equal layer thicknesses of 0.02 m, where one beam has the outermost boards in the longitudinal direction and the other beam has the outermost boards in the transverse direction. It can be seen in Equation 2.27 that the MoE does not affect the value of κ if the transverse MoE is assumed as zero, leaving the shear moduli G_R and G_0 as the remaining varying factors if the geometry is held constant. Figures 2.8 and 2.9 illustrate how κ varies with G_R for different values of G_0 . The values suggested by Jöbstl are also illustrated as rings for each line, respectively.

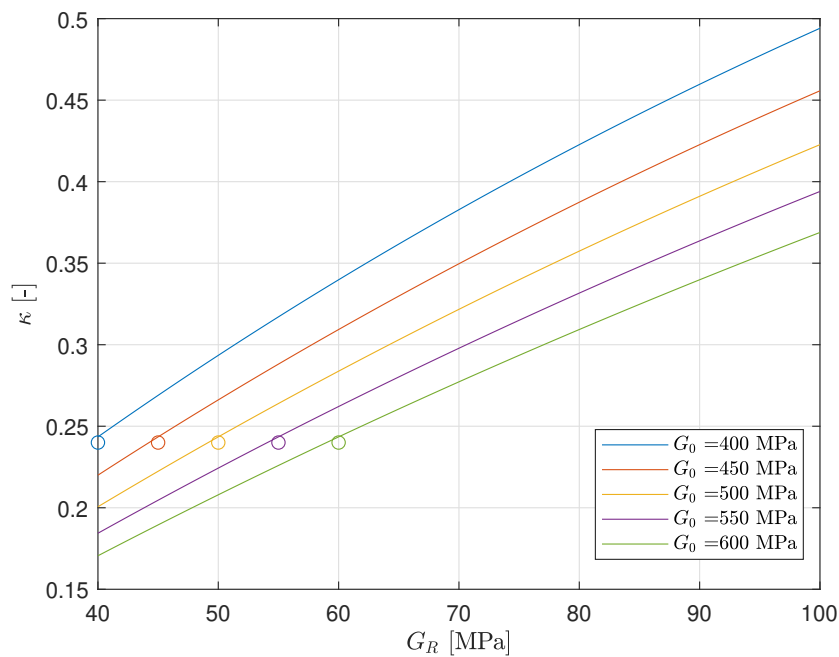


Figure 2.8: Relation between κ for different values of G_0 for a five layer beam with the outermost boards in the longitudinal direction.

2.5.4 Comparison between analytical methods

As the analytical methods are used to evaluate the stiffness parameters of a beam later in this dissertation it is of great interest to study the differences between the two methods. The main difference between using BE-theory in conjunction with the Gamma method, as opposed to Timoshenko theory, is that Timoshenko theory accounts for shear strains in the beam, whereas the Gamma method amplifies the deformation pat-

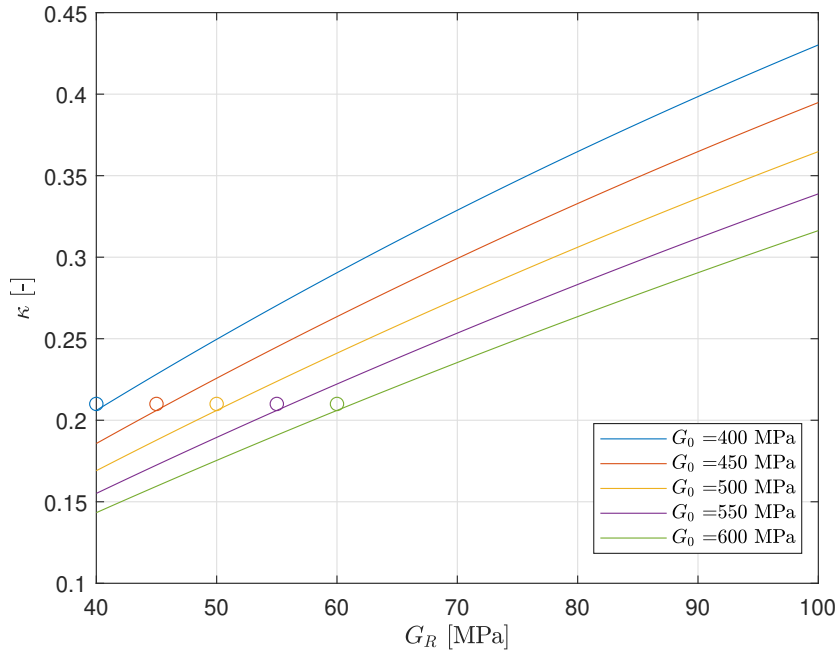


Figure 2.9: Relation between κ for different values of G_0 for a five layer beam with the outermost boards in the transverse direction.

tern of BE-theory through a reduced moment of inertia. This can be illustrated by plotting the deformation patterns using equations 2.23 and 2.25.

The deformation pattern is illustrated for both in-plane loading and out-of-plane loading for two different spans L_1 and L_2 , respectively. The spans that are illustrated represent some of the spans that were used for the experimental tests. However, only layups where the boards of the outermost layer oriented in the longitudinal direction are illustrated here. Layups where the outermost layer is oriented in the transverse direction could have also been included here. Although, the cross section of such a beam can be simplified to only consist of three constituent layers. This is due to the fact that the outermost layers are assumed not to transfer any bending or shear stresses during bending. Therefore it is superfluous to illustrate the deformation pattern of such beams here, as it will be similar to that of a 5 layer CLT beam. The following deformation patterns are illustrated below.

1. Beam loaded out-of-plane, $L_1 = 1.0$ m, see Figure 2.10.
2. Beam loaded out-of-plane, $L_1 = 1.4$ m, see Figure 2.11.
3. Beam loaded in-plane, $L_1 = 1.0$ m, see Figure 2.12.
4. Beam loaded in-plane, $L_1 = 1.4$ m, see Figure 2.13.

The stiffness parameters in this study were set to: $E_L = 12000$ MPa, $G_{LT} = 690$ MPa, $G_{RT} = 50$ MPa for all illustrations. The deformations in Figures 2.10 – 2.13 were normalised in comparison to BE-theory deformations using the net moment of inertia in order to show the relative difference in deformation between the analytical methods

used. As can be noted from the graphs the deformation only differs substantially in the middle. Thus, when using these methods to evaluate stiffness properties from deformation curves obtained by experimental tests, measuring the deformations in the mid span would be of most interest.

Considering that linear elastic conditions are applied, and that the stiffness parameters are held constant, Gamma method and Timoshenko theory will yield the same relative increase of deformation compared to BE-theory for loading in-plane and loading out-of-plane, respectively. This is illustrated for different beam spans in Figures 2.14 and 2.15, respectively.

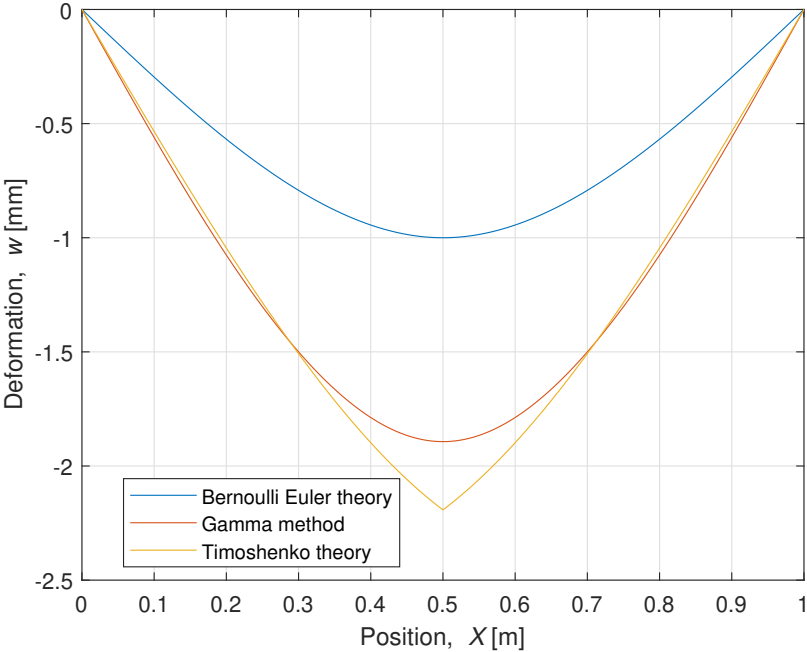


Figure 2.10: Deformation pattern for different analytical methods. Beam loaded out-of-plane, $L_1 = 1.0$ m.

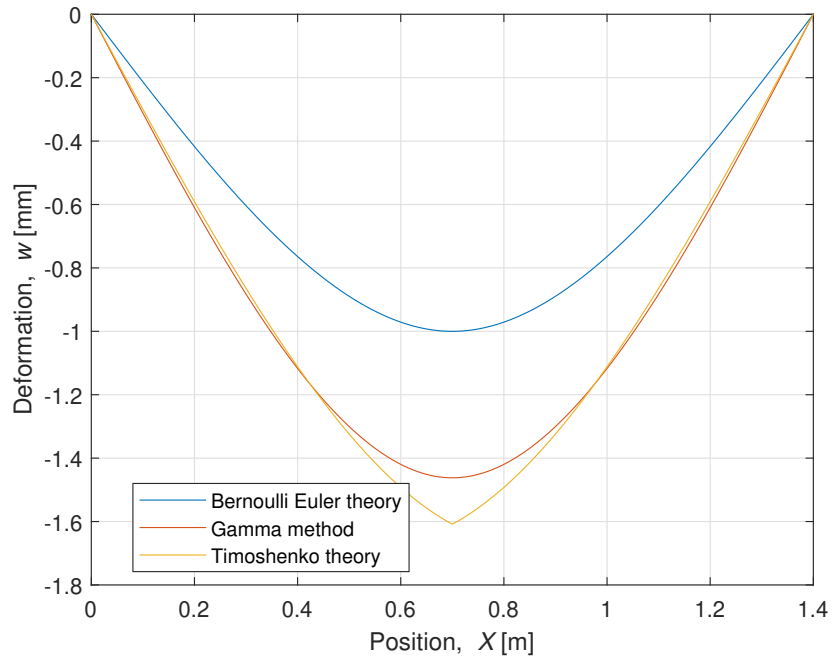


Figure 2.11: Deformation pattern for different analytical methods. Beam loaded out-of-plane, $L_2 = 1.4$ m.

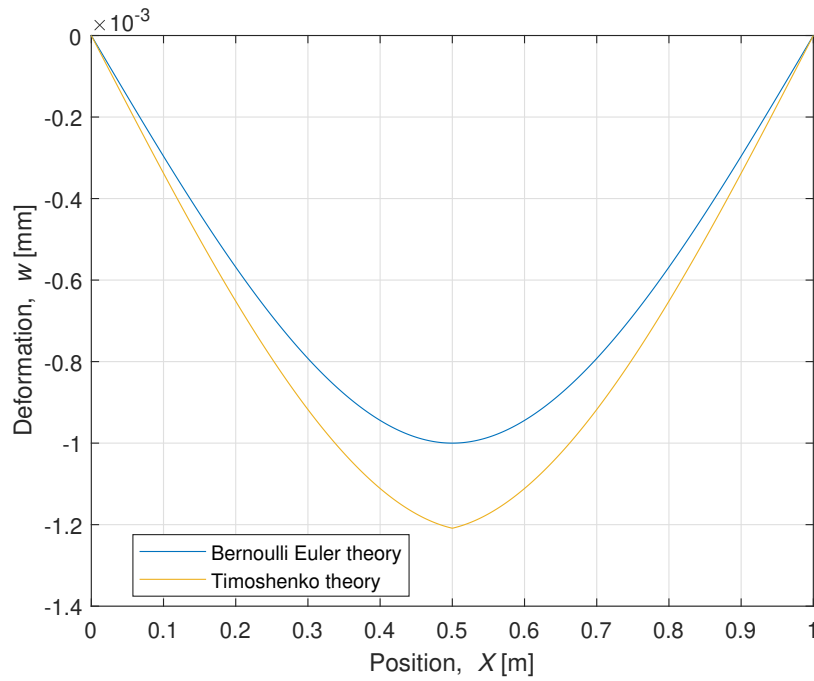


Figure 2.12: Deformation pattern for different analytical methods. Beam loaded in-plane, $L_1 = 1.0$ m.

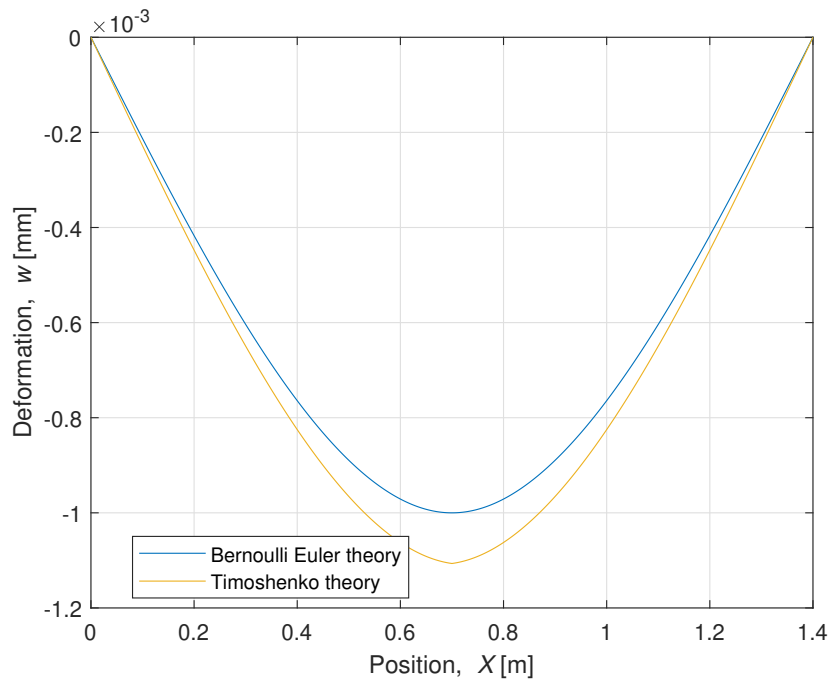


Figure 2.13: Deformation pattern for different analytical methods. Beam loaded in-plane, $L_2 = 1.4$ m.

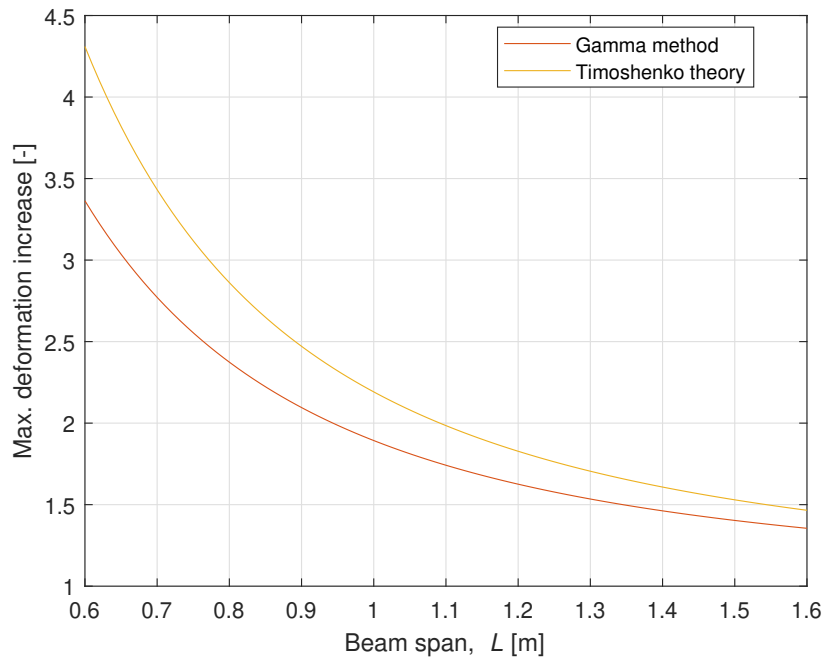


Figure 2.14: Max. deformation in relation to BE-theory for a beam loaded out-of-plane, where constant stiffness parameters are applied.

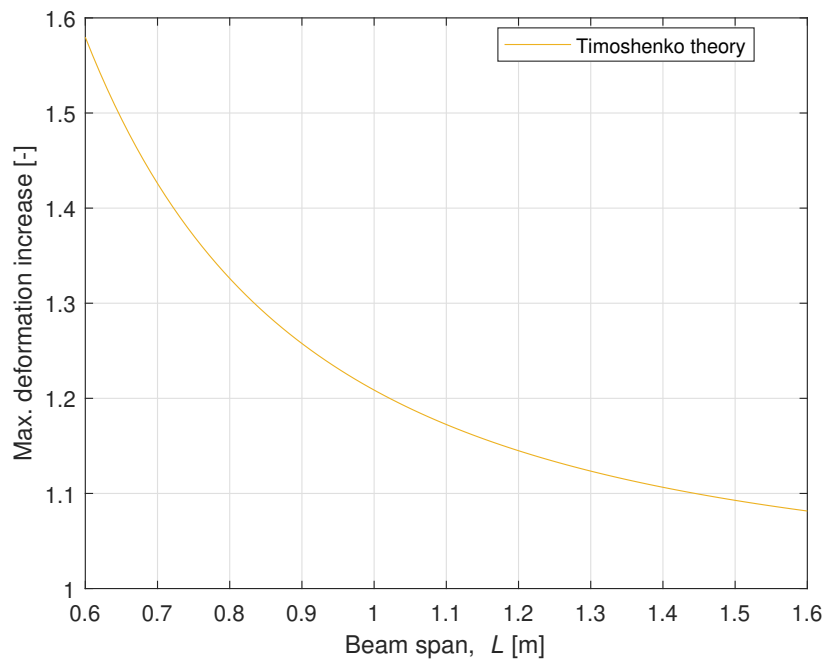


Figure 2.15: Max. deformation in relation to BE-theory for a beam loaded in-plane, where constant stiffness parameters are applied.

2.6 Bending stiffness (according to Eurocode)

The European assessment document (EAD) [3], which is the currently harmonized technical specification of solid wooden slabs, refer to Eurocodes [12] and other standards [14, 15] as a method of determining the bending stiffness EI of CLT. It is specified that the Gamma method may be used when determining the bending stiffness through a 4-point bending test, according to Figure 2.16. The rolling shear modulus G_R should then be approximated as 50 MPa. However, three potential difficulties have been identified in the above mentioned methodology. Firstly, for determining the MoE of the CLT the relative deformation between the two point loads is measured, as no shear strains occur in this span. For relatively short CLT beams this deformation is usually a few millimeters at most, whereas high accuracy and possibly high-end equipment is needed to correctly measure these deformations. Secondly, as can be seen in Section 3.6.1 the conventional value of 50 MPa proved to be rather conservative when the annual ring orientation of the boards are considered. Lastly, the rolling shear modulus exhibits the same uncertainty when measured as other mechanical properties of wood, whereas a static approximation might yield deviating results for lower or higher percentile values of G_R .

In conclusion, the difficulty of correctly measuring the deformation as well as the lower-end approximation of G_R might yield an overly deviating bending stiffness. Methods where the rolling shear modulus can be measured in accordance to the other stiffness parameters might yield more accurate results.

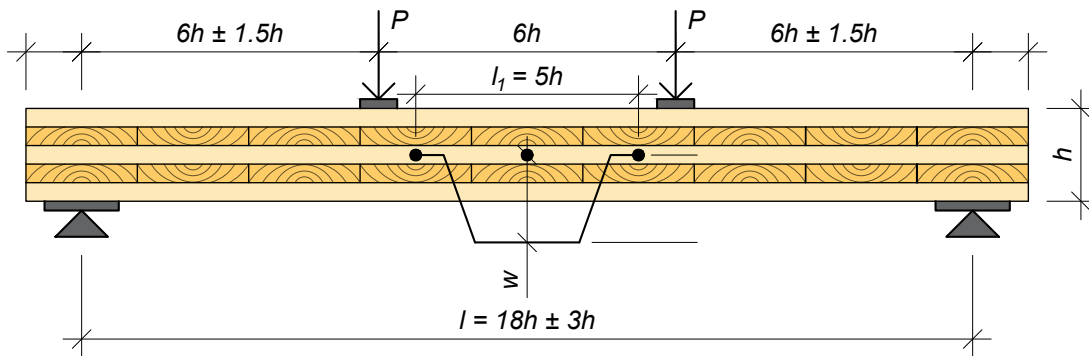


Figure 2.16: Test arrangement for measuring bending stiffness according to [14]

3 Finite element modeling

3.1 General

Most of the problems within engineering mechanics can be described by differential equations. Generally these equations are too complicated to solve analytically whereas a *numerical approach* can be utilised. The *finite element method* (FE-method) is an effective way of solving complicated problems numerically.

The FE-method is based on the assumption that differential equations, describing the physical phenomena, hold over a certain region which may be one, two or three dimensional. Conventionally, a studied body is often divided into smaller parts, so called *finite elements*, whereas the differential equations hold for each element, respectively. The collection of elements over the considered body is called a *finite element mesh*.

A variable varying in a non linear fashion over a body, may instead be modelled with a linear variation in each element, respectively. Given that the body is divided into a fine enough mesh, this approximation will converge toward the exact solution. The approximation which is to be applied over each element is chosen depending on the problem at hand. The approximation is based on the number of *nodal points* in the element, i.e. points where the variable are determined, and is expressed as an interpolation between these points. These nodal points are often located at the boundary of the element. The interpolation is usually polynomial and may be of linear, quadratic or cubic variation etc. When the approximations have been established for each element, the elements are patched together following certain rules in order to provide an approximate solution for the entire body. For further explanation of the FE-method, and derivation of the numerical model equations that make up the FE-method it is referred to [16].

3.2 Scope and limitations

The main purpose of the FE-models was to study the validity of the characterised stiffness properties calculated by applying analytical methods, presented in Section 2.5, to the experimental data obtained from conducting experimental tests. Therefore the FE-models were created in as close resemblance as possible to the experimental setups, in order to not compromise the efficacy. Given that a large number of tests were conducted, simplifications concerning the geometry of the models were made where the efficiency would be improved as a result. Furthermore, as wood is a heterogeneous and anisotropic material, with a large variety in material properties with respect to the spatial distribution of the beam, some general assumptions and simplifications were made in order to reduce the complexity of the models. The general assumptions and simplifications, applying to all FE-models, are listed below:

- Variation in material properties due to moisture content or temperature is not accounted for.
- Linear elastic material behaviour is assumed, plasticity or other nonlinear material behaviour is not included.
- Homogeneous material properties are considered.
- Plane stress is considered in the 2D-models.
- Glue lines are not modelled explicitly. There is assumed to be no difference in elastic coefficients in the interfaces between the boards compared to the rest of the cross section.

Assumptions and simplifications applying to the FE-models presented in Sections 3.4.1 and 3.4.2 are listed below:

- Symmetry is utilized with respect to the X -direction for the 2D-models.
- Symmetry is utilized with respect to both the X - and Y -directions for the 3D-models.
- Roller supports were modelled with respect to symmetry for the 2D- and 3D-models.
- Contact conditions between transverse boards in the same layer were not modelled.
- Annual ring pattern is not modelled. The effect of annual ring pattern is assumed to be reflected by the use of the characterised value G_{RT} , according to Section 3.6.1.
- The width of the transverse boards was measured as 147 mm but modelled with a width of 150 mm as a simplification. Furthermore only uncut boards were assumed in the transverse layers as a simplification.
- The overhang of all beams is modelled but the effect not studied explicitly.

3.3 Abaqus

There are several different commercial softwares available on the market today that utilise the FE-method. In this project the software suite *Abaqus FEA* was used for pre-processing, analyzing and post-processing. The program consists of different software applications where the following were used in this project:

- Abaqus/CAE [17] A software application for modelling, assigning mechanical properties and meshing of elements (pre-processing). It also includes a visualising tool after the analysis have been performed where pertinent parameters can be highlighted graphically (post-processing).
- Abaqus/Standard [18] A FE-analyzer that utilises implicit integration to solve equation systems. Suitable for e.g. static problems.

A characteristic feature of Abaqus is that units are not specified explicitly. Typically, unit conventions are used in order to specify input parameters and receive output parameters of correct measure. Dimensions in this project were modelled in millimeters, whereas the stiffness properties were specified in MPa resulting in the output parameter of e.g. the equivalent stiffness k being calculated in N/mm.

The Abaqus/CAE kernel is *Python* based. Every action performed in the graphical user interface (GUI) generates a Python code that is sent directly to the kernel. These code segments are stored in a *.rpy*-file for each active session of Abaqus. By copying pertinent segments from the *.rpy*-file and assembling them into a script, macros can be created in order to automatize certain functions. This has been utilised effectively throughout the FE-analysis of this project.

3.4 Representative beam models

3.4.1 2D models

The beams exerted to out-of-plane loading were modelled as two-dimensional (2D). Based on the fact that the width of the beam is relatively small in comparison to the length of the beam, and that deformation in the out-of-plane direction is not prevented, plane stress was assumed for all constituent elements. Thus, the 2D-model represent the stress distribution as homogeneous throughout the entire width of the (3D) beam, which should be a reasonable assumption. A illustration of the FE-model (corresponding to point 4 in the list below) is shown in Figure 3.1.

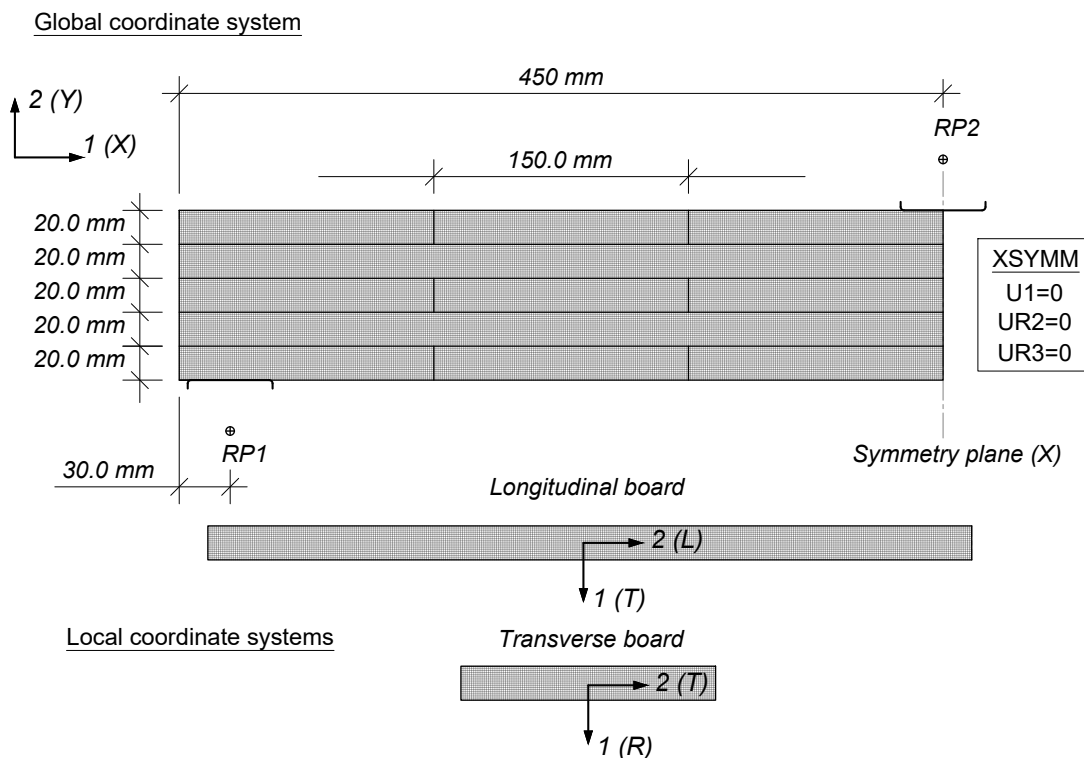


Figure 3.1: Schematic illustration of the 2D representative beam model.

The boundary conditions shown in Figure 3.1 apply to all the 2D-beam models, whereas the span, length and layer composition of the beams vary. When modelling the beams, symmetry was utilised along the X -axis, meaning that only half the beams were modelled. Thus, the degrees of freedom (dofs) along the symmetry plane were prevented to move in the X -direction ($u_X = 0$), see Figure 3.1. The beams were modelled in accordance with the tested beam specimen in the out-of-plane direction and corresponded to four different models:

1. Beam with a length of 750 mm (with respect to symmetry in the X -direction). The distance between the centre point of the support and the outer edge is 250 mm. This corresponds to the 1500 mm beams with a span of 1000 mm tested for out-of-plane loading.

2. Beam with a length of 750 mm (with respect to symmetry in the X -direction). The distance between the centre point of the support and the outer edge is 50 mm. This corresponds to the 1500 mm beams with a span of 1400 mm tested for out-of-plane loading.
3. Beam with a length of 450 mm (with respect to symmetry in the X -direction). The distance between the centre point of the support and the outer edge is 150 mm. This corresponds to the 900 mm beams with a span of 600 mm tested for out-of-plane loading.
4. Beam with a length of 450 mm (with respect to symmetry in the X -direction). The distance between the centre point of the support and the outer edge is 30 mm. This corresponds to the 900 mm beams with a span of 840 mm tested for out-of-plane loading.

The longitudinal and transverse boards were defined as two individual parts, where a local Cartesian coordinate system was created for both parts. Both local coordinate systems were oriented in the same way, however, the axes were defined for different *material directions*, as can be seen in Figure 3.1. The MoE and shear modulus parallel to grain and rolling shear modulus were variables determined from the experimental tests, whereas other variables were kept constant. The stiffness properties used are shown in Table 3.1 for the longitudinal and transverse boards, respectively.

Table 3.1: Mechanical properties used for the longitudinal and transverse boards, where $G_{LT} = G_{LR}$. A fixed value signifies a permanent value, whereas "var." represents a varying property.

Longitudinal boards		Transverse boards	
$E_1 = E_T$ [MPa]	800	$E_1 = E_R$ [MPa]	800
$E_2 = E_L$ [MPa]	var.	$E_2 = E_T$ [MPa]	500
$\nu_{12} = \nu_{LT}$	0.02	$\nu_{12} = \nu_{RT}$	0.3
$G_{12} = G_{LT}$ [MPa]	var.	$G_{12} = G_{RT}$ [MPa]	var.
$G_{13} = G_{RT}$ [MPa]	var.	$G_{13} = G_{LT}$ [MPa]	var.
$G_{23} = G_{LR}$ [MPa]	var.	$G_{23} = G_{LR}$ [MPa]	var.

The element type used are called *shell elements* or more specifically "CPS4 - four node bilinear plane stress quadrilateral" according to Abaqus naming convention [19, 20]. This means that it is a four node isoparametric element with linear variation for the shape functions in both the X - and Y -direction. The out-of-plane thickness is specified as 100 mm. Furthermore, full integration is applied in order to avoid "*hour-glass modes*". Hour-glass modes are also called *spurious zero-energy modes* and can occur when reduced integration is used for isoparametric elements. The phenomena is derived from the fact that internal strain of the element can not be represented by the *gauss points (integration points)* of the reduced integration and thus no elastic energy is created by these modes. Therefore, these modes tend to disturb the FE-model as the elements provide no resistance at all towards the zero energy modes [16]. *Constraints* between the longitudinal and transverse boards were modelled as *ties*, meaning that there is no relative motion between the connected dofs along the contact surface [21]. The surface of the longitudinal boards were always taken as *master surface*.

The supports were modelled as analytical rigid surfaces [22] (see Figures 3.1 and 3.2) and were connected to a reference point governing the surface motion of the analytical rigid surfaces. The dimensions of these corresponded to that of the steel plates used in the experimental tests, with a width of 50 mm. The corners were modelled with a *fillet* in order to avoid stress concentrations. The reference point was modelled at a distance of 30 mm from the analytical rigid, serving as the centre of rotation (CoR), corresponding to the CoR of the support used in the laboratory. Furthermore, translation in the Y -direction was prevented ($u_Y = 0$) in the reference point. Consequently the analytical rigid surface is also prevented translate Y -direction. However, it was still free to rotate around the CoR and translate in the X -direction, theoretically simulating a roller support. For the tests both a fix ($u_X = u_Y = 0$) and roller ($u_Y = 0$) support were used, but preventing translation in the X -direction resulted in non realistic tensile stresses between the analytical rigids of the support and load application.

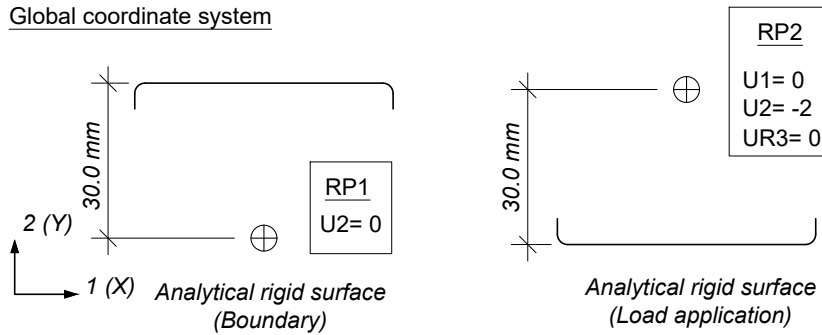


Figure 3.2: Boundary conditions and dimensions for the analytical rigids that apply to all the 2D beam models.

The load application surface was also modelled as an analytical rigid surface, and geometrically modelled the same way as the supports (see Figures 3.1 and 3.2), but rotated 180°. However, only half of the load application surface was in contact with the opposite boards, whereas the other half was protruding the symmetry plane. Utilising symmetry in this manner, as opposed to modelling a full beam (analogous to the symmetry beam), could result in small discrepancies in the results between the two models due to the difference in the surface area between the frictional constraints. This difference, however, was deemed negligible and was not further investigated.

The reference point connected to the analytical rigid (load application surface) was prevented to translate in the X -direction ($u_X = 0$) as well as rotate around the Z -axis ($\theta_Z = 0$) due to symmetry in the mid plane. The deformation in the reference point was specified as 2 mm in the Y -direction ($u_Y = -2$), governing the deformation of the entire beam. The deformation corresponded to a unit deformation multiplied by a factor two, with respect to symmetry in the X -direction. The resulting reaction force in the Y -direction was extracted from the reference point in the post-processing. Due to the aforementioned use of unit deformation the reaction force corresponded to the equivalent stiffness k (N/mm) for the beam model. It should be noted, that extracting the reaction force for a deformation of 1 mm and 2 mm, respectively, should result in a factor 2 between the results due to linear elastic conditions. However, very small discrepancies were found between the resulting reaction forces ($< 0.1\%$), which were

assumed to be a result of the non linear behaviour due to the frictional constraint of the analytical rigids. This difference was deemed negligible, and too small to affect the results.

The contact condition between the analytical rigids and the opposite boards were created where the *normal behaviour* was defined as *hard contact* [23], the out-of-plane geometry was specified for a width of 100 mm and the *tangential behaviour* was modelled as *penalty*, [24] with a friction coefficient of $\mu = 0.25$. The analytical rigid was chosen as master surface for the interaction, whereas *finite sliding* was specified for the constraint. This interaction between the analytical rigid and a deformable body gives rise to a complex non linear behaviour [25] which was not studied in this project. The friction coefficient is dependant on several different factors, e.g. value of applied pressure, angle of load to grain, moisture content and plate roughness [26], making it hard to establish a correct value. However, based on [26] choosing a value of μ within the interval of $0.2 \leq \mu \leq 0.3$ was deemed reasonable. The combination of the frictional constraint and the symmetry condition also prevented rigid body motion of the beam.

3.4.2 3D-models

The beams exerted to in-plane loading were modelled as three-dimensional (3D). This was done mainly due to the fact that stress distribution in the out-of-plane direction is not homogeneous due to the difference in mechanical properties between the transverse and longitudinal layers. The model is therefore a representative geometrical body of the complete beam used for the tests. A illustration of the FE-model (corresponding to point 3 in the list below) is shown in Figure 3.3.

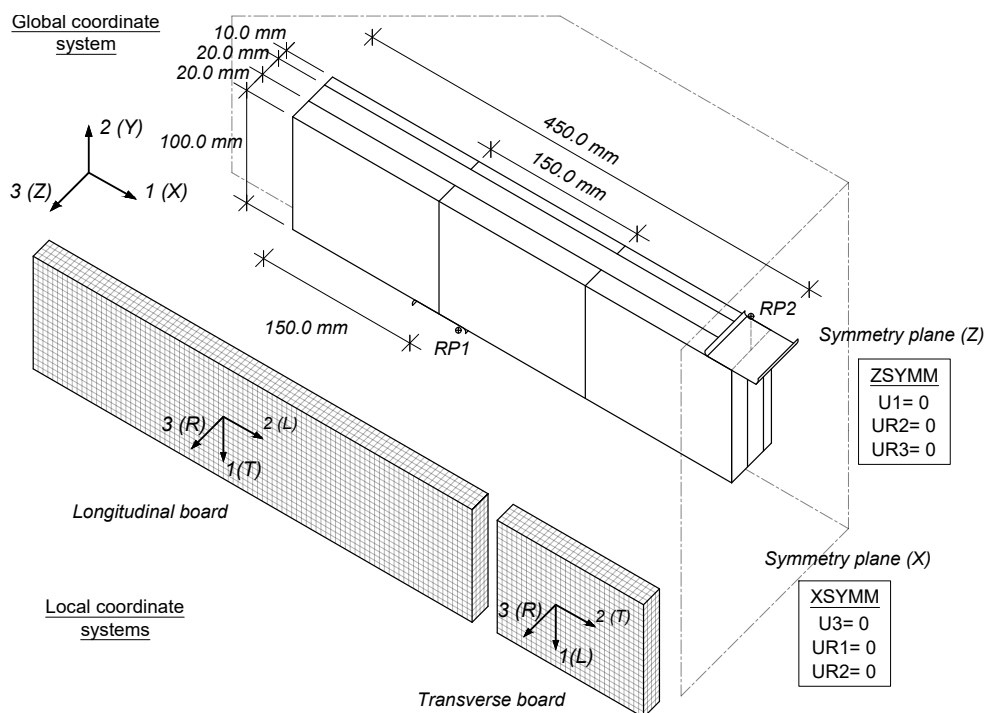


Figure 3.3: Schematic illustration of the 3D representative beam model.

The boundary conditions shown in Figure 3.3 apply to all the 3D-beam models, whereas the span, length and layer composition of the beam vary. When modelling the beams, symmetry was utilised along both the X -axis and the Y -axis meaning that a quarter of the beams were modelled. *Encastre* was used to model the symmetry on the symmetry planes. The dofs on the XZ -symmetry plane were prevented to move in the X -direction ($u_X = 0$) and rotate around the Y - and Z -axis ($\theta_Y = \theta_Z = 0$). The dofs on the YZ -symmetry plane were prevented to move in the Z -direction ($u_Z = 0$) and rotate around the X - and Y -axis ($\theta_X = \theta_Y = 0$). The beams were modelled in accordance with the tested beam specimen in the in-plane direction and corresponded to four different models:

1. Beam with a length of 750 mm and a width of 50 mm (with respect to symmetry in the X - and Z -direction, respectively). The distance between the centre point of the support and the outer edge is 250 mm. This corresponds to the 1500 mm beams with a span of 1000 mm tested for in-plane loading.
2. Beam with a length of 750 mm and a width of 50 mm (with respect to symmetry in the X - and Z -direction, respectively). The distance between the centre point of the support and the outer edge is 50 mm. This corresponds to the 1500 mm beams with a span of 1400 mm tested for in-plane loading.
3. Beam with a length of 450 mm and a width of 50 mm (with respect to symmetry in the X - and Z -direction, respectively). The distance between the centre point of the support and the outer edge is 150 mm. This corresponds to the 900 mm beams with a span of 600 mm tested for in-plane loading.
4. Beam with a length of 450 mm and a width of 50 mm (with respect to symmetry in the X - and Z -direction, respectively). The distance between the centre point of the support and the outer edge is 30 mm. This corresponds to the 900 mm beams with a span of 840 mm tested for in-plane loading.

The longitudinal and transverse boards were defined as two individual parts, where a local Cartesian coordinate system was created for both parts. Both local coordinate systems were oriented in the same way, however, the axes were defined for different *material directions*, as can be seen in Figure 3.3. The MoE and shear modulus parallel to grain and rolling shear modulus were variables determined from the experimental tests, whereas other variables were kept constant. The mechanical properties used are shown in Table 3.2 for the longitudinal and transverse boards, respectively.

The element type used are called *solid elements* or more specifically "C3D8 - eight node brick element", according to Abaqus naming convention [27]. This means that it is a eight node isoparametric solid element with linear variation for the shape function in the X -, Y - and Z -directions. Full integration is applied similarly to Section 3.4.1, where in this case eight integration points are used. This element type is more resource intensive compared to shell elements, which motivated the use of two symmetry planes instead of just one.

The constraints between the longitudinal and transverse boards were modelled in accordance to Section 3.4.1.

Table 3.2: Mechanical properties used for the longitudinal and transverse boards, where $G_{LT} = G_{LR}$. A fixed value signifies a permanent value, whereas "var." represents a varying property.

Longitudinal boards		Transverse boards	
$E_1 = E_T$ [MPa]	500	$E_1 = E_L$ [MPa]	var.
$E_2 = E_L$ [MPa]	var.	$E_2 = E_T$ [MPa]	500
$E_3 = E_R$ [MPa]	800	$E_3 = E_R$ [MPa]	800
$\nu_{12} = \nu_{LT}$	0.02	$\nu_{12} = \nu_{LT}$	0.02
$\nu_{13} = \nu_{RT}$	0.3	$\nu_{13} = \nu_{LR}$	0.02
$\nu_{23} = \nu_{LR}$	0.02	$\nu_{23} = \nu_{RT}$	0.3
$G_{12} = G_{LT}$ [MPa]	var.	$G_{12} = G_{LT}$ [MPa]	var.
$G_{13} = G_{RT}$ [MPa]	var.	$G_{13} = G_{LR}$ [MPa]	var.
$G_{23} = G_{LR}$ [MPa]	var.	$G_{23} = G_{RT}$ [MPa]	var.

The supports were modelled as analytical rigid shells (see Figures 3.3 and 3.4 with a width of 50 mm, as described in Section 3.4.1. The analytical rigids were also modelled with a width in the Z -direction of 50 mm, corresponding to half the total width of the beam. The corners were modelled with a fillet in order to avoid stress concentrations. A connection was made to a reference point, offset 30 mm from the geometrical centre point of the analytical rigid. In order to simulate a roller support and account for the symmetry in the Z -direction, only movement in the X -direction and rotation around the Z -axis were allowed ($u_Y = u_Z = 0$ and $\theta_X = \theta_Y = 0$).

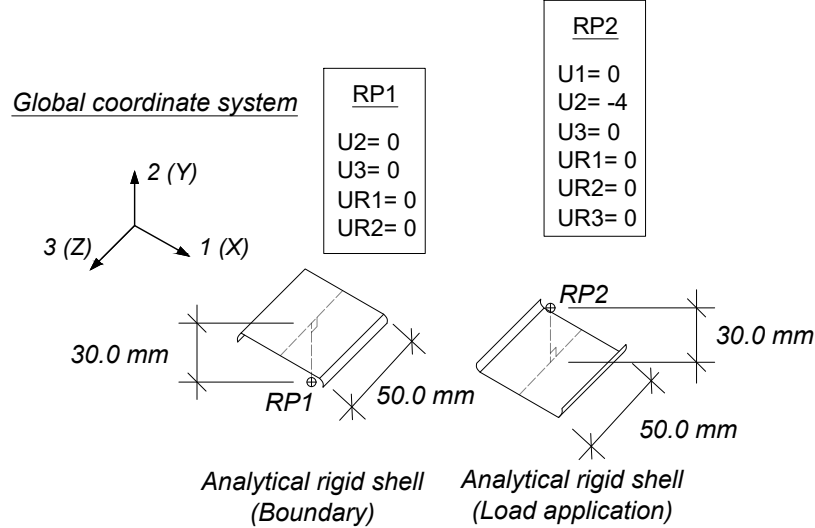


Figure 3.4: Boundary conditions and dimensions for the analytical rigids that apply to all the 3D beam models.

The load application surface was also modelled as an analytical rigid shell, geometrically modelled the same way as the supports (see Figures 3.3 and 3.4, but rotated 180° corresponding to the description in Section 3.4.1.

The reference point connected to the analytical rigid (load application surface) was prevented to rotate around all axes, and only allowed to move in the Y -direction ($u_X = u_Z = 0$ and $\theta_X = \theta_Y = \theta_Z = 0$), due to symmetry in both the longitudinal

and transverse mid plane of the beam. The deformation in the reference point was specified as 4 mm in the Y -direction ($u_Y = -4$), governing the deformation of the entire beam. In similarity to Section 3.4.1, a unit deformation was specified and then multiplied by a factor four, with respect to symmetries around the X - and Z -planes. Thus, the reaction force corresponded to the equivalent beam stiffness k (N/mm) for the beam model.

The contact condition between the analytical rigids and the opposite boards were created in similarity to Section 3.4.1, with the exception of the out-of-plane geometry not being specified.

3.5 Convergence study

In order to examine the sensitivity of the FE-models towards the size of the finite element mesh the equivalent stiffness k was calculated for four different beam models of varying mesh density. In order to include the size of the FE-model as a parameter in the study, two beam lengths were examined for the 2D and 3D models, respectively. The models included in the convergence study were:

1. 2D model. Beam with a length of 450 mm. The distance between the centre point of the support and the outer edge is 150 mm. This corresponds to the 900 mm beams with a span of 600 mm tested for out-of-plane loading.
2. 2D model. Beam with a length of 750 mm. The distance between the centre point of the support and the outer edge is 50 mm. This corresponds to the 1500 mm beams with a span of 1400 mm tested for out-of-plane loading.
3. 3D model. Beam with a length of 450 mm and a width of 50 mm. The distance between the centre point of the support and the outer edge is 150 mm. This corresponds to the 900 mm beams with a span of 600 mm tested for in-plane loading.
4. 3D model. Beam with a length of 750 mm and a width of 50 mm. The distance between the centre point of the support and the outer edge is 50 mm. This corresponds to the 1500 mm beams with a span of 1400 mm tested for in-plane loading.

The element size was chosen so that only rectilinear quadrilateral or cubic elements would be generated. A starting value of 10 mm for the element side length was chosen, whereas this value was then halved for each subsequent test. Analyses were carried out until the limit of 250000 nodes due to the restriction of the Abaqus teaching licence was exceeded. Due to the significant amount of FE-analyses conducted in this project, the efficiency of each model was also studied by including the computational time.

What is deemed sufficient convergence in a project usually depends on the problem at hand and the purpose of the FE-analysis. In this project, the intention of the numerical models is to verify the analytical models used to calculate certain stiffness properties. The accuracy of the models were thought to improve if any deviation due to mesh density could be eliminated. However, considering the significant amount of FE-models and analyses that were conducted, sufficient convergence was assumed when a finer mesh resulted in small deviations of k , and the computational time was heavily affected. The result of the convergence analysis can be seen in Figures 3.5 and 3.6 for the 2D models, and Figures 3.7 and 3.8 for the 3D models.

The models corresponding to the shorter beams seemed more sensitive to the mesh density. This can be seen clearly for the 2D models, as k converges towards a certain value for the model corresponding to Figure 3.6, but not for the model corresponding to Figure 3.5. This could be due to the fact that the relative size between the mesh-element and model is greater for the short beams in comparison to the long beams.

Generally, for models exerted to static loading the stiffness decreases for a greater mesh density. This is due to the fact that more dofs are introduced in the model, thus making it more "flexible". This is the case for the longer beams. However, for the shorter beams, the stiffness is increasing with a greater mesh density, see Figures 3.5 and 3.7. This discrepancy is thought to be a result of the nonlinear behaviour between the analytical rigids and boards, however it was not examined further in this project.

It can be seen in Figure 3.7 that even though symmetry across two planes were used for the 3D models, they quickly become quite cumbersome. For a model with a mesh containing elements with a size of 2.5 mm it takes almost two hours to complete the analysis. However, the absolute difference between the resulting stiffness k of using elements with a size of 5 mm as opposed to 2.5 mm proved less than 10 N/mm, and the relative difference less than 0.2 %. Therefore, an element size of 5 mm was used for the 3D models representing the short beams. As the models representing short beams proved more sensitive to mesh density, an element size of 5 mm was also used for the 3D models representing the long beams.

An element size of 2.5 mm were used for the 2D models representing the longer beams as a finer mesh resulted in a absolute difference of k less than 0.1 N/mm. Referring to Figure 3.5 the absolute difference of k with respect to using a mesh with an element size of 1.25 mm as opposed to 0.625 mm proved less than 4 N/mm, and the relative difference less than 0.2 %. Taking this into consideration, together with the 450 % increase of the computational time for the corresponding mesh refinement, the element size of 1.25 mm was deemed more efficient and was used for the 2D models representing the shorter beams.

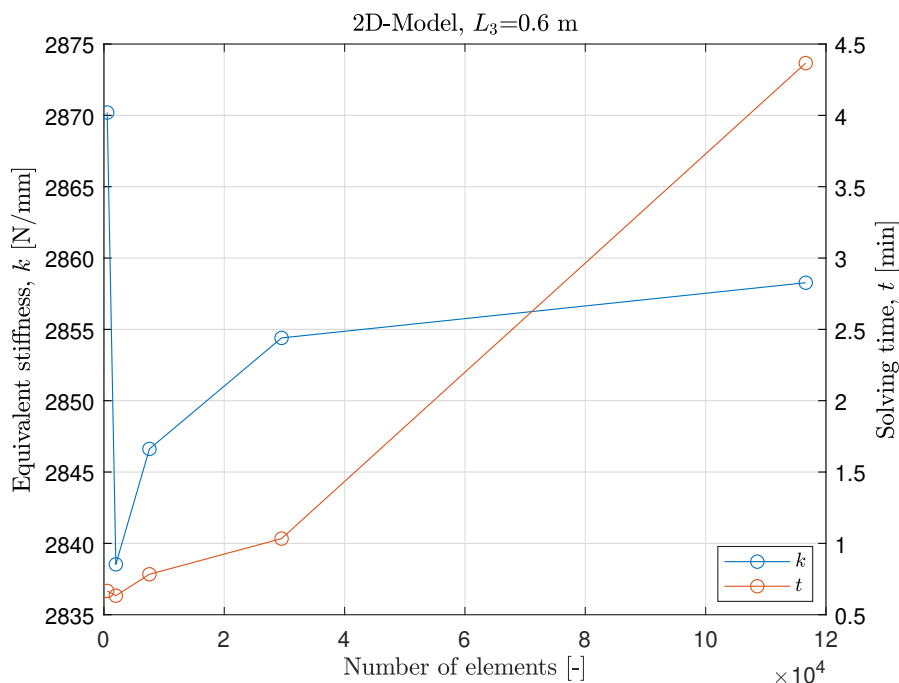


Figure 3.5: Five tests were performed corresponding to an element size of 10 mm, 5 mm, 2.5 mm, 1.25 mm and 0.625 mm from left to right.

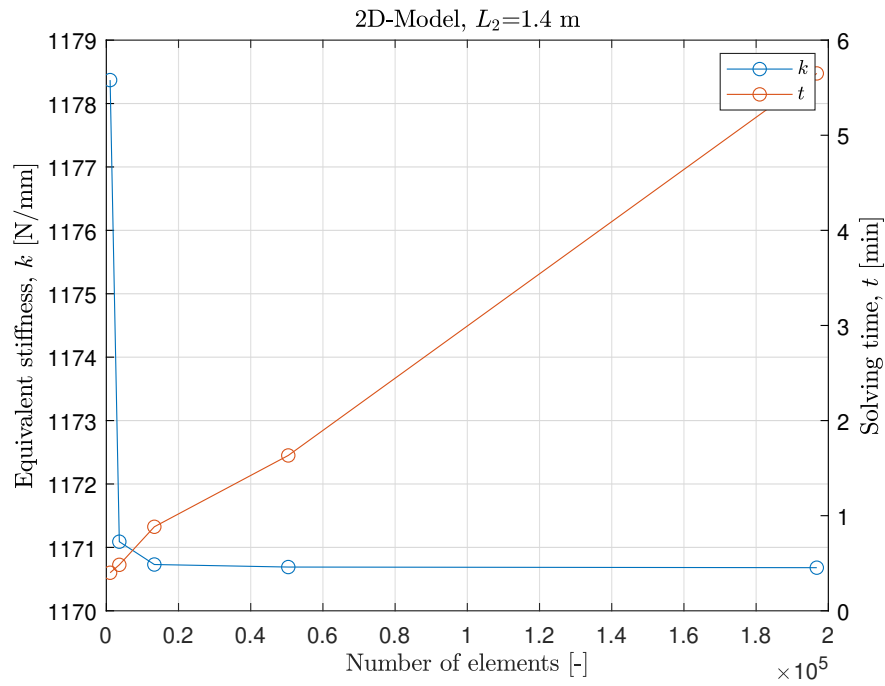


Figure 3.6: Five tests were performed corresponding to an element size of 10 mm, 5 mm, 2.5 mm, 1.25 mm and 0.625 mm from left to right.

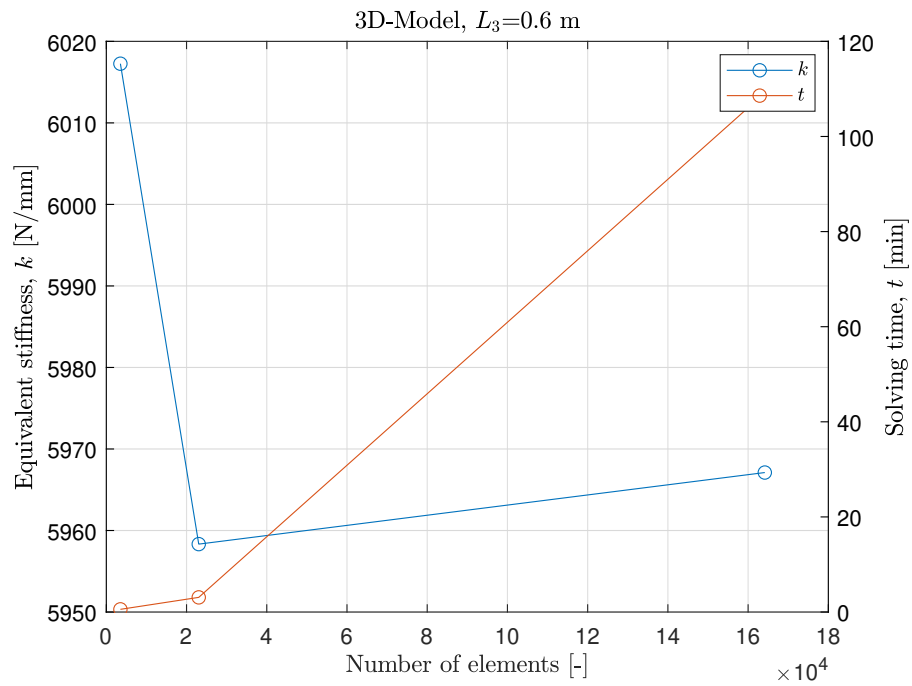


Figure 3.7: Three tests were performed corresponding to an element size of 10 mm, 5 mm and 2.5 mm from left to right.

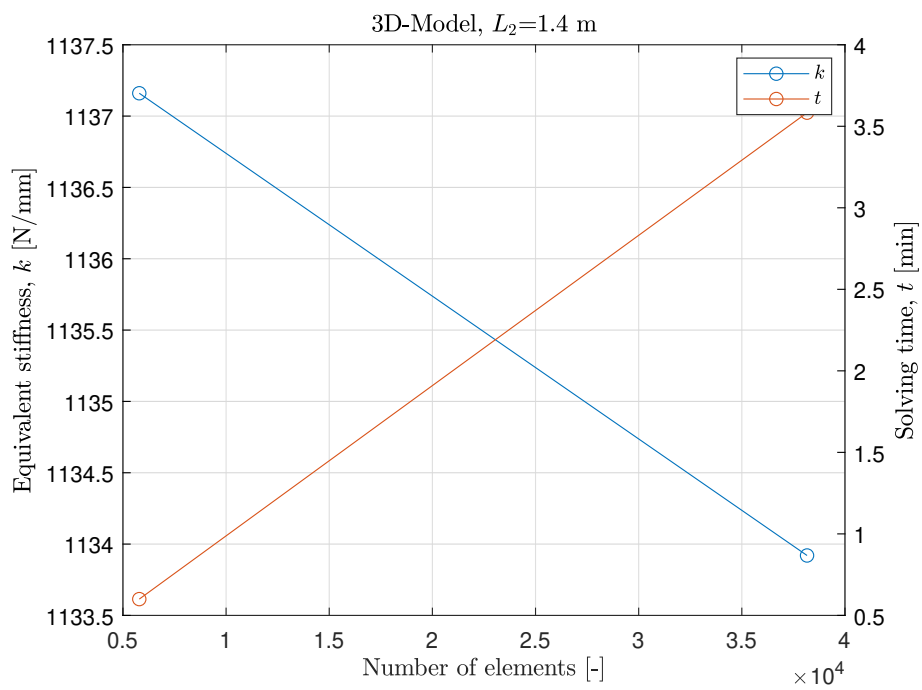


Figure 3.8: Two tests were performed corresponding to an element size of 10 mm and 5 mm from left to right.

3.6 Preliminary finite element analysis

3.6.1 Simple shear model

It has been previously mentioned in Chapter 2 that the rolling shear modulus has a significant impact on the stiffness of CLT, when out-of-plane loading is considered. Based on Section 2.4.2 the rolling shear modulus is not an intrinsic material property, but rather an apparent property, governed by the geometry, principal direction stiffnesses and annual ring orientation. This section investigates the effect of the annual ring orientation on the apparent rolling shear modulus $G_{R,app}$.

The setup was based on idealized conditions of a transverse board when the CLT is exposed to bending. The board is modelled in Abaqus where the CPS4 - four node bilinear plane stress quadrilateral elements are used (the same elements used for the analyses presented in Section 3.4.1).

The board is exposed to simple shear as shown in Figure 3.9. The board is completely fixed ($u_x = u_y = 0$) along the lower edge, whereas a unit deformation ($\Delta u_x = 1$) was applied along the complete length of the upper edge. This, in turn, resulted in a resultant shear force F along the upper edge. It should be noted that the boundary conditions used differ from a real bending situation, but are deemed to provide a valid representation of the basic influences that were considered.

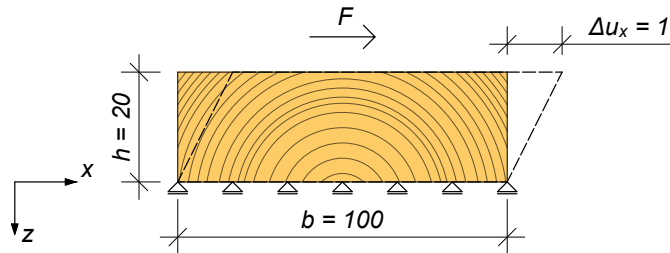


Figure 3.9: Simplified model for determining apparent rolling shear modulus, measurements in mm.

An apparent shear modulus $G_{R,app}$ was calculated according to

$$G_{R,app} = \frac{\tau}{\gamma} = \frac{Fh}{b\Delta u_x} \quad (3.1)$$

where

- τ is the shear stress along the upper surface of the board, whereas $\tau = F/A$.
- A is the top area of the board, calculated as $A = bt$.
- t is the out-of-plane thickness (in this case the shear force was calculated per mm thickness), here $t = 1$ mm.
- γ is the shear strain of the board, calculated as $\gamma = \Delta u_x/h$.

The geometry and the principal direction stiffness coefficients were kept constant, in order to only regard the annual ring orientation. The stiffness properties in this study were set to: $E_R = 600$ MPa, $E_T = 700$ MPa, $G_{RT} = 50$ MPa, resulting in a ratio of $E_R:E_T:G_{RT} = 1:1.16:0.083$, and $\nu_{TR} = 0.4$. The local orthotropic coordinate system was represented by a cylindrical coordinate system, originating from the pith. The global Cartesian coordinate system was set to the bottom edge of the board. Thus, the individual material coordinate systems were aligned according to Figure 3.10.

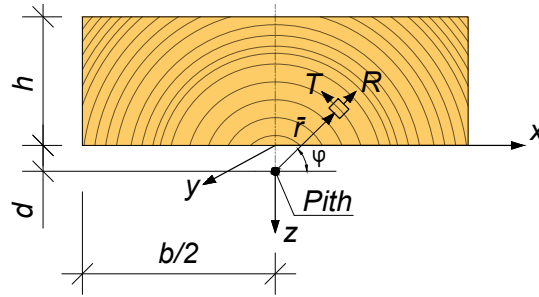


Figure 3.10: Definition of global Cartesian coordinate system and local cylindrical coordinate system.

A parametric study was conducted where the distance from the global coordinate system to the pith was increased by increments of 2 mm in the upwards direction (negative z -direction), whereas the apparent shear modulus was calculated according to Equation 3.1 for each pith position. The results were normalized in relation to a reference value of 50 MPa [3] and is shown in Figure 3.11.

In Figure 3.11 it can be seen that the board configurations containing the pith ($0 \leq d \leq 20$ mm) have a lower apparent rolling shear modulus compared to configurations where the pith is relatively close ($d \leq 84$ mm). The maximum value of $G_{R,app}$ is almost 3 times greater than the prescribed value of the material stiffness G_{RT} . The idealized board configuration with horizontal annual ring orientation converges with the prescribed rolling shear modulus of 50 MPa.

Based on the results above, a viable alternative to including the annual ring orientation in 2D FE-models by use of a cylindrical coordinate system, is to instead model the transverse layers with a Cartesian coordinate system and homogeneous orientation of the material principal directions. A higher value of G_{RT} in the model would then correspond to an increase in pith distance (up to a certain point).

Furthermore, based on Figure 3.11 the value of the apparent rolling shear modulus is likely to be in the range of $1.4G_{RT} \leq G_{R,app} \leq 2.8G_{RT}$ for realistic pith configurations. It should be noted that this range is derived from idealised boundary conditions, a perfectly cylindrical annual ring orientation, and a board with a width of 100 mm. The specimen tested in this project had a width of 150 mm. Taking these facts into consideration, the aforementioned range should serve more as an indication that the characterised rolling shear moduli (by means of analytical models) should be higher than the principal direction rolling shear modulus G_{RT} .

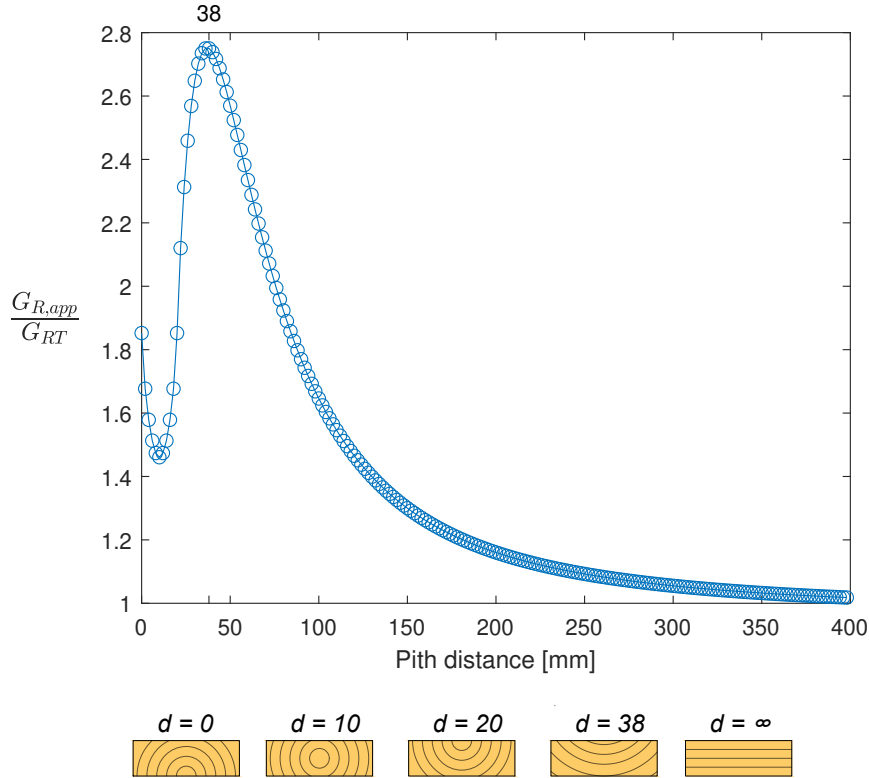


Figure 3.11: Influence of annual ring orientation on apparent rolling shear stiffness $G_{R,app}$ of a transverse board. Five of the analyzed sawing patterns are illustrated for clarity where $d = \infty$ represents a board with horizontal annual rings.

3.6.2 Shear stress distribution

Based on Section 2.4.3, the shear stress distribution in the transverse layers were assumed as zero for in-plane loading considered (see Figure 2.4). This assumption was based on the assumption of no bending stresses being present in these layers. As a consequence, the stiffness contribution of these layers should be neglected and only the area of the longitudinal layers A_{net} should be considered when calculating the shear stiffness. This section investigates the shear stress distribution by means of representative 3D-models corresponding to two of the tested Specimen. The purpose is to analyse how well the assumed shear stress distribution of a one-dimensional beam model corresponds to the shear stress distribution of a three-dimensional FE-model.

The analysis was based on the hypothesis that the shear stress distribution in the longitudinal direction τ_{LT} (corresponding to τ_{12} for the global directions defined in Figure 3.12) would vary mainly depending on the layup and span of the beam. Therefore, in order to highlight these parameters in the analysis, the 3D-models corresponding to point 2 (with a span of 600 mm) and point 3 (with a span of 1400 mm) in Section 3.4.2 were tested. Note that the layup of these beams were partly different, as shown in Figure 3.12. Boundary conditions according to Figure 3.3 and 3.4 apply for both models.

The shear stress distribution τ_{LT} in the models was analysed by defining a set of *paths* throughout the beam. Data pairs, in terms of τ_{LT} and the corresponding nodal co-

ordinate in the path direction, was then extracted from all nodes along the path. The paths were specified by defining the end points corresponding to the global coordinate system in which the elements were assembled. Three paths (1–3) were defined throughout the entire length of the beam in the X -direction, as shown in Figure 3.12. These paths were located in the middle of each constituent layer in the transverse directions of the beam (both in the Y - and Z -directions). Two additional paths (4–5) were defined throughout the width of the model in the Z -direction. Path 4 was defined along the middle of a joint between two adjacent transverse boards, and Path 5 was defined as a cut-through the mid section of the most central transverse board in the X -direction. The coordinates used to define the paths are shown in Table 3.3.

Table 3.3: Path coordinates for the long beam (Specimen 1) and the short beam (Specimen 2).

	Specimen 1		Specimen 2	
	Start	End	Start	End
Path 1	(-600, 50, 10)	(150, 50, 10)	(-600, 50, 30)	(-150, 50, 30)
Path 2	(-600, 50, -10)	(150, 50, -10)	(-600, 50, 10)	(-150, 50, 10)
Path 3	(-600, 50, -30)	(150, 50, -30)	(-600, 50, -10)	(-150, 50, -10)
Path 4	(-150, 50, 20)	(-150, 50, -30)	(-300, 50, 40)	(-300, 50, -10)
Path 5	(-225, 50, 20)	(-225, 50, -30)	(-375, 50, 40)	(-375, 50, -10)

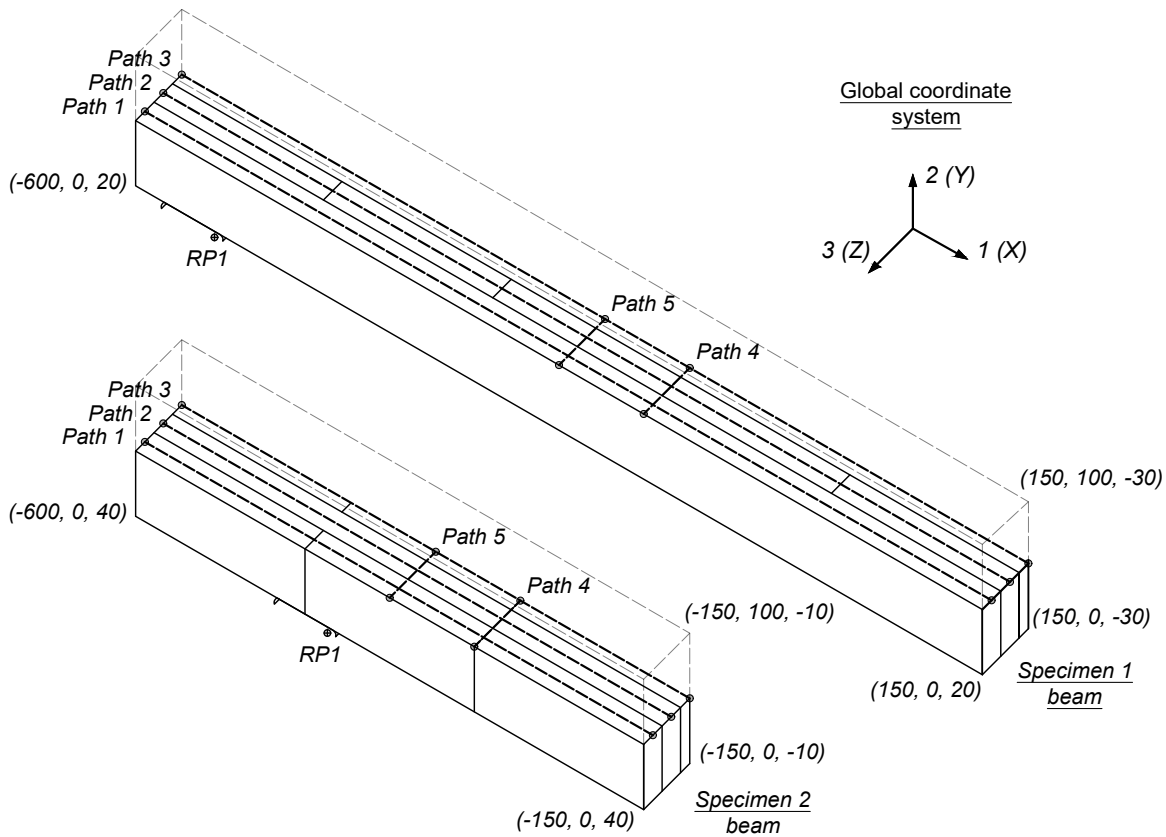


Figure 3.12: Path definitions and global coordinates for the corner points of the beam models.

Figures 3.13 and 3.14 show the stress distribution for the Specimen 1 beams, and Figures 3.15 and 3.16 for the Specimen 2 beams. The mechanical properties used in the analysis are equal to those of Table 3.2, and where $E_L = 15622$ MPa, $G_{LT} = G_{LR} = 261$ MPa and $G_{RT} = 79$ MPa were used for the Specimen 1 beams. Accordingly, $E_L = 9968$ MPa, $G_{LT} = G_{LR} = 279$ MPa and $G_{RT} = 134$ MPa were used for the Specimen 2 beams. The shear moduli presented above represent the values calculated analytically with Timoshenko theory, according to Equations 4.12 and 4.14. For the shear moduli parallel to grain, the gross area A_{gross} was used in the Equation 4.12. Furthermore, the values correspond to those of beam 1, and beam 4 presented later in Chapter 5.

As a comparison, the shear stresses were calculated according to BE-theory with respect to a rectangular cross section. The max shear stresses occur in the middle of the cross section and considering the gross area A_{gross} and gross moment of inertia $I_{x,gross,z}$ the expression takes the following form

$$\tau_{XY} = \frac{3}{2} \frac{V_Y}{A_{gross}} \quad (3.2)$$

where

V_Y is the shear force, calculated with respect to the symmetry planes in the X - and Z -directions as $4F/2$, where F is the reaction force calculated in the reference point.

A_{gross} is the gross area, 0.01 m^2 for the Specimen 1 and 2 beam, respectively.

The reaction force F was calculated as 1134 N for the Specimen 1 beam, and 5187 N for the Specimen 2 beam. According to Equation 3.2 this results in a shear stress τ_{XY} of 0.34 MPa and 1.56 MPa for the Specimen 1 and Specimen 2 beam, respectively.

It can be seen from Figures 3.14 and 3.16 that the area beneath the curves of the shear stresses corresponding to BE-theory and Path 5 are seemingly equal, indicating that the total shear flow is the same in the mid section, and that the gross area is a good representation of the shear stress distribution in the middle of the transverse boards. Considering Path 4 in Figures 3.14 and 3.16, the shear stresses assume different values at certain coordinates. Furthermore, the shear stresses should equal to zero in the transverse layer ($0 \leq Z \leq 40$) and the gradients between the points could be misleading at the intersections as these are connected linearly. These discrepancies are a result of the coarse mesh in combination with the extrapolation and approximation of the stresses in the integration points [28, 29].

Analysing Figures 3.13 and 3.15 a transfer of shear stresses between the longitudinal and transverse layers can be seen, where the edge-gap between the transverse boards are located. This is a consequence of shear stresses not able to transfer between non-edge glued boards, and results in the spikes seen in the graphs, where these are more distinct for the longitudinal layers encased between two transverse layers. By looking at Figures 3.14 and 3.16 it can be seen that the shear stress distribution in the mid section of the transverse layer analysed is rather homogeneous. A comparison

between the shear stresses of the mid section of the transverse and longitudinal layers (i.e. $Z = 10$ mm, $Z = 30$ mm and $Z = 50$ mm) in Figures 3.14 and 3.16 were made for for path 5. In both cases the shear stresses in the longitudinal layer compared to the transverse layer did not exceed 40 %.

Based on the results of this chapter, compared to the assumption made in Section 2.4.3 (where it is assumed that no shear stresses are transferred in the transverse layers for in-plane loading), it is more likely that a upper bound value of the area, closer to A_{gross} would produce better results than using A_{net} .

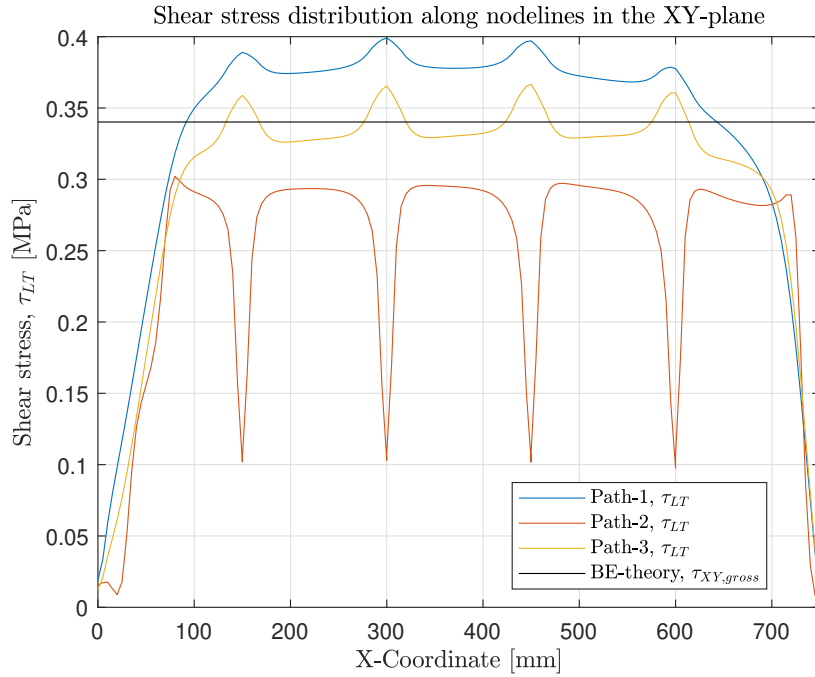


Figure 3.13: Path definitions and global coordinates for the corner points of the Specimen 1 beam model. The X -coordinates for the centre points of the support and load application are 50 mm and 750 mm, respectively.

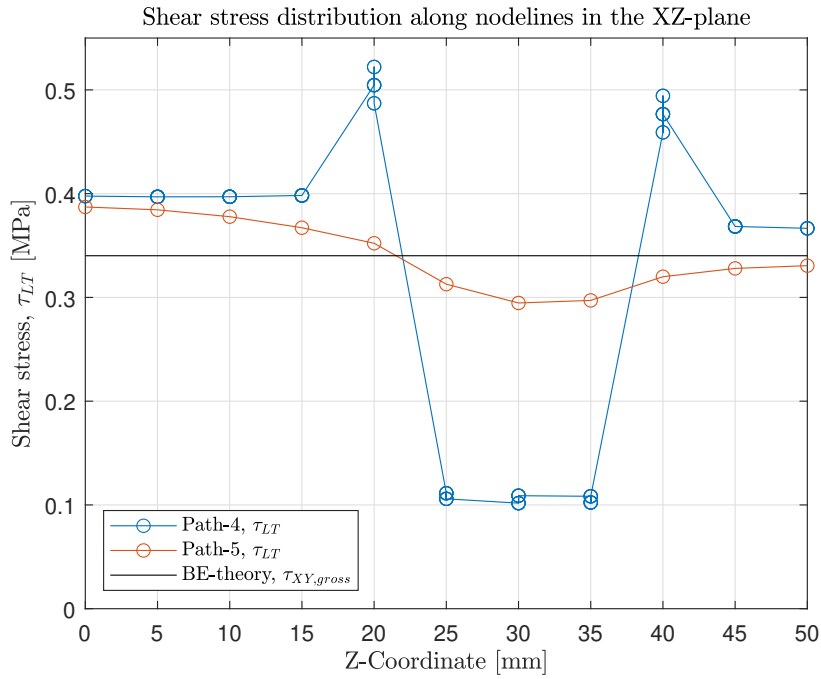


Figure 3.14: Path definitions and global coordinates for the corner points of Specimen 1 beam model. The longitudinal boards are located within the ranges of $Z = 0\text{--}20$ mm and $Z = 40\text{--}50$ mm. The transverse boards are located within the range of $Z = 20\text{--}40$ mm.

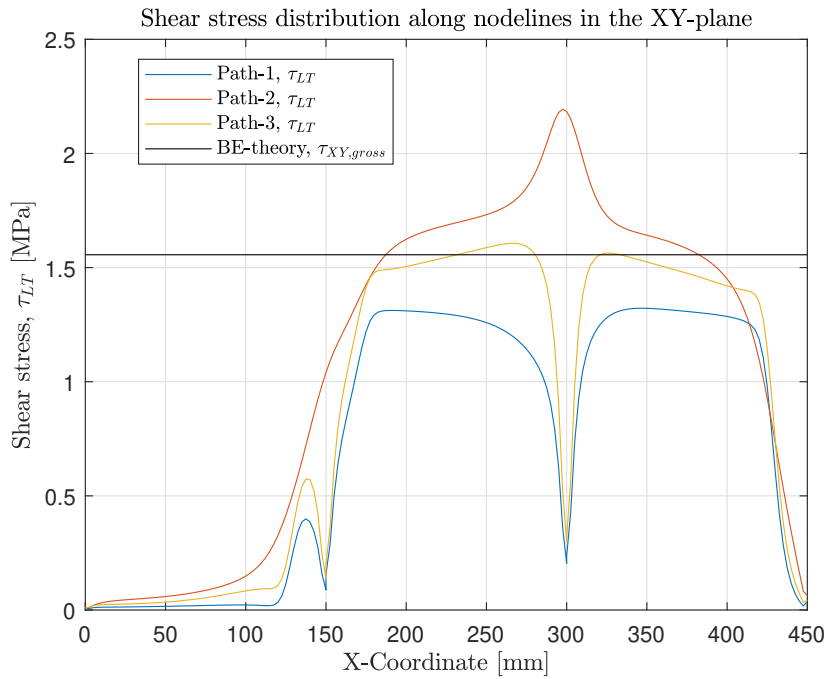


Figure 3.15: Path definitions and global coordinates for the corner points of Specimen 2 beam model. The X -coordinates for the centre points of the support and load application are 150 mm and 450 mm, respectively.

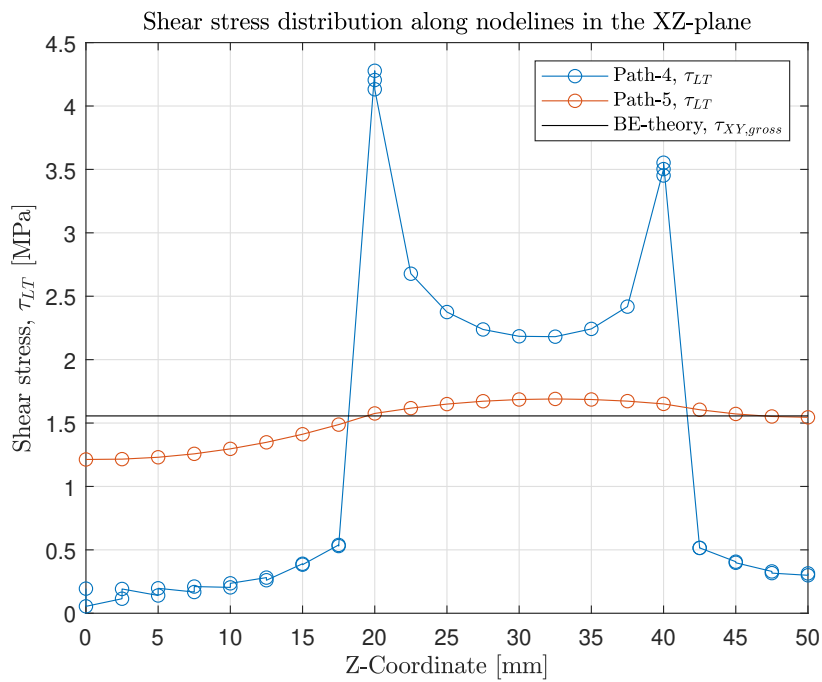


Figure 3.16: Path definitions and global coordinates for the corner points of Specimen 2 beam model. The longitudinal boards are located within the range of $Z = 20\text{--}40$ mm. The transverse boards are located within the ranges of $Z = 0\text{--}20$ mm and $Z = 40\text{--}50$ mm

4 Testing and evaluation methods

4.1 Specimen preparation

A 5-layer symmetrical CLT plate was used for the beam cut-outs. The constituent boards of the plate were 20 mm thick and approximately 146–147 mm wide. The total thickness of the plate was 100 mm. The material was provided by a Swedish manufacturer, Södra [30] and originated from cut-outs for door openings. The wood was produced from Norway spruce and the boards were of quality C24. In production Polyurethane was used for face gluing and no structural edge gluing was performed. There were also no edge gaps between the boards. Boards containing finger joints were used, and can be assumed to be present in each beam, respectively.

Nine prismatic beam specimen with a square cross section of $100 \times 100 \text{ mm}^2$ were cut out from the CLT, see Figure 4.1. The beams were cut in two directions with regard to the outermost boards: in the direction of the boards and perpendicular to the boards. Thus, the cut out beams had the outermost boards oriented in the longitudinal direction of the beam (denoted Specimen 1) or in the transverse direction of the beam (denoted Specimen 2). Specimen 1 was cut to a length of 1500 mm and Specimen 2 was cut to a length of 900 mm. Cutting was done centrally in regards to the longitudinal boards, resulting in only one board being present in the longitudinal layers of the beam. As the beams were somewhat shorter in length than the original length and width of the CLT plate, the outermost transverse layers of the beams were asymmetrical in the regard that they were of different width. This was mainly affecting the Specimen 2 beams.

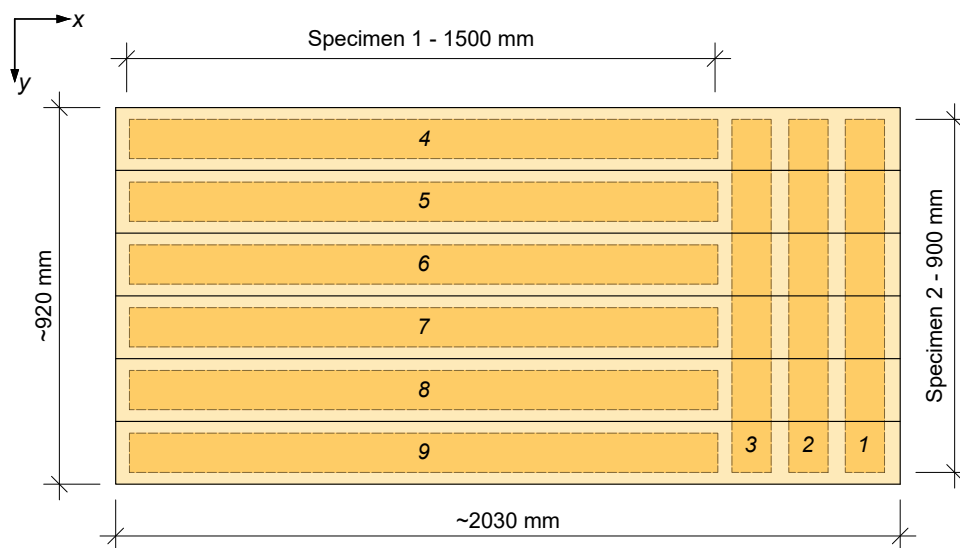


Figure 4.1: CLT plate and cut-out pattern of the beams.

Before the tests, each beam was also measured to control the that the length, width

and height coincided with the prescribed dimensions. The weight was measured in order to calculate the density. The moisture content (MC) was measured with a *testo-606-2* moisture meter in six different locations of each beam. Three times on the side of the beam in one of the middle longitudinal layers: in the middle and 5 cm from each end. Three times on the top of the beam, if the top layer consists of a longitudinal board: in the middle and 5 cm from each end. The moisture meter could only measure the MC in the interval of 8.8 % to 54.8 % in relation to the dry weight (0 % MC) of the wood. As the beams were initially very dry from acclimatizing too fast, containing drying cracks both in the longitudinal and transverse boards, a subjective grading of the cracks was created in order to note possible deviations due to severe cracks. The grading is as follows:

1. A few cracks in the transverse and longitudinal layers. No cracks exceed 1 mm in width.
2. A few cracks in the transverse and longitudinal layers. Some cracks exceed 1 mm in width.
3. Many cracks in the transverse and longitudinal layers. Many cracks exceed 1 mm in width.

The result of the measurements are presented in Tables 4.1 and 4.2.

Table 4.1: Geometric measurements (including weight and density) for each beam.

Beam	Length [m]	Weight [g]	Cross section, b×h [m]	Density [kg/m ³]
1	0.901	3980.0	100×99	446
2	0.900	4474.8	100×99	502
3	0.901	4414.2	100×99	495
4	1.500	7386.7	100×99	497
5	1.500	7731.7	100×99	521
6	1.500	7269.2	100×100	485
7	1.500	6992.5	100×100	466
8	1.499	7164.4	99×99	488
9	1.499	6589.2	99×99	448

Table 4.2: Moisture content and subjective grading of drying for each beam.

Beam	Mean moisture content [%]	Grade [-]
1	<8.8	3
2	<8.8	3
3	<8.8	3
4	<8.8	2
5	<8.8	3
6	<8.8	1
7	<8.8	1
8	<8.8	3
9	<8.8	2

4.2 Equipment

The tests were carried out using a "MTS 810 servo-hydraulic testing machine" [31] under displacement control (in resemblance to what was done in a similar project [32]). A pre-fabricated loading rig, consisting of an I-beam welded to a clamping plate was mounted on the MTS machine. The boundaries and the beam were then mounted on top of the I-beam. Steel plates of size $50 \times 100 \text{ mm}^2$ were placed at the supports and loading point to reduce local indentations. The test setup is shown schematically in Figure 4.2, and pictures from experimental tests can be seen in Appendix B.

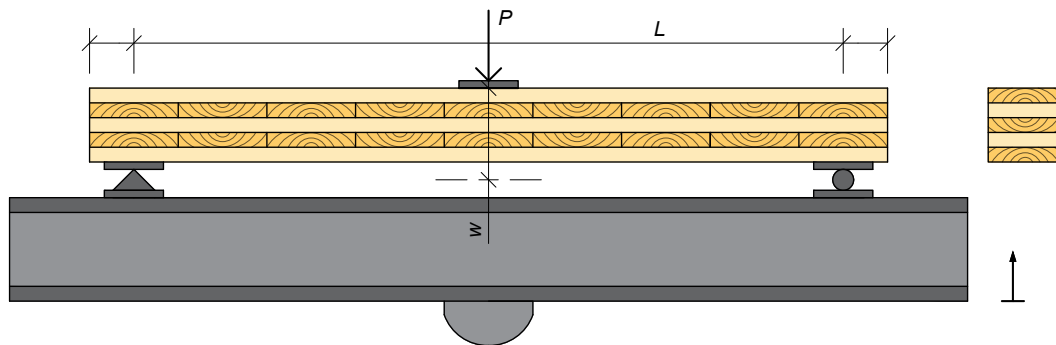


Figure 4.2: Schematic illustration of the test setup.

The bottom piston governs the translation of the I-beam in the upwards direction, whereas the relative deformation w of the beam is measured in the linear variable differential transformer (LVDT) of the bottom piston. The beams were loaded to an extent where the maximum bending or shear stress in any point of the beam did not exceed approximately 40 % of the expected capacity, according to Table 2.1. The load was applied through a steel cylinder, assuming a line load over the width of the beam. The loading rate was adjusted accordingly in order to reach the maximum load value after a period of 3–5 minutes. However, due to the high variance of mechanical properties of the beams, the maximum load value in reality was reached after 3–12 minutes. The sampling rate used was 5 Hz and the cross-head speed varied between 0.004–0.010 mm/s including the first tests where the loading speed, span length and sensitivity of the tests were calibrated.

The test parameters relating to maximum stress (or load) and loading rate were derived from specifications SS-EN 408 [14]. However, these specifications are stated for methods with different loading conditions and were used as reference but not strictly followed. Therefore, some discrepancies may occur within this project, e.g the stresses being slightly higher at some point of the cross section, or that the max load is reached after a time slightly exceeding the specifications for some tests. The following specifications are stated in [14]:

- The maximum load applied shall not exceed $0.4 P_{max}$ of the capacity.
- Load P shall be applied at a constant rate of loading-head movement so adjusted that the load P_{max} is reached within $(300 \pm 120) \text{ s}$.

4.3 Specimen setups

Each beam was tested with two different spans, denoted as setups, where the supports were adjusted symmetrically around the centre of the beam in the longitudinal direction. Furthermore, each beam were tested for both in-plane loading and out-of-plane loading. Thus, each specimen was tested two times for each setup, i.e. four times in total. For the nine beam specimen that were cut out, a total of 36 tests were performed, excluding any tests that were done for calibration purposes. The setups for each specimen, respectively, are shown in Figures 4.4 and 4.5, where both the local coordinate system for the beam (X, Y), and the global coordinate system for the plate is illustrated (x, y) as well.

The following naming pattern were used to quantify the measured data from the experiments, see Figure 4.3

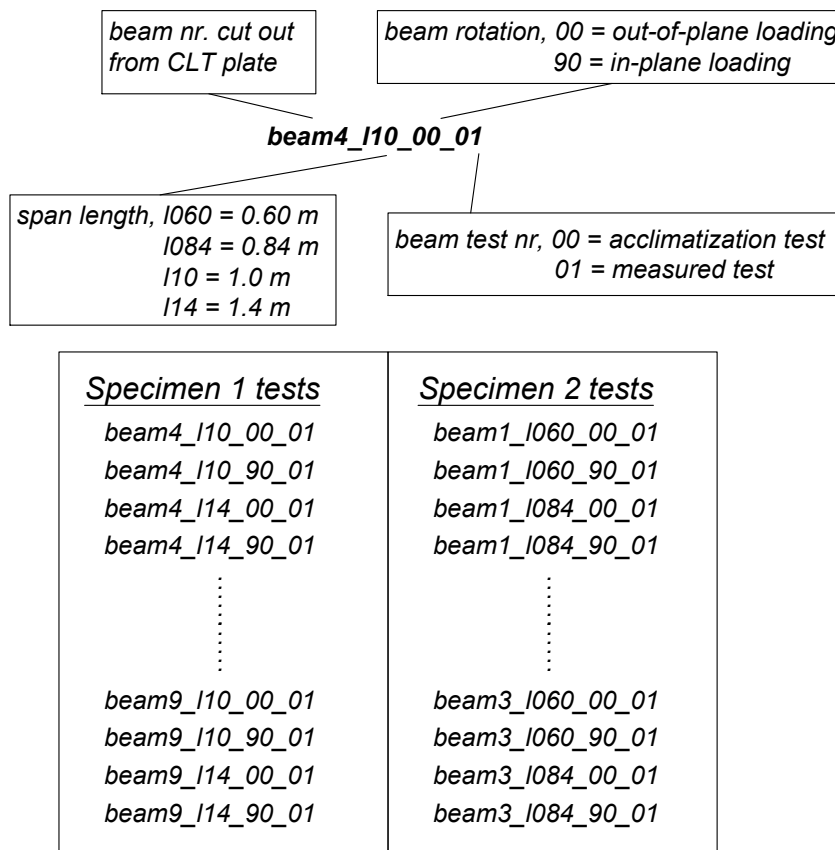


Figure 4.3: Naming pattern for quantifying experimental data. Note that the lists only show the measured data used. For every measured test, a calibration test was performed before.

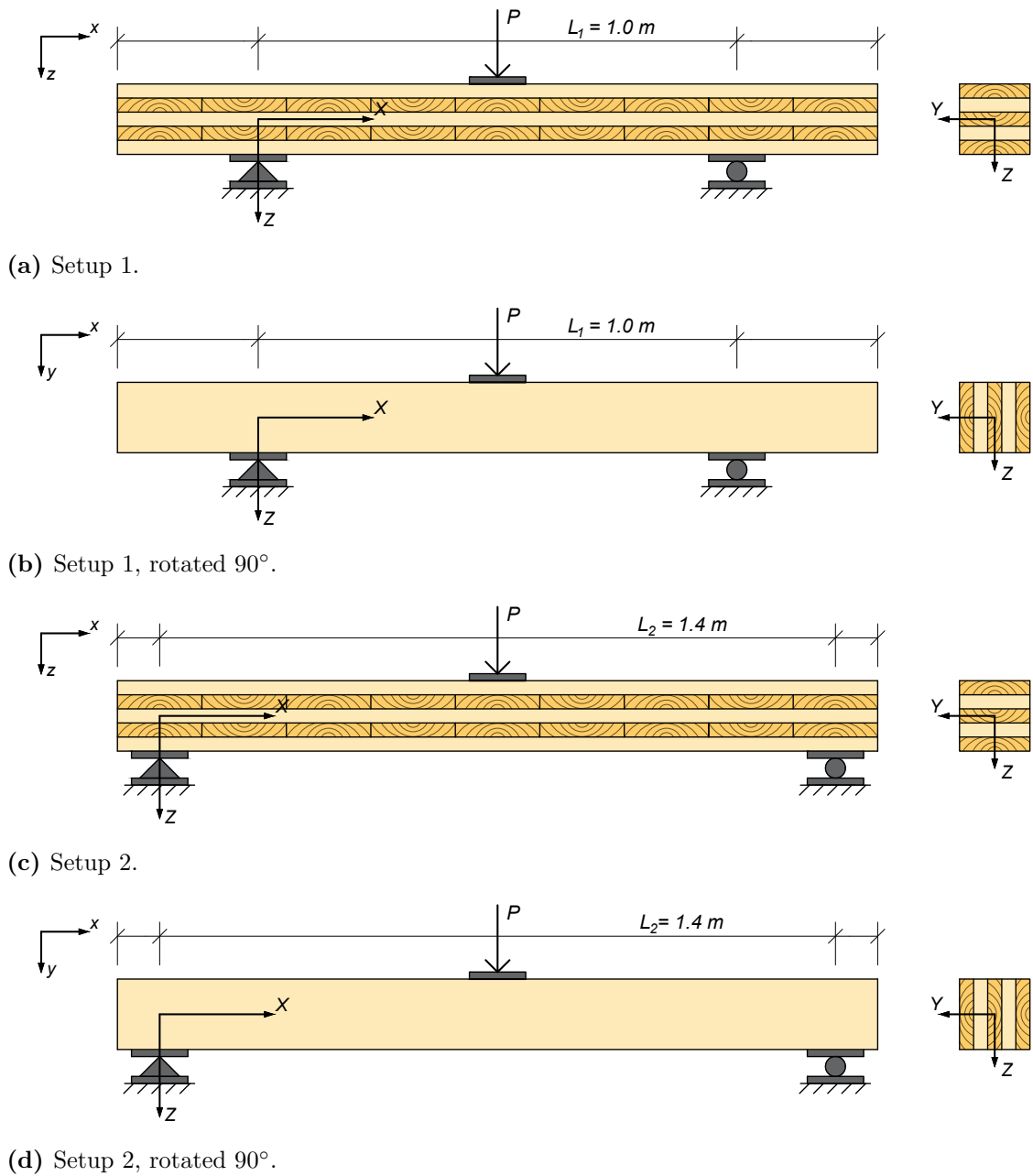
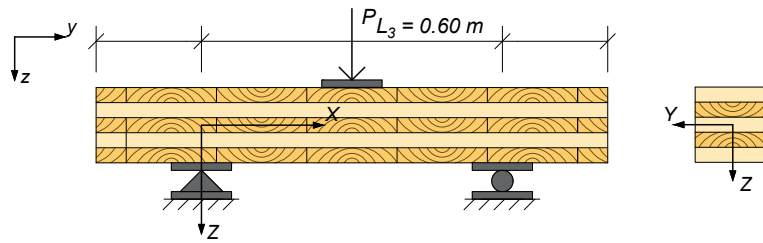
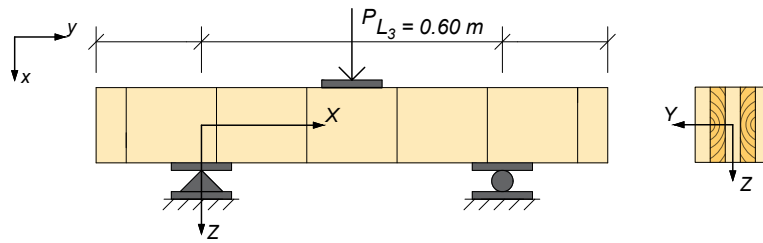


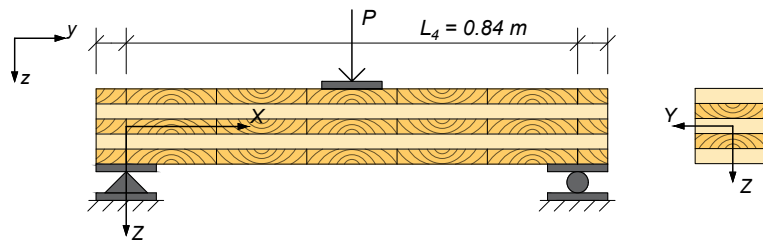
Figure 4.4: Setups for the Specimen 1 tests.



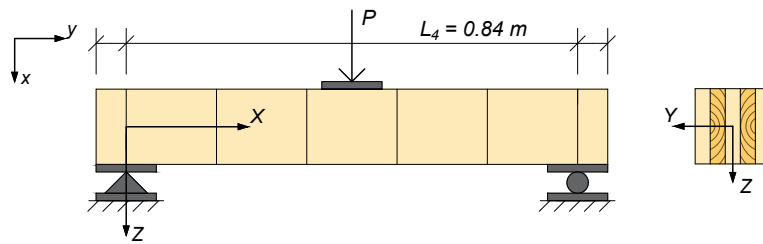
(a) Setup 3.



(b) Setup 3, rotated 90°.



(c) Setup 4.



(d) Setup 4, rotated 90°.

Figure 4.5: Setups for the Specimen 2 tests.

4.4 Evaluation methods

In order to characterise the stiffness properties of the CLT beams, the analytical expressions established in Sections 2.5.1 and 2.5.2 were applied. By reformulating Equations 2.24 and 2.25 with respect to the mid span of the beam ($X = L/2$), Equations 4.1 and 4.2 are obtained. Equation 4.1 signifies the mid span deformation according to the Gamma method

$$w(L/2) = \frac{P}{12 \cdot E_0 I_{x,ef}} \cdot \left(\frac{L}{2}\right)^3 - \frac{PL^2}{16 \cdot E_0 I_{x,net}} \cdot \frac{L}{2}$$

$$w = \frac{PL^3}{48 \cdot E_0 I_{x,ef}} \quad (4.1)$$

and Equation 4.2 signifies the mid span deformation according to Timoshenko theory

$$w(L/2) = \frac{P}{12 \cdot E_0 I_{x,net}} \left(\frac{L}{2}\right)^3 - \frac{P}{E_0 I_{x,net}} \left(\frac{L^2}{16} - \frac{\alpha}{2}\right) \cdot \frac{L}{2}$$

$$w = \frac{PL^3}{48 \cdot E_0 I_{x,net}} + \frac{PL\alpha}{4 \cdot E_0 I_{x,net}} \quad (4.2)$$

where

- $E = E_0$ is the MoE parallel to grain.
- $I_{x,net}$ is the net moment of inertia with respect to the global axes and load cases, as shown in Figure 2.5. It is calculated as $I_{x,net,z}$ when in-plane loading is considered, and as $I_{x,net,y}$ when out-of-plane loading is considered.

Considering the constituent stiffness properties that govern Equations 4.1 and 4.2, it can be seen that Equation 4.1 is governed by E_0 and G_R through $I_{x,ef}$. Equation 4.2 is governed by E_0 , G_0 for in-plane loading, and E_0 , G_0 and G_R for out-of-plane loading. As mentioned previously in Section 1.3, the approach was to first characterise E_0 and G_0 from in-plane bending tests, whereas Equation 4.2 was used. Consequently, Equation 4.2 was simplified by using Equation 2.32

$$w = \frac{PL^3}{48 \cdot E_0 I_{x,net,z}} + \frac{3 \cdot PL}{10 \cdot G_0 A} \quad (4.3)$$

where

- A is the assumed effective area of the cross section, given by either A_{net} or A_{gross} , according to Section 2.5.2.
- $\kappa = 5/6$ is the shear correction coefficient of a rectangular cross section.

SS-EN 408 [14] specifies that the MoE for a beam exerted to 4-point bending can be characterised from force-deformation data obtained experimentally, where the section

between $0.1P_{max} < P < 0.4P_{max}$ should be used. This methodology was adopted with discrepancies due to the different loading conditions in this project. For example, the interval was changed to $0.5P_{max} < P < P_{max}$ as the tested specimen in this project are only loaded to approximately 40 % of their characteristic strength in total. Using all the data points within this interval a linear regression was performed using *MATLAB* [33], and the built in function *fitlm* [34], see Appendix D. The resulting relation between load and deformation for the regression takes the following form

$$\bar{P} = \bar{w}k + q \quad (4.4)$$

where

$$\begin{aligned} \bar{P} & \text{ is the total applied load.} \\ \bar{w} & \text{ is the deflection.} \\ k = \frac{\Delta\bar{P}}{\Delta\bar{w}} & \text{ is the slope of regression line.} \\ q & \text{ is the intercept of regression line.} \end{aligned}$$

SS-EN 408 [14] also states that the coefficient of correlation r must be 0.99 or higher for the regression line, if the slope k is to be used to characterise the MoE. If this is not fulfilled, the regression has to be disregarded. The slope k can also be seen as the equivalent stiffness of the beam, with respect to linear elastic conditions. Reformulating Equation 4.3 with respect to k , and solving for either E_0 or G_0 results in four expressions for in-plane loading and Timoshenko theory considered

$$E_0 = \frac{10 \cdot G_0 AkL^3}{480 \cdot G_0 I_{x,net,z} A - 144 \cdot I_{x,net,z} kL} \quad (4.5)$$

$$G_0 = \frac{144 \cdot E_0 I_{x,net,z} kL}{480 \cdot E_0 I_{x,net,z} A - 10 \cdot AkL^3} \quad (4.6)$$

$$E_0 = \frac{kL^3}{48 \cdot I_{x,net,z}} + \frac{E_0 3 \cdot kL}{G_0 10 \cdot A} \quad (4.7)$$

$$G_0 = \frac{G_0}{E_0} \frac{kL^3}{48 \cdot I_{x,net,z}} + \frac{3 \cdot kL}{10 \cdot A} \quad (4.8)$$

Two methods of utilising Equations 4.5 and 4.6 to characterise E_0 and G_0 were considered. The simpler of the two methods is to assume a value of G_0 in Equation 4.5 and solve for E_0 , and correspondingly, assume a value of E_0 in Equation 4.6 and solve for G_0 . This method requires only one test, as the Equations are solved for one unknown parameter, respectively. However, the drawback of this method is that the characterised properties are sensitive to the assumptions. The other method is to establish equation systems based on the data of two individual tests, corresponding to testing two different span of the same beam with respect to in-plane loading. The equation systems were solved numerically with the built in *MATLAB* function *fzero* [35]. More specifically, the equation system with respect to Equation 4.5 would be used to characterise G_0 , and the equation system with respect to Equation 4.6 would

be used to characterise E_0 . The equation systems are presented later in Section 4.5 as Equations 4.11 and 4.12.

Equations 4.7 and 4.8 were solved by assuming a relation between E_0 and G_0 . Relations between the stiffness parameters can be found in literature and design codes. One example is derived from [36], where a relation between $E_0/G_0 = 16$ can be found for C24 timber, although it is not explicitly stated. This method suffer the same drawback of the first method described above, namely, that it is sensitive to the assumption of the ratio. Assuming the wrong ratio might result in non-realistic values of E_0 and G_0 .

In accordance to the procedure above for characterising E_0 and G_0 from data obtained from in-plane loading tests, similar expressions can also be formulated for characterising G_R from data obtained from out-of-plane loading tests. These expressions also include the equivalent stiffness k , uniquely determined for each tested span and beam, with respect to out-of-plane loading. Furthermore, these expressions are based on that the parameter E_0 (and G_0 when Timoshenko theory is utilised) have been previously characterised. As G_R is embedded in the parameters $I_{x,ef}$ in Equation 4.1, and κ in Equation 4.2, solving the equations for G_R in accordance to Equations 4.5–4.8 becomes quite cumbersome. However, by using *MATLAB* and *fzero* the equations for characterising G_R can be formulated differently. By reformulating Equations 4.1 and 4.2 with respect to k , two expressions for solving G_R are obtained. Equation 4.9 represents the Gamma method with respect to out-of-plane loading

$$\frac{kL^3}{48 \cdot EI_{x,ef}} - 1 = 0 \quad (4.9)$$

where

$I_{x,ef}$ is the effective moment of inertia calculated with Equation 2.16 for a 5-layer CLT-beam, or Equation 2.19 for a 3-layer CLT-beam.

Equation 4.10 represents Timoshenko theory with respect to out-of-plane loading

$$\frac{kL^3}{48 \cdot E_0 I_{x,net}} + \frac{kL\alpha}{4 \cdot E_0 I_{x,net}} - 1 = 0 \quad (4.10)$$

where

α is the ratio between the bending stiffness and effective shear stiffness, calculated with Equation 2.33 for a 5-layer CLT-beam, or Equation 2.34 for a 3-layer CLT-beam.

When characterising G_R according to Equation 4.10, κ can either be calculated with Equations 2.27–2.31, according to Section 2.5.2, or assume the approximated values according to Section 2.5.3. Use of Equations 4.9 and 4.10 is presented in Section 4.5 by Equations 4.13 and 4.14.

4.5 Preliminary testing

The alternative test method could be sensitive to loading speed, sampling frequency, boundary conditions, loading conditions, accuracy of measurements, beam inhomogeneities, stress distribution, local indentation and possibly other not mentioned parameters. All of these parameters could affect the *reliability*, i.e. to what extent the results can be reproduced when repeated under the same conditions, and the *validity*, i.e. how well the results measure what they are intended to measure. For a complete collection of the preliminary test results, as well as the corresponding load-deformation graphs, it is referred to Appendix A.

In order to test the reliability a beam specimen was chosen at random (beam number 5, according to Figure 2.4), whereas a number of tests both in-plane and out-of-plane were performed according to Figure 4.4, a) - d). The tests were conducted for span lengths of 1.0 m and 1.4 m, corresponding to a height to length ratio of 10:1 and 14:1, respectively. For the results of the preliminary tests, see Appendix A. Most of the tests were performed in a sequence, meaning that the beam was loaded, unloaded and then directly loaded again. For some of the tests considering a span of 1.4 m the sensitivity to measurements were also controlled for. This was done by remounting the beam in between each test. For these tests the beam was also rotated 180° as opposed to the previous setups. As can be seen from Table 4.3 the coefficient of variation is below 3 % for all tests, indicating a good reliability. Furthermore, by looking at the results of Table A.1 in Appendix A, a slight increase in the stiffness coefficient k can be noted after each subsequent test.

Table 4.3: Mean values, standard deviation and the coefficient of variation of the measured stiffness coefficients.

Beam5_	110.00_01-05	110.90_01-03	114.00_01-06	114.90_01-05
mean, k	2476	2851	1212	1193
std	49	66	16	18
cov	1.97 %	2.32 %	1.35 %	1.53 %

In order to test the validity of the different analytical methods, the data from the preliminary test was used in conjunction with the methods presented in Section 4.4. The purpose was to evaluate if the resulting stiffness properties are characterised within a reasonable interval, e.g. according to Table 2.2. Note that Table 2.2 was only used for reference as the presented stiffness properties are derived with respect to Norway spruce and clear wood. Considering Equations 4.5–4.8, these equations were based on assumptions being made for the different moduli or ratio. These assumptions are presented below, along with definitions of the different characterised moduli with respect to each method, respectively. Furthermore, the MoE was also calculated according to BE-theory, using Equation 4.1 with respect to $I_{x,net,z}$ instead of $I_{x,ef}$. This was used as a comparative lower-end reference value, as the characterised MoE by means of Timoshenko theory were expected to be of greater value.

The following definitions refer to Table 4.4 and concern the MoE and shear modulus parallel to grain (E_0 and G_0).

- $E_{0,1}$ was calculated with BE-theory, as mentioned previously.
- $E_{0,2}$ was calculated with Equation 4.5, where G_0 was assumed as 700 MPa according to Table 2.2.
- $E_{0,3}$ was calculated with Equation 4.7, where a ratio of $E_0/G_0 = 16$ was assumed according to Section 4.4.
- $G_{0,1}$ was calculated with Equation 4.6, where E_0 was assumed as 14000 MPa according to Table 2.2.
- $G_{0,2}$ was calculated with Equation 4.8, where a ratio of $G_0/E_0 = 1/16$ was assumed according to Section 4.4.

Table 4.4: Moduli of elasticity, and longitudinal shear moduli with respect to the data from the preliminary tests. Note that each value corresponds to one test, see Figure 4.3.

	P_{max} [N]	k [N/mm]	r [-]	q [N]	$E_{0,1}$ [MPa]	$E_{0,2}$ [MPa]	$E_{0,3}$ [MPa]	$G_{0,1}$ [MPa]	$G_{0,2}$ [MPa]
Beam5_110.90_01	4014	2776	0.999	-2171	11565	13127	12898	479	806
Beam5_110.90_02	4035	2875	0.999	-1887	11981	13665	13361	598	835
Beam5_110.90_03	4007	2901	0.999	-1930	12087	13803	13480	637	842
Beam5_114.90_01	2864	1167	0.999	-840	13345	14349	14129	1047	883
Beam5_114.90_02	2869	1204	0.999	-893	13761	14832	14570	2964	911
Beam5_114.90_03	2867	1216	0.999	-812	13899	14993	14716	7099	920
Beam5_114.90_04	2862	1187	0.999	-834	13575	14617	14373	1644	898
Beam5_114.90_05	2869	1191	1.000	-792	13622	14671	14423	1855	901

As can be seen from Table 4.4 seemingly reasonable values are obtained for all methods except for $G_{0,1}$, where the assumption of E_0 resulted in non-realistic results. By analysing Figures A.1 and A.2 in Appendix A a distinct shift in slope in the beginning of the curves can be noted. This is most likely mainly caused by a slight gap between the one end underlying steel plate and the cylindrical solid used to apply the load, as shown in Appendix B. The gap was measured as approximately 1 mm, which corresponds to the slope of Figures A.1 and A.2 in Appendix A. Furthermore, after the load is evenly applied, a slight shift in slope can be seen before the curves assumes a constant slope. This is probably caused by redistribution of stresses and irregularities. However, due to the interval chosen for the regression, the irregularities and imperfections did not seem to affect the equivalent stiffness k , and consequently the stiffness properties.

However, as previously mentioned the stiffness properties found in Table 4.4 are governed by assumptions. Every tested beam specimen will possess large varieties in material properties, which in turn will be reflected by the measured equivalent stiffness k . Based on the assumption made, the characterised stiffness properties would be more or less accurate depending on the tested beam specimen. Thus, utilising assumptions would require knowledge about the stiffness properties of the beam prior to testing it.

A more consistent method of characterising E_0 and G_0 is through equation systems, as described in Section 4.4. In order to test this method the mean value of k was calculated for each setup and orientation, see Table 4.3. Equations 4.5 and 4.6 were utilised in order to create the equation systems by determining E_0 and G_0 from a system of two equations based on two tests performed on the same beam, but using different span lengths (L_1 and L_2). Based on tested setups, see Figure 4.4 (b) and (d), the equation system took the following form

$$\frac{144 \cdot E_0 I_{x,net,z} k_1 L_1}{480 \cdot E_0 I_{x,net,z} A - 10 \cdot A k_1 L_1^3} - \frac{144 \cdot E_0 I_{x,net,z} k_2 L_2}{480 \cdot E_0 I_{x,net,z} A - 10 \cdot A k_2 L_2^3} = 0 \quad (4.11)$$

$$\frac{10 \cdot G_0 A k_1 L_1^3}{480 \cdot G_0 I_{x,net,z} A + 144 \cdot I_{x,net,z} k_1 L_1} - \frac{10 \cdot G_0 A k_2 L_2^3}{480 \cdot G_0 I_{x,net,z} A + 144 \cdot I_{x,net,z} k_2 L_2} = 0 \quad (4.12)$$

where

- k_1 is the mean equivalent stiffness of the setup 1 in-plane tests.
- k_2 is the mean equivalent stiffness of the setup 2 in-plane tests.
- L_1 is the span of the beam according to setup 1.
- L_2 is the span of the beam according to setup 2.
- A is the gross area, A_{gross} .

The resulting stiffness properties were characterised as $E_0 = 16760$ MPa and $G_0 = 294$ MPa, corresponding to a ratio of $E_0/G_0 = 57$. This method yielded a substantially higher MoE, and lower shear modulus parallel to grain, when compared to Table 4.4. Furthermore, these stiffness properties were used in conjunction with the mean values of k for the out-of-plane bending tests, with respect to the two tested span (see Table 4.3). The rolling shear modulus G_R was calculated for with the Gamma method according to Equation 4.9

$$\frac{k_j L_j^3}{48 \cdot E I_{x,ef}} - 1 = 0 \quad (4.13)$$

and with Timoshenko theory according to Equation 4.10

$$\frac{k_j L_j^3}{48 \cdot E_0 I_{x,net}} + \frac{k_j L_j \alpha}{4 \cdot E_0 I_{x,net}} - 1 = 0 \quad (4.14)$$

where

- j denotes the considered setup (span), with respect to out-of-plane loading.
- k_j is the (mean) equivalent stiffness of the considered tests for setup j .
- L_j is the span of beam for the considered setup j .

Using the Gamma method (Equation 4.13) resulted in the rolling shear moduli being characterised as $G_R = 54$ MPa for both span, $L_1 = 1.0$ m and $L_2 = 1.4$ m.

Using Timoshenko theory (Equation 4.14), where κ was calculated numerically, resulted in the rolling shear moduli being characterised as $G_R = 87$ MPa and $G_R = 84$ MPa for both span, $L_1 = 1.0$ m and $L_2 = 1.4$ m.

Using Timoshenko theory (Equation 4.14), where κ was approximated as 0.24 according to Section 2.5.3, resulted in the rolling shear moduli being characterised as $G_R = 768$ MPa and $G_R = 742$ MPa for both span, $L_1 = 1.0$ m MPa and $L_2 = 1.4$ m.

A high validity of the characterised stiffness properties using equation systems was indicated by the consistent yield of values within the ranges suggested by Table 2.2. It should however, be noted that the MoE parallel to grain resulting from the equation systems was slightly higher than expected, whereas the shear modulus parallel to grain was significantly lower than expected. The rolling shear moduli characterised by means of the Gamma method were slightly lower than expected. Considering Timoshenko theory, the method using the approximate value of κ was disregarded, as it resulted in non-realistic values of the rolling shear moduli. The most significant results were obtained from using Timoshenko theory, with respect to κ being calculated numerically. Realistic values of the rolling shear moduli were obtained, which based on the slightly higher values, also indicated that the annual ring pattern was taken into consideration.

In conclusion, the analytical approach using equation systems referring to Equations 4.11–4.14 was considered the most practical approach considering the consistency of the method. The analytical methods based on Equations 4.5–4.8 were disregarded and not further evaluated within this project, due to the inconsistency of the characterised moduli with respect to the assumptions made.

Lastly, conclusions were also made for the tested setup. The height to length ratio of 1:10 and 1:14, with respect to the Specimen 1 beams, was deemed appropriate for further tests. Correspondingly, this relation was also applied to the Specimen 2 beams. As the equivalent height of these beams are 60 mm (out-of-plane loading considered), the corresponding spans were chosen as $L_1 = 0.6$ m and $L_2 = 0.84$, respectively.

The loading speed, sampling frequency, boundary conditions and loading conditions used were also calibrated through the preliminary tests, whereas the final results have been previously described in Section 4.2. The same conditions were applied for both the Specimen 1 and 2 tests.

The size of the steel plates used to reduce local indentations were controlled for by calculating the local deformation for the beam with the greatest load. The local indentation was assumed to only occur in the outermost layer, with a thickness of 20 mm. This resulted in a maximum local deformation within the range of 10^{-5} m, which was deemed negligible.

In order to account for the slight increase of k after each consequent test, as can be seen in Appendix A, an "acclimatization test" where the beam is loaded to approximately 40 % of its capacity was performed prior to every measured test henceforth.

5 Results

5.1 Stiffness properties

The stiffness properties presented in this section are based of the analytical method using Equation systems 4.11–4.14, as described in Sections 4.4 and 4.5. The MoE in the longitudinal direction E_0 is obtained as a single value for each beam, respectively. The longitudinal shear moduli, $G_{0,net}$ and $G_{0,gross}$ depend on the cross-sectional area used in the analysis, whereas the relation between the two moduli equals that of the corresponding two areas A_{net} and A_{gross} . For the Specimen 1 beams the relation is $A_{net}/A_{gross} = 0.6$ and for the Specimen 2 beams the relation is $A_{net}/A_{gross} = 0.4$. Consequently, using Timoshenko theory the rolling shear moduli will differ depending on what value of the longitudinal shear modulus is used in the equation system. Further, as Equation systems 4.13 and 4.14 are based on a single unknown parameter, G_R , one modulus can be calculated for each span of the tested beams. Therefore, the rolling shear moduli using Timoshenko theory are presented as $G_{R1,net}$ or $G_{R1,gross}$ for the short span beams, and $G_{R2,net}$ or $G_{R2,gross}$ for the long span beams. The rolling shear moduli calculated with the Gamma method is independent of G_0 . Therefore, only two rolling shear moduli, G_{R1} , and G_{R2} are presented for the two spans of each beam, respectively.

5.1.1 Specimen 1 beams

The results for the Specimen 1 beams, corresponding to the tested beams 4 – 9 (with a total length of 1.5 m) in terms of E_0 , $G_{0,net}$ and $G_{0,gross}$ are given in Table 5.1. The variables k_1 and k_2 signify the measured equivalent stiffness for $L_1 = 1.0$ m and $L_2 = 1.4$ m, respectively. Equations used for calculations are also given in the table.

The results in terms of G_{R1} , G_{R2} , $G_{R1,net}$, $G_{R2,net}$, $G_{R1,gross}$ and $G_{R2,gross}$ are given in Table 5.2, where the indices 1 and 2 correspond to a span of $L_1 = 1.0$ m and $L_2 = 1.4$ m, respectively. Equations used for calculations are also given in the table.

Studying the mean values of the stiffness parameters given in Table 5.1 and 5.2 shows that using $G_{0,gross}$ instead of $G_{0,net}$ corresponds to an increase of approximately 10 % for the resulting rolling shear moduli, whereas the longitudinal shear moduli decreases with 40 %, due to the 40 % difference in assumed effective area.

Table 5.1: Moduli of elasticity E_0 and longitudinal shear moduli G_0 for the Specimen 1 beams, calculated analytically with Timoshenko theory.

	k_1 [N/mm]	k_2 [N/mm]	E_0 [MPa] (4.11)	$G_{0,net}$ [MPa] (4.12)	$G_{0,gross}$ [MPa] (4.12)
Beam 4	2629	1120	15622	435	261
Beam 5	2910	1216	16419	556	334
Beam 6	2506	1018	13220	597	358
Beam 7	2280	927	12063	537	322
Beam 8	2623	1087	14497	533	320
Beam 9	2001	814	10599	469	282
mean	2490	1031	13737	521	313
std	314	144	2202	59	35
cov	12.62 %	13.94 %	16.03 %	11.31 %	11.31 %

Table 5.2: Rolling shear moduli G_R for the Specimen 1 beams, calculated analytically with the Gamma method or Timoshenko theory.

	k_1 [N/mm]	k_2 [N/mm]	Gamma method		Timoshenko theory (calculated with $G_{0,net}$ or $G_{0,gross}$)			
			G_{R1} [MPa] (4.13)	G_{R2} [MPa] (4.13)	$G_{R1,net}$ [MPa] (4.14)	$G_{R2,net}$ [MPa] (4.14)	$G_{R1,gross}$ [MPa] (4.14)	$G_{R2,gross}$ [MPa] (4.14)
Beam 4	2343	1127	52	50	76	71	85	79
Beam 5	2509	1212	57	56	81	78	89	85
Beam 6	2205	1025	55	52	77	71	83	77
Beam 7	2012	909	50	44	70	59	76	64
Beam 8	2293	1053	54	47	76	65	83	70
Beam 9	1883	844	51	45	72	63	79	69
mean	2208	1028	53	49	75	68	83	74
std	228	136	3	5	4	7	4	8
cov	10.33 %	13.20 %	4.87 %	9.24 %	5.07 %	10.00 %	5.34 %	10.72 %

5.1.2 Specimen 2 beams

The results for the Specimen 2 beams, corresponding to the tested beams 1 – 3 (with a total length of 0.9 m) in terms of E_0 , $G_{0,net}$ and $G_{0,gross}$ are given in Table 5.3. The variables k_1 and k_2 signify the measured equivalent stiffness for $L_3 = 0.6$ m and $L_4 = 0.84$ m, respectively. Equations used for calculations are also given in the table.

The results in terms of G_{R1} , G_{R2} , $G_{R1,net}$, $G_{R2,net}$, $G_{R1,gross}$ and $G_{R2,gross}$ are given in Table 5.4, where the indices 1 and 2 correspond to a span of $L_3 = 0.6$ m and $L_4 = 0.84$ m, respectively. Equations used for calculations are also given in the table.

Studying the mean values of the stiffness parameters given in Table 5.3 and 5.4 shows that using $G_{0,gross}$ instead of $G_{0,net}$ corresponds to an increase of approximately 24 % for the resulting rolling shear moduli, whereas the longitudinal shear moduli decreases with 60 %, due to the 60 % difference in assumed effective area.

Table 5.3: Moduli of elasticity E_0 and longitudinal shear moduli G_0 for the Specimen 2 beams, calculated analytically with Timoshenko theory.

	k_1 [N/mm]	k_2 [N/mm]	E_0 [MPa] (4.11)	$G_{0,net}$ [MPa] (4.12)	$G_{0,gross}$ [MPa] (4.12)
Beam 1	5001	2165	9968	697	279
Beam 2	6518	2954	14659	734	294
Beam 3	6295	3070	17559	549	220
mean	5938	2729	14062	660	264
std	819	493	3830	98	39
cov	13.80 %	18.05 %	27.24 %	14.84 %	14.84 %

Table 5.4: Rolling shear moduli G_R for the Specimen 2 beams, calculated analytically with the Gamma method and Timoshenko theory.

	k_1 [N/mm]	k_2 [N/mm]	Gamma method		Timoshenko theory (calculated with $G_{0,net}$ or $G_{0,gross}$)			
			G_{R1} [MPa] (4.13)	G_{R2} [MPa] (4.13)	$G_{R1,net}$ [MPa] (4.14)	$G_{R2,net}$ [MPa] (4.14)	$G_{R1,gross}$ [MPa] (4.14)	$G_{R2,gross}$ [MPa] (4.14)
Beam 1	2336	1066	20	52	108	114	134	144
Beam 2	2833	1356	-12	29	102	99	123	120
Beam 3	2828	1479	-40	15	88	95	111	122
mean	2666	1300	-11	32	99	103	123	128
std	286	212	30	19	10	10	12	13
cov	10.72 %	16.32 %	-	58.40 %	10.04%	9.74%	9.45 %	10.44 %

5.1.3 Summary

All of the stiffness properties calculated for beams 1–9 are presented in Table 5.5, together with non-weighted mean values of each property, respectively. Furthermore, a comparison between the clear wood properties, referring to Table 2.1 in Section 2.3, and the characterised properties is given in Table 5.6.

Table 5.5: Summary of stiffness properties presented in Sections 5.1.1 and 5.1.2.

	E_0 [MPa]	$G_{0,net}$ [MPa]	$G_{0,gross}$ [MPa]	G_{R1} [MPa]	G_{R2} [MPa]	$G_{R1,net}$ [MPa]	$G_{R2,net}$ [MPa]	$G_{R1,gross}$ [MPa]	$G_{R2,gross}$ [MPa]
Beam 1	9968	697	279	20	52	108	114	134	144
Beam 2	14659	734	294	-12	29	102	99	123	120
Beam 3	17559	549	220	-40	15	88	95	111	122
Beam 4	15622	435	261	52	50	76	71	85	79
Beam 5	16419	556	334	57	56	81	78	89	85
Beam 6	13220	597	358	55	52	77	71	83	77
Beam 7	12063	537	322	50	44	70	59	76	64
Beam 8	14497	533	320	54	47	76	65	83	70
Beam 9	10599	469	282	51	45	72	63	79	69
mean	13845	567	296	32	43	83	79	96	92
std	2445	91	40	33	12	13	18	20	27
cov	17.66 %	16.10 %	13.34 %	104.60 %	28.50 %	15.14 %	22.36 %	20.88 %	29.45 %

Table 5.6: Comparison between clear wood properties and corresponding characterised properties of CLT beams.

Clear wood prop. Norway spruce [7] [MPa]		Characterised stiffness prop. Specimen 1 Specimen 2 [MPa] [MPa]		
E_L	13500 – 16700	E_0	10599 – 16419	9968 – 17559
G_{LT}	500 – 850	$G_{0,net}$	435 – 597	549 – 734
		$G_{0,gross}$	261 – 358	220 – 294
G_{RT}	29 – 39	G_R	45 – 57	-40 – 52
		$G_{R,net}$	59 – 81	88 – 114
		$G_{R,gross}$	64 – 89	111 – 144

5.2 Finite element models

The results presented in the tables of this section are calculated with the FE-models described in Sections 3.4.1 and 3.4.2. For every beam tested in laboratory, a combination of stiffness properties E_0 , G_0 and G_R have been presented according to the Gamma method or Timoshenko theory, see Table 5.5. These combinations of stiffness properties were used in the FE-models where the combinations depend on the load case, specimen type or span length. The load case is characterised by either out-of-plane loading, corresponding to the 2D-models, or in-plane loading, corresponding to the 3D-models. The specimen type is characterised by either the Specimen 1 beams (with a length of 0.9 m), or the Specimen 2 beams (with a length of 1.5 m). The span is either $L_1 = 1.0$ m or $L_2 = 1.4$ m for the Specimen 2 beams, or $L_3 = 0.6$ m or $L_4 = 0.84$ m for the Specimen 1 beams.

Tables depicting the varying stiffness properties used for each combination are presented, followed by tables presenting both the measured equivalent stiffness k_t as well as the calculated equivalent stiffness k_m from the FE-model. The ratio between k_m and k_t signify how well the stiffness properties derived by analytical models correspond to the total stiffness of the FE-models. The ratio can be used to analyse the validity of the calculated stiffness properties. Tables 3.1 and 3.2 from Sections 3.4.1 and 3.4.2 are shown below in order to illustrate the assumed constant and varying stiffness properties used for each model, respectively.

Table 5.7: Stiffness properties used for the longitudinal and transverse boards in the 2D-models, where $E_L = E_0$, $G_{LT} = G_{LR} = G_0$ and $G_{RT} = G_R$.

Longitudinal boards		Transverse boards	
$E_1 = E_T$ [MPa]	800	$E_1 = E_R$ [MPa]	800
$E_2 = E_L$ [MPa]	var.	$E_2 = E_T$ [MPa]	500
$\nu_{12} = \nu_{LT}$	0.02	$\nu_{12} = \nu_{RT}$	0.3
$G_{12} = G_{LT}$ [MPa]	var.	$G_{12} = G_{RT}$ [MPa]	var.
$G_{13} = G_{RT}$ [MPa]	var.	$G_{13} = G_{LT}$ [MPa]	var.
$G_{23} = G_{LR}$ [MPa]	var.	$G_{23} = G_{LR}$ [MPa]	var.

Table 5.8: Stiffness properties used for the longitudinal and transverse boards in the 3D-models, where $E_L = E_0$, $G_{LT} = G_{LR} = G_0$ and $G_{RT} = G_R$.

Longitudinal boards		Transverse boards	
$E_1 = E_T$ [MPa]	500	$E_1 = E_L$ [MPa]	var.
$E_2 = E_L$ [MPa]	var.	$E_2 = E_T$ [MPa]	500
$E_3 = E_R$ [MPa]	800	$E_3 = E_R$ [MPa]	800
$\nu_{12} = \nu_{LT}$	0.02	$\nu_{12} = \nu_{LT}$	0.02
$\nu_{13} = \nu_{RT}$	0.3	$\nu_{13} = \nu_{LR}$	0.02
$\nu_{23} = \nu_{LR}$	0.02	$\nu_{23} = \nu_{RT}$	0.3
$G_{12} = G_{LT}$ [MPa]	var.	$G_{12} = G_{LT}$ [MPa]	var.
$G_{13} = G_{RT}$ [MPa]	var.	$G_{13} = G_{LR}$ [MPa]	var.
$G_{23} = G_{LR}$ [MPa]	var.	$G_{23} = G_{RT}$ [MPa]	var.

5.2.1 Specimen 1 beams

For the Specimen 1 beams four different combinations of stiffness properties based of the results from Section 5.1 were tested. These are denoted "Test A–D" and are specified further below. For a collection of the stiffness properties used it is referenced to Table 5.5.

Test A – Timoshenko theory (net area) & Gamma method

The longitudinal shear moduli $G_{0,net}$ are calculated with Timoshenko theory and are based of the net area $A_{net} = 0.006 \text{ m}^2$. The rolling shear moduli G_{R1} and G_{R2} are calculated with the Gamma method. Table 5.9 shows the stiffness properties used for each model and the results from the FE-analysis are given in Table 5.10.

Table 5.9: Stiffness properties used in FE-models for test A.

	E_0	$G_{0,net}$	G_{R1}	G_{R2}
	[MPa]	[MPa]	[MPa]	[MPa]
Beam 4	15622	435	52	50
Beam 5	16419	556	57	56
Beam 6	13220	597	55	52
Beam 7	12063	537	50	44
Beam 8	14497	533	54	47
Beam 9	10599	469	51	45

Table 5.10: Equivalent stiffnesses and the corresponding ratio for test A.

	In-plane (3D-models)			Out-of-plane (2D-models)		
	k_t	k_m	Ratio, $\frac{k_m}{k_t}$	k_t	k_m	Ratio, $\frac{k_m}{k_t}$
	[N/mm]	[N/mm]		[N/mm]	[N/mm]	
<u>Beam 4</u>						
$L_1 = 1.0 \text{ m}$	2620	2991	114.1 %	2343	2108	90.0 %
$L_2 = 1.4 \text{ m}$	1120	1219	108.8 %	1127	1033	91.7 %
<u>Beam 5</u>						
$L_1 = 1.0 \text{ m}$	2910	3262	112.1 %	2509	2286	91.1 %
$L_2 = 1.4 \text{ m}$	1216	1309	107.6 %	1212	1120	92.4 %
<u>Beam 6</u>						
$L_1 = 1.0 \text{ m}$	2506	2761	110.2 %	2205	2033	92.2 %
$L_2 = 1.4 \text{ m}$	1018	1085	106.6 %	1025	959	93.6 %
<u>Beam 7</u>						
$L_1 = 1.0 \text{ m}$	2280	2518	110.4 %	2012	1854	92.2 %
$L_2 = 1.4 \text{ m}$	927	990	106.7 %	909	854	94.0 %
<u>Beam 8</u>						
$L_1 = 1.0 \text{ m}$	2623	2927	111.6 %	2293	2098	91.5 %
$L_2 = 1.4 \text{ m}$	1087	1166	107.3 %	1053	976	92.7 %
<u>Beam 9</u>						
$L_1 = 1.0 \text{ m}$	2001	2220	110.9 %	1883	1734	92.1 %
$L_2 = 1.4 \text{ m}$	814	872	107.1 %	844	789	93.5 %

Test B – Timoshenko theory (gross area) & Gamma method

The longitudinal shear moduli $G_{0,net}$ are calculated with Timoshenko theory and are based of the gross area $A_{gross} = 0.01 \text{ m}^2$. The rolling shear moduli G_{R1} and G_{R2} are calculated with the Gamma method. Table 5.11 shows the stiffness properties used for each model and the results from the FE-analysis are given in Table 5.12.

Table 5.11: Stiffness properties used in FE-models for test B.

	E_0 [MPa]	$G_{0,gross}$ [MPa]	G_{R1} [MPa]	G_{R2} [MPa]
Beam 4	15622	261	52	50
Beam 5	16419	334	57	56
Beam 6	13220	358	55	52
Beam 7	12063	322	50	44
Beam 8	14497	320	54	47
Beam 9	10599	282	51	45

Table 5.12: Equivalent stiffnesses and the corresponding ratio for test B.

	In-plane (3D-models)			Out-of-plane (2D-models)		
	k_t [N/mm]	k_m [N/mm]	Ratio, $\frac{k_m}{k_t}$	k_t [N/mm]	k_m [N/mm]	Ratio, $\frac{k_m}{k_t}$
<u>Beam 4</u>						
$L_1 = 1.0 \text{ m}$	2620	2637	100.6 %	2343	2007	85.7 %
$L_2 = 1.4 \text{ m}$	1120	1130	100.9 %	1127	1000	88.8 %
<u>Beam 5</u>						
$L_1 = 1.0 \text{ m}$	2910	2926	100.6 %	2509	2192	87.3 %
$L_2 = 1.4 \text{ m}$	1216	1227	100.9 %	1212	1089	89.9 %
<u>Beam 6</u>						
$L_1 = 1.0 \text{ m}$	2506	2529	100.9 %	2205	1963	89.0 %
$L_2 = 1.4 \text{ m}$	1018	1032	101.3 %	1025	938	91.5 %
<u>Beam 7</u>						
$L_1 = 1.0 \text{ m}$	2280	2305	101.1 %	2012	1790	89.0 %
$L_2 = 1.4 \text{ m}$	927	941	101.4 %	909	836	91.9 %
<u>Beam 8</u>						
$L_1 = 1.0 \text{ m}$	2623	2643	100.7 %	2293	2015	87.9 %
$L_2 = 1.4 \text{ m}$	1087	1098	101.0 %	1053	952	90.4 %
<u>Beam 9</u>						
$L_1 = 1.0 \text{ m}$	2001	2032	101.5 %	1883	1671	88.7 %
$L_2 = 1.4 \text{ m}$	814	829	101.8 %	844	771	91.3 %

Test C – Timoshenko theory (net area)

The longitudinal shear moduli $G_{0,net}$ are calculated with Timoshenko theory and are based of the net area $A_{net} = 0.006 \text{ m}^2$. The rolling shear moduli $G_{R1,net}$ and $G_{R2,net}$ are calculated with Timoshenko theory. Table 5.13 shows the stiffness properties used for each model and the results from the FE-analysis are given in Table 5.14.

Table 5.13: Stiffness properties used in FE-models for test C.

	E_0 [MPa]	$G_{0,net}$ [MPa]	$G_{R1,net}$ [MPa]	$G_{R2,net}$ [MPa]
Beam 4	15622	435	76	71
Beam 5	16419	556	81	78
Beam 6	13220	597	77	71
Beam 7	12063	537	70	59
Beam 8	14497	533	76	65
Beam 9	10599	469	72	63

Table 5.14: Equivalent stiffnesses and the corresponding ratio for test C.

	In-plane (3D-models)			Out-of-plane (2D-models)		
	k_t [N/mm]	k_m [N/mm]	Ratio, $\frac{k_m}{k_t}$	k_t [N/mm]	k_m [N/mm]	Ratio, $\frac{k_m}{k_t}$
<u>Beam 4</u>						
$L_1 = 1.0 \text{ m}$	2620	3004	114.7 %	2343	2461	105.1 %
$L_2 = 1.4 \text{ m}$	1120	1222	109.1%	1127	1156	102.6 %
<u>Beam 5</u>						
$L_1 = 1.0 \text{ m}$	2910	3275	112.6 %	2509	2637	105.1 %
$L_2 = 1.4 \text{ m}$	1216	1312	107.9 %	1212	1242	102.5 %
<u>Beam 6</u>						
$L_1 = 1.0 \text{ m}$	2506	2770	110.5 %	2205	2312	104.8 %
$L_2 = 1.4 \text{ m}$	1018	1087	106.8 %	1025	1050	102.5 %
<u>Beam 7</u>						
$L_1 = 1.0 \text{ m}$	2280	2527	110.8 %	2012	2110	104.9 %
$L_2 = 1.4 \text{ m}$	927	992	107.0 %	909	935	102.8 %
<u>Beam 8</u>						
$L_1 = 1.0 \text{ m}$	2623	2938	112.0 %	2293	2403	104.8 %
$L_2 = 1.4 \text{ m}$	1087	1169	107.5 %	1053	1085	103.0 %
<u>Beam 9</u>						
$L_1 = 1.0 \text{ m}$	2001	2227	111.3 %	1883	1961	104.1 %
$L_2 = 1.4 \text{ m}$	814	874	107.4 %	844	866	102.6 %

Test D – Timoshenko theory (gross area)

The longitudinal shear moduli $G_{0,gross}$ are calculated with Timoshenko theory and are based of the gross area $A_{gross} = 0.01 \text{ m}^2$. The rolling shear moduli $G_{R1,gross}$ and $G_{R2,gross}$ are calculated with Timoshenko theory. Table 5.15 shows the stiffness properties used for each model and the results from the FE-analysis are given in Table 5.16.

Table 5.15: Stiffness properties used in FE-models for test D.

	E_0 [MPa]	$G_{0,gross}$ [MPa]	$G_{R1,gross}$ [MPa]	$G_{R2,gross}$ [MPa]
Beam 4	15622	261	85	79
Beam 5	16419	334	89	85
Beam 6	13220	358	83	77
Beam 7	12063	322	76	64
Beam 8	14497	320	83	70
Beam 9	10599	282	79	69

Table 5.16: Equivalent stiffnesses and the corresponding ratio for test D.

	In-plane (3D-models)			Out-of-plane (2D-models)		
	k_t [N/mm]	k_m [N/mm]	Ratio, $\frac{k_m}{k_t}$	k_t [N/mm]	k_m [N/mm]	Ratio, $\frac{k_m}{k_t}$
<u>Beam 4</u>						
$L_1 = 1.0 \text{ m}$	2620	2652	101.2 %	2343	2423	103.5 %
$L_2 = 1.4 \text{ m}$	1120	1134	101.2 %	1127	1149	102.0 %
<u>Beam 5</u>						
$L_1 = 1.0 \text{ m}$	2910	2941	101.1 %	2509	2603	103.7 %
$L_2 = 1.4 \text{ m}$	1216	1231	101.2 %	1212	1234	101.8 %
<u>Beam 6</u>						
$L_1 = 1.0 \text{ m}$	2506	2540	101.3 %	2205	2282	103.5 %
$L_2 = 1.4 \text{ m}$	1018	1035	101.6 %	1025	1046	102.1 %
<u>Beam 7</u>						
$L_1 = 1.0 \text{ m}$	2280	2314	101.5 %	2012	2087	103.7 %
$L_2 = 1.4 \text{ m}$	927	943	101.7 %	909	933	102.6 %
<u>Beam 8</u>						
$L_1 = 1.0 \text{ m}$	2623	2655	101.2 %	2293	2371	103.4 %
$L_2 = 1.4 \text{ m}$	1087	1101	101.3 %	1053	1077	102.3 %
<u>Beam 9</u>						
$L_1 = 1.0 \text{ m}$	2001	2040	101.9 %	1883	1939	103.0 %
$L_2 = 1.4 \text{ m}$	814	831	102.1 %	844	863	102.2 %

5.2.2 Specimen 2 beams

For the Specimen 2 beams three different combinations of stiffness properties based of the results from Section 5.1 were tested. These are denoted "Test E–G" and are specified further below. The rolling shear moduli obtained through use of the Gamma method were not included in the tests, as they in some cases were represented by negative non-realistic values. For a collection of the stiffness properties used it is referenced to Table 5.5.

Test E – Timoshenko theory (net area)

The longitudinal shear moduli $G_{0,net}$ are calculated with Timoshenko theory and are based of the net area $A_{net} = 0.004 \text{ m}^2$. The rolling shear moduli $G_{R1,net}$ and $G_{R2,net}$ are calculated with Timoshenko theory. Table 5.17 shows the stiffness properties used for each model and the results from the FE-analysis are given in Table 5.18.

Table 5.17: Stiffness properties used in FE-models for test E.

	E_0 [MPa]	$G_{0,net}$ [MPa]	$G_{R1,net}$ [MPa]	$G_{R2,net}$ [MPa]
Beam 1	9968	697	108	114
Beam 2	14659	734	102	99
Beam 3	17559	549	88	95

Table 5.18: Equivalent stiffnesses and the corresponding ratio for test E.

	In-plane (3D-models)			Out-of-plane (2D-models)		
	k_t [N/mm]	k_m [N/mm]	Ratio, $\frac{k_m}{k_t}$	k_t [N/mm]	k_m [N/mm]	Ratio, $\frac{k_m}{k_t}$
<u>Beam 1</u>						
$L_3 = 0.60 \text{ m}$	5001	6410	128.2 %	2336	2881	123.3 %
$L_4 = 0.84 \text{ m}$	2165	2567	118.6 %	1066	1251	117.3 %
<u>Beam 2</u>						
$L_3 = 0.60 \text{ m}$	6518	8615	132.2 %	2833	3472	122.6 %
$L_4 = 0.84 \text{ m}$	2954	3549	120.2 %	1356	1553	114.5 %
<u>Beam 3</u>						
$L_3 = 0.60 \text{ m}$	6295	9021	143.3 %	2828	3524	124.6 %
$L_4 = 0.84 \text{ m}$	3070	3910	127.4 %	1479	1685	113.9 %

Test F – Timoshenko theory (gross area)

The longitudinal shear moduli $G_{0,gross}$ are calculated with Timoshenko theory and are based of the gross area $A_{gross} = 0.01 \text{ m}^2$. The rolling shear moduli $G_{R1,gross}$ and $G_{R2,gross}$ are calculated with Timoshenko theory. Table 5.19 shows the stiffness properties used for each model and the results from the FE-analysis are given in Table 5.20.

Table 5.19: Stiffness properties used in FE-models for test F.

	E_0 [MPa]	$G_{0,gross}$ [MPa]	$G_{R1,gross}$ [MPa]	$G_{R2,gross}$ [MPa]
Beam 1	9968	279	134	144
Beam 2	14659	294	123	120
Beam 3	17559	220	111	122

Table 5.20: Equivalent stiffnesses and the corresponding ratio for test F.

	In-plane (3D-models)			Out-of-plane (2D-models)		
	k_t [N/mm]	k_m [N/mm]	Ratio, $\frac{k_m}{k_t}$	k_t [N/mm]	k_m [N/mm]	Ratio, $\frac{k_m}{k_t}$
<u>Beam 1</u>						
$L_3 = 0.60 \text{ m}$	5001	5177	103.5 %	2336	2820	120.7 %
$L_4 = 0.84 \text{ m}$	2165	2251	104.0 %	1066	1242	116.5 %
<u>Beam 2</u>						
$L_3 = 0.60 \text{ m}$	6518	6608	101.4 %	2833	3357	118.5 %
$L_4 = 0.84 \text{ m}$	2954	2996	101.4 %	1356	1535	113.2 %
<u>Beam 3</u>						
$L_3 = 0.60 \text{ m}$	6295	6364	101.1 %	2828	3360	118.8 %
$L_4 = 0.84 \text{ m}$	3070	3085	100.5 %	1479	1656	112.0 %

Test G – Timoshenko theory (gross area) & mean values

A good correlation could be found between k_t and k_m for the 3D-models when the shear moduli corresponding to the gross area were used, as shown in Table 5.20. However, this did not significantly improve the correlation between k_t and k_m for the 2D-models. An assumption was made that these models were mainly governed by the rolling shear moduli. It was seen fit to instead test the rolling shear moduli derived from the tests of the Specimen 1 beams. Therefore, a third test was conducted where the mean values of $G_{R1,gross}$ and $G_{R2,gross}$ from Table 5.5 would be used. The other stiffness properties were the same as for Test F. Table 5.21 shows the stiffness properties used for each model and the results from the FE-analysis are given in Table 5.22.

Table 5.21: Stiffness properties used in FE-models for test G.

	E_0 [MPa]	$G_{0,gross}$ [MPa]	$G_{R1,mean}$ [MPa]	$G_{R2,mean}$ [MPa]
Beam 1	9968	279	83	74
Beam 2	14659	294	83	74
Beam 3	17559	220	83	74

Table 5.22: Equivalent stiffnesses and the corresponding ratio for test G.

	In-plane (3D-models)			Out-of-plane (2D-models)		
	k_t [N/mm]	k_m [N/mm]	Ratio, $\frac{k_m}{k_t}$	k_t [N/mm]	k_m [N/mm]	Ratio, $\frac{k_m}{k_t}$
<u>Beam 1</u>						
$L_3 = 0.60$ m	5001	5126	102.5 %	2336	2497	106.9 %
$L_4 = 0.84$ m	2165	2228	102.9 %	1066	1092	102.4 %
<u>Beam 2</u>						
$L_3 = 0.60$ m	6518	6538	100.3 %	2833	2982	105.3 %
$L_4 = 0.84$ m	2954	2966	100.4 %	1356	1359	100.2 %
<u>Beam 3</u>						
$L_3 = 0.60$ m	6295	6310	100.2 %	2828	3065	108.3 %
$L_4 = 0.84$ m	3070	3051	99.4 %	1479	1448	97.9%

6 Discussion

6.1 Test method

The scatter in measured equivalent stiffness proved to be very low, with a coefficient of variation of less than 3 % for the preliminary test results of the Specimen 1 beam, see Table 4.3. Some of the preliminary tests included remounting the beam, and rotating it 180° about its longitudinal axis compared to the previous tests, indicating that the reliability is overall good for the Specimen 1 beams considering the tested setups.

However, a small increase in the coefficient of variation was noted for a decreasing span of the Specimen 1 beam, which implies that the reliability may be negatively affected by a shorter span. In hindsight, preliminary tests should also have been conducted for a Specimen 2 beam. It should also be noted that the same sized steel plates (50×100 mm) were used at the supports and loading point for both the Specimen 1 and 2 beams, respectively. Local indentations were assumed to be negligible for both the Specimen 1 and 2 beams. However, the decrease in span due to the width of steel plates, relative to the beam length, should be more noticeable for the Specimen 2 beams. The effect of this was not studied within this project.

Furthermore, a small increase of the measured equivalent stiffness was noted from the results of each subsequent test conducted during the preliminary tests. For all tests considered, this increase was not greater than 5 %, where the majority of the increase was measured between the first and second test. Performing only one acclimatization test was therefore deemed adequate, given the time span of this project.

Due to a slight slope in the transverse direction of the test rig used for the MTS-machine, the load was unevenly applied in the beginning of each test. Before each test, the steel cylinder used for the load application was mounted so that one edge was barely in contact with the underlying steel plate, see Appendix B. This resulted in a 1 mm gap between the the opposing edge of the steel cylinder and plate, respectively. This can be seen in the beginning of the load-deformation curves in Appendix A, where the incline of the slope is lesser until a deformation of approximately 1 mm. It is also illustrated in Appendix B. However, by testing the beams to approximately 40 % of their assumed capacity and then performing the regression including only the values between $0.5P_{max} < P < P_{max}$, it is assumed that initial imperfections of the test rig (or beam specimen) did not have an impact on the end results.

6.2 Stiffness properties

Three different methods of characterising the MoE and shear modulus parallel to grain (E_0 and G_0) from in-plane bending tests using Timoshenko theory were tested in this project. The methods were based on either: assuming a certain value of the MoE or shear modulus parallel to grain, assuming a certain ratio between the two aforementioned moduli, or establishing equation systems and using test results from two independent tests. Based on the inconsistency of the characterised properties according to the first two methods, these proved not suitable for this test method.

Assumptions using conventional values or a ratio of the two moduli were tested for the first two methods. However, based on the third method the characterised moduli deviate from the conventional values, significantly so when considering the ratio between the moduli. Thus, the first two methods are likely to result in inaccurate moduli, and will not be further discussed within this project.

Three different methods of characterising the rolling shear modulus (G_R) from out-of-plane bending tests were studied in this project: using the gamma method or using Timoshenko theory with respect to the shear correction factor κ either being approximated or calculated numerically. The simplified analytical model using Timoshenko theory and approximate values of κ did not yield representative values of the rolling shear modulus. By analysing the rolling shear moduli determined by the more complex method, where κ was calculated according to Equations 2.27 – 2.31, showed that these moduli normally resulted in values above 70 MPa. Considering Figures 2.8 and 2.9 it could be seen that the approximate value of κ , suggested by Jöbstl [13], corresponded to much lower values of the rolling shear moduli than those determined by the more complex method. Consequently, using the lower κ -value would result in a significant overestimation of the rolling shear moduli.

6.2.1 In-plane loading

The MoE parallel to grain were mostly characterised in the expected range of values, 13500–16700 MPa according to Table 2.2. Albeit, these values were somewhat low for some specimen, it could simply be the result of some specimen possessing lower stiffness properties. It could also be the result of the different cutting pattern of the boards, in accordance with what is presented in Section 2.3.

The characterised shear modulus parallel to grain vary depending on how the shear stiffness is calculated. Timoshenko theory assumes an equivalent shear stiffness of the cross section governed by the parallel to grain shear modulus, and assumptions of κ and the effective area. Kappa was assumed as 5/6 based on the initial assumption that shear stresses would only be transferred in the longitudinal layers. The corresponding effective area was assumed to be rectangular consisting of the longitudinal layers only, denoted net area A_{net} . However, the shear stresses were analysed by means of FE-models in Section 3.6.2, showing that a great portion of shear stresses are also transferred through the transverse layers. In order to study the effect of the area governing the shear stiffness, the gross area A_{gross} was considered as an upper limit

value. This resulted in the characterised shear moduli parallel to grain being significantly lower than the conventional values presented in Table 5.6. However, according to [37] the shear stiffness is lower for a CLT beam, compared to e.g. a homogeneous beam, due to discontinuities and the traction free surface of the narrow-face edges in the transverse layers. Furthermore, the shear stress distribution varies both in the width and longitudinal direction of the beam. It can be seen in Figures 3.13–3.16 that the shear stresses decreases significantly at the intersections of the transverse layers, where in theory the effective area should be that of the longitudinal layers only A_{net} . It is therefore likely that the shear stress distribution depends on the transverse board width, the width of the gap between transverse boards, and the number of transverse layers, which in turn should be reflected by the effective area used. As the gross area is a upper limit value, it is also likely that the characterised shear moduli parallel to grain are underestimated. Consequently this would also mean that the rolling shear moduli characterised with Timoshenko theory are slightly overestimated.

Comparing the mean shear modulus parallel to grain, characterised with respect to the gross area for the Specimen 1 and 2 beams, respectively, shows that the modulus for the Specimen 2 beam is approximately 20 % lower. This further implies that the number of transverse layers impact the shear stress distribution and therefore the effective area. Most likely the effective area should be lower for the Specimen 2 beams, as these contain three transverse layers as opposed to two when regarding the Specimen 1 beams.

6.2.2 Out-of-plane loading

Based on the FE-analysis conducted in this project with respect to the effect of annual ring pattern, the values of the characterised rolling shear modulus were expected within the range of $1.4G_R - 2.8G_R$. This results in values between 70 – 140 MPa, when the principal direction rolling shear modulus G_{RT} is assumed to be 50 MPa, according to the conventional value stated in [3]. However, the same comparison can be made when the principal direction rolling shear modulus is assumed to be that of clear wood $G_{RT} = 29 - 39$ MPa, according to Table 2.2. This results in values between 40.6 – 109.2 MPa. Thus, it is hard to determine an exact range in which the resulting rolling shear moduli should be characterised. Furthermore, the FE-analysis was based on a simple shear model, whereas the shear deformation of the transverse boards will differ in a CLT plate exerted to bending. However, this information provides an indication of the effect of the annual ring pattern, and whether or not the characterised rolling shear moduli reflect this phenomenon.

Considering the Specimen 1 beams, the mean value of the rolling shear moduli characterised using Timoshenko theory with respect to the gross shear modulus parallel to grain $G_{0,gross}$ were in the range of 74 – 84 MPa. The corresponding range of the mean values for the Specimen 2 beams were in the range of 123 – 128 MPa. Given that the values presented for the Specimen 2 beams correspond to an upper limit value of the ranges discussed above, this would require that the transverse layers of the Specimen 2 beams are comprised mainly of boards with optimum pith distance, with respect to the apparent rolling shear stiffness. This was not studied explicitly, but regarded as highly unlikely. Furthermore, it was mentioned in the previous section that the assumption

of the effective area could result in the the rolling shear stiffness being significantly overestimated for the Specimen 2 beams. The rolling shear moduli for the Specimen 1 beams are therefore likely to be more representative values of the CLT-beams.

Characterising the rolling shear moduli using the Gamma method resulted in lower values compared to using Timoshenko theory. For the Specimen 2 beams even negative (non-realistic) values were obtained. The Gamma method is based on Bernoulli-Euler theory, where shear strains are assumed as zero. Instead, the shear strains are accounted for by a reduction of the moment of inertia using Gamma factors, which are partly governed by the span of the beam. A shorter span will in general result in relatively larger shear strains, which is compensated by the Gamma method as a larger reduction of the moment of inertia. However, compared to Timoshenko theory the Gamma method assumes a more stiff behaviour for the tested span of this project, as can be seen in Figures 2.10–2.15. It seems that the Gamma method can only be applied to a certain extent based on the span and measured stiffness, if the rolling shear modulus is to be characterised. Most likely, considering the Specimen 2 beams, the Gamma method could in most cases not predict the large shear strains, which resulted in the aforementioned negative (non-realistic) values.

There is a slight increase in the values of the rolling shear moduli for the Specimen 1 beams, given a longer span. For the Specimen 2 beams the opposite is true, namely, a longer span results in a slight decrease of the rolling shear moduli. It is hard to determine the reason of this discrepancy. As the phenomena is present when characterising the rolling shear moduli according to both the Gamma method and Timoshenko theory, a hypothesis is that it is caused by the difference in layups of the beams, which is partly reflected in the analytical models by the difference of the moment of inertia.

Lastly, a significant decrease in the shear moduli parallel to grain resulted in a relatively small decrease of the rolling shear moduli when using Timoshenko theory. Thus, indicating that the equivalent stiffness of the beam is mainly governed by the rolling shear modulus. By studying the mean values of the results in Tables 5.1 and 5.2, it can be seen that for the Specimen 1 beams a 40 % decrease of the longitudinal shear moduli resulted in an increase of the rolling shear moduli by 8.8 – 10.7 %, depending on the span. For the Specimen 2 beams (see Tables 5.3 and 5.4) a 60 % decrease of the longitudinal shear moduli resulted in an increase of the rolling shear moduli by 24.2 – 24.3 %. By comparing the decrease of the longitudinal shear moduli, relative to the increase of the rolling shear moduli for the aforementioned cases, the corresponding ratio for the Specimen 1 beams (approximately 40/10) was 4:1, compared to (approximately 60/24) 2.5:1 for the Specimen 2 beams. This indicates that the equivalent stiffness of the Specimen 1 beams is governed by the rolling shear modulus to a greater degree than the Specimen 2 beams. This may sound counter-intuitive as two transverse layers are assumed to be exposed to rolling shear for the Specimen 1 beams, as opposed to one layer for the Specimen 2 beams. However, as the Specimen 2 beams are significantly shorter in length, the equivalent stiffness of these beams are likely to also be significantly affected by longitudinal shear strains.

6.3 Validity of results

The validity of the characterised stiffness moduli discussed in the previous section are evaluated in this section mainly depending to two parameters: the difference in measured equivalent stiffness and calculated equivalent stiffness (denoted ratio), and the consistency in the determined ratio for each test, respectively.

The former parameter indicates if the stiffness properties characterised by the analytical model are representative values for the constituent layers of the CLT-beam. It should however be noted that the results are based of FE-models where the properties of each board are considered as homogeneous and where the longitudinal shear moduli are assumed to be of equal value.

The latter parameter indicates if the variation in mechanical properties between the tested beam specimen are consistently reflected by the characterised moduli of each beam, respectively.

6.3.1 Specimen 1 beams

The best overall correlation was obtained for Test D, through use of Timoshenko theory and by calculating the shear stiffness with respect to the gross area. The 3D-models only overestimated the measured stiffness by up to 2.1 %, and the 2D-models only overestimated the stiffness by up to 3.7 %. These results indicate that the shear stress distribution, and in turn the shear stiffness of the cross section is better represented by the gross area in comparison to the net area. However, it does not mean that the gross area is the best representative value, but rather implies that the area should be close to a upper bound value of the gross area.

The 2D-models corresponding to Test A and Test B, where the Gamma method was used to characterise the rolling shear moduli, underestimated the measured stiffness by up to 14.3 %. Thus, further implying that the rolling shear moduli characterised by use of the Gamma method are underestimated.

The best consistency in ratios was obtained for Test D. The deviation of the ratios for the 3D-models did not exceed 0.3 %, and correspondingly for the 2D-models did not exceed 2 %.

6.3.2 Specimen 2 beams

Based on the results for the Specimen 1 beams, Test F (corresponding to Test D) was assumed to produce the best result for the Specimen 2 beams. The 3D-models for Test F showed good correlation, only overestimating the stiffness by up to 4.0 %. However, the 2D-models showed significantly worse correlation, overestimating the stiffness by up to 20.7 %. Based on the previous section, the Specimen 2 beams should be affected by the assumption of the effective area to a greater extent compared to the Specimen 1 beams. The consequences would most likely be that the shear modulus parallel to grain is underestimated, whereas the rolling shear moduli is overestimated. The combination

of these inaccurate moduli could partly explain the significant overestimation of the stiffness for the 2D-models. Another plausible explanation could be that Timoshenko theory is not entirely applicable for the Specimen 2 beams, due to the bending and shear stresses being highly non-linear throughout the majority of the beam. The increase in deviation when comparing the test results between the shorter span and the longer span of the Specimen 2 beams, respectively, could be an indication of this.

In Test G the mean values of the rolling shear moduli for the Specimen 1 beams were tested together with the other stiffness properties used in Test F. The correlation improved for both the 3D-model and 2D-model. Significantly so for the 2D-model, where the difference in equivalent stiffnesses did not exceed 8.3 %. It has been previously noted that both the shear modulus parallel to grain and rolling shear moduli could be inaccurate, whereas these results serve more as an indication that the rolling shear moduli should be significantly lower for the Specimen 2 beams.

The best consistency in ratios was obtained for Test F. The deviation of the ratios for the 3D-models did not exceed 3.5 %, and correspondingly for the 2D-models did not exceed 8.7 %.

7 Conclusion

7.1 Concluding remarks

This project comprise an analysis of a suggested alternative method where 5-layer cross laminated timber (CLT) beams have been tested at in-plane and out-of-plane loading, respectively. The tested beam specimens were prismatic and of equal cross-sectional dimensions, whereas the length and layup of the beams varied. The analysis was conducted with respect to defining the effect of different material and geometry parameters, determining the reliability of the method and the validity of the resulting stiffness properties.

In total 9 different beams were tested, whereas 6 had a length of 1500 mm and the outermost boards in the longitudinal direction (denoted Specimen 1), and 3 had a length of 900 mm and the outermost board in the transverse direction (denoted Specimen 2).

Considering the validity of the results, different methods for the analytical models were tested and evaluated. The effects of annual ring pattern and shear stress distribution were studied by means of FE-models, as these parameters were considered to have a high impact on the outcome. The stiffness properties characterised by means of the analytical models and results of experimental tests were used as input parameters in FE-models with homogenised properties, where the calculated equivalent stiffness was compared to the equivalent stiffness measured from experimental tests.

Remarks on reliability & test method

The reliability for the Specimen 1 beams was very good, with a coefficient of variation of only 3 % concerning the equivalent stiffness measured from the preliminary tests. The increase of the coefficient of variation due to a decrease in span, and the increase of measured equivalent stiffness after each subsequent test should be considered if further testing are to be conducted.

Remarks on shear stress distribution

The shear stress distribution in the transverse layers should be considered when characterising the shear modulus parallel to grain by means of Timoshenko theory. This could be reflected by the use of an effective area when calculating the shear stiffness. The width of the transversal boards, the gap between these boards and number of the transverse layers should be considered when assuming the effective area. However, further analysis is needed to determine the impact of these parameters. Based of the correlation between the test results and the FE-models, the use of the gross area serves as a good approximation when characterising the shear moduli with Timoshenko theory (with respect to the Specimen 1 beams).

Remarks on annual ring pattern

The annual ring pattern has a large impact on the apparent rolling shear modulus and should be considered when establishing FE-models corresponding to the tested beam specimen. Using a Cartesian coordinate system, and assuming the rolling shear modulus equal to that of the apparent rolling shear modulus proved to be a viable and simple method of accounting for the effect of typical annual ring pattern in FE-models.

Remarks on stiffness properties

The characterised moduli for the Specimen 2 beams showed large deviations from the expected range of values and should not be regarded as representative values. For future tests, a larger span should be considered.

Characterisation of the rolling shear moduli with respect to Timoshenko theory (and with respect to the shear modulus parallel to grain being calculated for the gross area) resulted in values of 64–89 MPa. These values indicate a high validity with respect to the effect of annual ring pattern and suggests that the rolling shear modulus should be higher than the conventional value of 50 MPa.

Characterisation of the rolling shear moduli by means of the Gamma method consistently resulted in underestimated values for the Specimen 1 and 2 beams, respectively. The cause of this was assumed to be the inherent overestimation of the beam stiffness when using the Gamma method for the beam specimen considered in this project.

Remarks on validity of results

The validity with respect to the ratio of measured and calculated equivalent stiffness was very high for Test D. The validity with respect to the consistency of the different ratio for each beam within a Test was high when considering the Test D, and significantly lower when considering the Test F.

7.2 Further analysis

It is indicated within this project that the use of the gross area, when evaluating the shear stiffness of the cross section according to Timoshenko theory, yields a more representative value of the parallel to grain shear modulus. However, depending on the type of support, loading and geometry and layout of the beam, the shear stress distribution could differ. Further analysis could improve the understanding of what parameters govern the shear stress distribution, and how the corresponding effective area should be approximated.

The method is based on a number of assumptions that were not evaluated within this project. Some of these assumptions are stated in Eurocode 5, Annex B [12]. Further understanding of these assumptions could possibly introduce a means of characterising the stiffness properties using the Gamma method for this test method.

Certain parameters were not included within this project because of the complexity it would add, or as a result of the limited time span. The parameters considered most pertinent for further studies are presented below:

- The MoE perpendicular to grain is assumed as negligible and zero for the analytical models as a simplification. However, non-zero MoE perpendicular to grain is still regarded in the FE-models. The impact of this assumption could be studied by including the MoE perpendicular to grain in the analytical models.
- As a simplification the contact restraints between the transverse boards in the FE-models were not modelled, as these surfaces were assumed not to transfer shear stresses. However, compressive normal stresses are likely to occur between transverse boards without a gap as a result of bending. The effect of this could be modelled as a contact restraint (for the upper boards) within a FE-model for further analysis.
- As two spans were tested for each beam, the shorter span resulted in a significant overhang which could induce restraints against shear deformations at the edges. The effect of this should be included in further analysis.

References

- [1] Reinhard Brandner, Robert Tomasi, Thomas Moosbrugger, Erik Serrano and Philipp Dietsch. *Properties, Testing and Design of Cross Laminated Timber*. Sept. 2018. ISBN: 978-3-8440-6143-7. DOI: 10.2370/9783844061437.
- [2] Swedish Wood. *The CLT Handbook*. May 2019. ISBN: 978-91-983214-4-3.
- [3] *EAD 130005-00-0304 - Solid Wood Slab Element to be Used as a Structural Element in Buildings*. eng. URL: <https://www.nlfnorm.cz/en/ehn/6210> (visited on 18/03/2021).
- [4] Sven Thelandersson and Hans J. Larsen. *Timber Engineering*. Wiley, 2003. ISBN: 0-470-84469-8.
- [5] Jozsef Bodig and Benjamin A. Jayne. *Mechanics of Wood and Wood Composites*. Van Nostrand Reinhold, 1982. ISBN: 0-442-00822-8.
- [6] J. M. Dinwoodie. *Timber its Nature and Behaviour*. Van Nostrand Reinhold, 1981. ISBN: 0442304455 ;
- [7] Kent Persson. “Micromechanical Modelling of Wood and Fibre Properties”. eng. PhD thesis. Lund University, 2000. ISBN: 91-7874-094-0. DOI: 10.13140/RG.2.1.1389.7685. URL: <http://rgdoi.net/10.13140/RG.2.1.1389.7685>.
- [8] Henrik Danielsson. “Perpendicular to Grain Fracture Analysis of Wooden Structural Elements - Models and Applications”. eng. PhD thesis. Lund University, 2013. URL: <https://lup.lub.lu.se/search/ws/files/6343447/3736629.pdf>.
- [9] Hans Joachim Blaß and Carmen Sandhaas. *Timber Engineering - Principles for Design*. 2017. ISBN: 978-3-7315-0673-7. DOI: 10.2370/9783844061437.
- [10] *Standard - Träkonstruktioner - Massivträ för Byggsystem - Krav SS-EN 16351:2021*. eng. URL: <https://www.sis.se/produkter/trateknik-15e6ae2b/trabaserade-skivor/plywood/ss-en-163512021/> (visited on 17/03/2021).
- [11] Simon Aicher and Gerhard Dill-Langer. “Basic Considerations to Rolling Shear Modulus in Wooden Boards”. In: *Otto-Graf-Journal* 11 (Jan. 2000), pp. 157–165.
- [12] *Standard - Eurokod 5: Dimensionering av Träkonstruktioner - Del 1-1: Allmänt - Gemensamma Regler och Regler förr Byggnader SS-EN 1995-1-1:2004*. sv. URL: <https://www.sis.se/produkter/byggnadsmaterial-och-byggnader/byggnadsindustrin/tekniska-aspekter/ssen1995112004/> (visited on 17/03/2021).
- [13] Markus Wallner-Novak, Josef Koppelhuber and Kurt Pock. *Cross-Laminated Timber Structural Design - Basic design and engineering principles according to Eurocode*. 2014. ISBN: 978-3-902926-03-6.

- [14] *Standard - Träkonstruktioner - Konstruktionsvirke och Limträ - Bestämning av Vissa Fysikaliska och Mekaniska Egenskaper SS-EN 408:2010+A1:2012*. eng. URL: <https://www.sis.se/produkter/trateknik-15e6ae2b/tra-sagtimmer-och-sagat-virke/ssen4082010a12012/> (visited on 17/03/2021).
- [15] *Standard - Träkonstruktioner - Provningsmetoder - Bestämning av Mekaniska Egenskaper hos Träbaserade Skivor SS-EN 789:2004*. eng. URL: <https://www.sis.se/produkter/trateknik-15e6ae2b/tra-sagtimmer-och-sagat-virke/ssen7892004/> (visited on 17/03/2021).
- [16] Niels Ottosen. *Introduction to the Finite Element Method*. New York: Prentice Hall, 1992. ISBN: 978-0-13-473877-2.
- [17] Dassault Systemés Simulia Corp. *Abaqus/CAE*. Version 2019.
- [18] Dassault Systemés Simulia Corp. *Abaqus/Standard*. Version 2019.
- [19] *Four-Node Plane Stress Element (CPS4 and CPS4R)*. URL: https://web.mit.edu/calculix_v2.7/CalculiX/ccx_2.7/doc/ccx/node41.html (visited on 03/05/2021).
- [20] *Eight-Node Plane Stress Element (CPS8 and CPS8R)*. URL: https://web.mit.edu/calculix_v2.7/CalculiX/ccx_2.7/doc/ccx/node43.html (visited on 03/05/2021).
- [21] *Defining Tie Constraints*. en. URL: <https://abaqus-docs.mit.edu/2017/English/SIMACAECAERefMap/simacae-t-itnhelptied.htm> (visited on 03/05/2021).
- [22] *Analytical rigid surface definition*. en. URL: <https://abaqus-docs.mit.edu/2017/English/SIMACAEEMODRefMap/simamod-c-rigidsurf.htm> (visited on 03/05/2021).
- [23] *Contact Pressure-Overclosure Relationships*. en. URL: <https://abaqus-docs.mit.edu/2017/English/SIMACAEITNRefMap/simaitn-c-normalinteraction.htm> (visited on 03/05/2021).
- [24] *Frictional Behavior*. en. URL: <https://abaqus-docs.mit.edu/2017/English/SIMACAEITNRefMap/simaitn-c-friction.htm> (visited on 03/05/2021).
- [25] *Small and Finite Sliding*. en. URL: <https://abaqus-docs.mit.edu/2017/English/SIMACAECSARefMap/simagsa-c-cntsmallfinlid.htm> (visited on 03/05/2021).
- [26] Michael Dorn, Karolína Habrová, Radek Koubek and Erik Serrano. “Determination of Coefficients of Friction for Laminated Veneer Lumber on Steel under High Pressure Loads”. en. In: *Friction* 9.2 (Apr. 2021), pp. 367–379. ISSN: 2223-7704. DOI: 10.1007/s40544-020-0377-0. URL: <https://doi.org/10.1007/s40544-020-0377-0> (visited on 03/05/2021).
- [27] *Eight-Node Brick Element (C3D8 and F3D8)*. URL: https://web.mit.edu/calculix_v2.7/CalculiX/ccx_2.7/doc/ccx/node26.html (visited on 04/05/2021).
- [28] *Understanding How Results Are Computed*. en. URL: <https://abaqus-docs.mit.edu/2017/English/SIMACAECAERefMap/simacae-c-resconceptcompute.htm> (visited on 20/05/2021).

- [29] *Controlling Result Averaging*. en. URL: <https://abaqus-docs.mit.edu/2017/English/SIMACAECAERefMap/simacae-t-resaverage.htm> (visited on 20/05/2021).
- [30] *Documents*. en. URL: <https://www.sodra.com/en/global/building-systems/documents/> (visited on 25/03/2021).
- [31] *MTS 810 & 858 Material Testing Systems*. en. URL: https://www.upc.edu/sct/documents_equipament/d_77_id-412.pdf (visited on 31/03/2021).
- [32] Erik Serrano and Henrik Danielsson. “Fracture Mechanics Based Design of CLT-plates – Notches at Supports and Half- and-Half Joints”. English. In: *International Network on Timber Engineering Research - Proceedings Meeting 53*. Ed. by Rainer Görlacher. International Network on Timber Engineering Research - Meeting 53, INTER ; Conference date: 17-08-2020 Through 19-08-2020. Timber Scientific Publishing, Karlsruhe, Germany, 2020.
- [33] 2020. The Mathworks Inc. *Matlab*. Version R2020a.
- [34] *Fit Linear Regression Model - MATLAB fitlm - MathWorks Nordic*. URL: <https://se.mathworks.com/help/stats/fitlm.html> (visited on 20/04/2021).
- [35] *Root of Nonlinear Function - MATLAB fzero - MathWorks Nordic*. URL: <https://se.mathworks.com/help/matlab/ref/fzero.html> (visited on 20/04/2021).
- [36] *Standard - Träkonstruktioner - Konstruktionsvirke - Hållfasthetsklasser SS-EN 338:2016*. sv. (Visited on 05/04/2021).
- [37] Henrik Danielsson, Mario Jeleč and Erik Serrano. *Strength and stiffness of cross laminated timber at in-plane beam loading*. eng. Tech. rep. TVSM-7164. Structural Mechanics, Lund University, June 2017. URL: <http://www.byggmek.lth.se/fileadmin/byggnadsmekanik/publications/tvsm7000/web7164.pdf>.

Appendix A

Test results

A.1 Preliminary tests

Table A.1: Measured data from preliminary experimental tests. Tests marked in **bold** correspond to tests where the beam was remounted after each subsequent test and/or mounted 180° as compared to previous tests.

Test	Ellapsed time [s]	Max def. [mm]	Max force [N]	r [-]	q [N]	k [N]
Beam5_l10_00_01	385	3.1	4964	0.9999	-2417	2392
Beam5_l10_00_02	386	3.1	4964	0.9999	-2691	2476
Beam5_l10_00_03	354	2.8	4953	0.9999	-2139	2498
Beam5_l10_00_04	342	2.7	4968	0.9999	-1910	2505
Beam5_l10_00_05	330	2.7	4965	0.9999	-1945	2509
Beam5_l10_90_01	556	2.2	4014	0.9997	-2171	2776
Beam5_l10_90_02	513	2.1	4035	0.9998	-1887	2875
Beam5_l10_90_03	511	2.0	4007	0.9997	-1930	2901
Beam5_l14_00_01	383	3.8	3771	1.0000	-764	1183
Beam5_l14_00_02	364	3.6	3776	1.0000	-690	1225
Beam5_l14_00_03	358	3.6	3775	1.0000	-622	1230
Beam5_l14_00_04	380	3.8	3773	1.0000	-822	1211
Beam5_l14_00_05	380	3.8	3778	1.0000	-821	1209
Beam5_l14_00_06	374	3.7	3766	1.0000	-769	1213
Beam5_l14_90_01	352	3.2	2864	0.9999	-840	1167
Beam5_l14_90_02	347	3.1	2869	1.0000	-893	1204
Beam5_l14_90_03	336	3.0	2867	1.0000	-812	1216
Beam5_l14_90_04	345	3.1	2862	1.0000	-834	1187
Beam5_l14_90_05	341	3.1	2869	1.0000	-792	1191

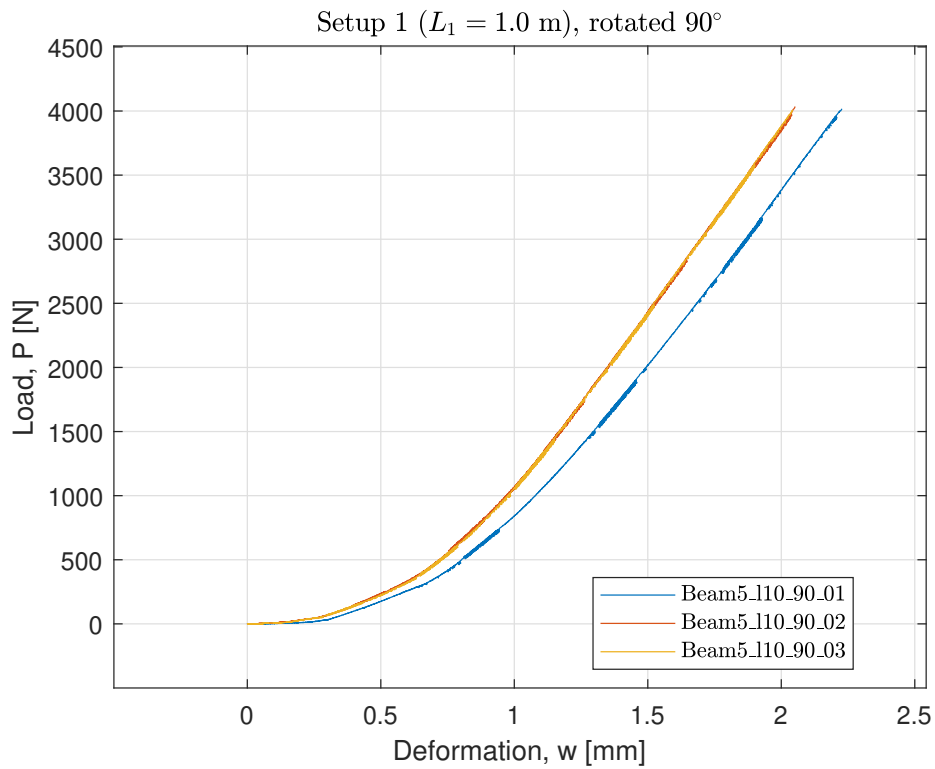


Figure A.1: Load-deformation curves for beam specimen 5 exerted to in-plane bending.

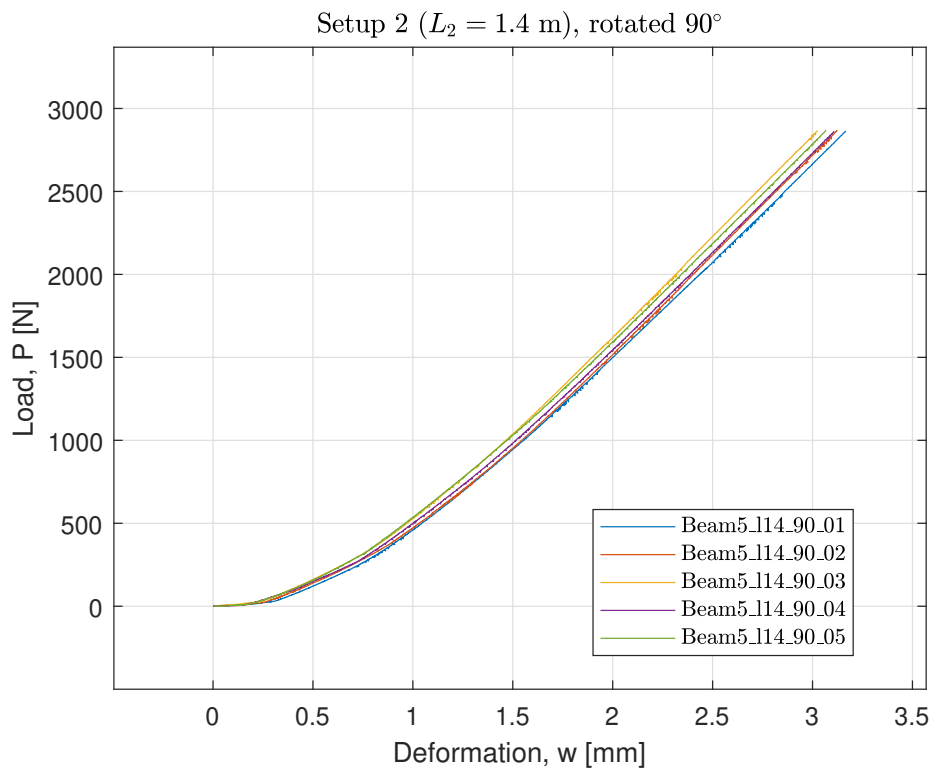


Figure A.2: Load-deformation curves for beam specimen 5 exerted to in-plane bending.

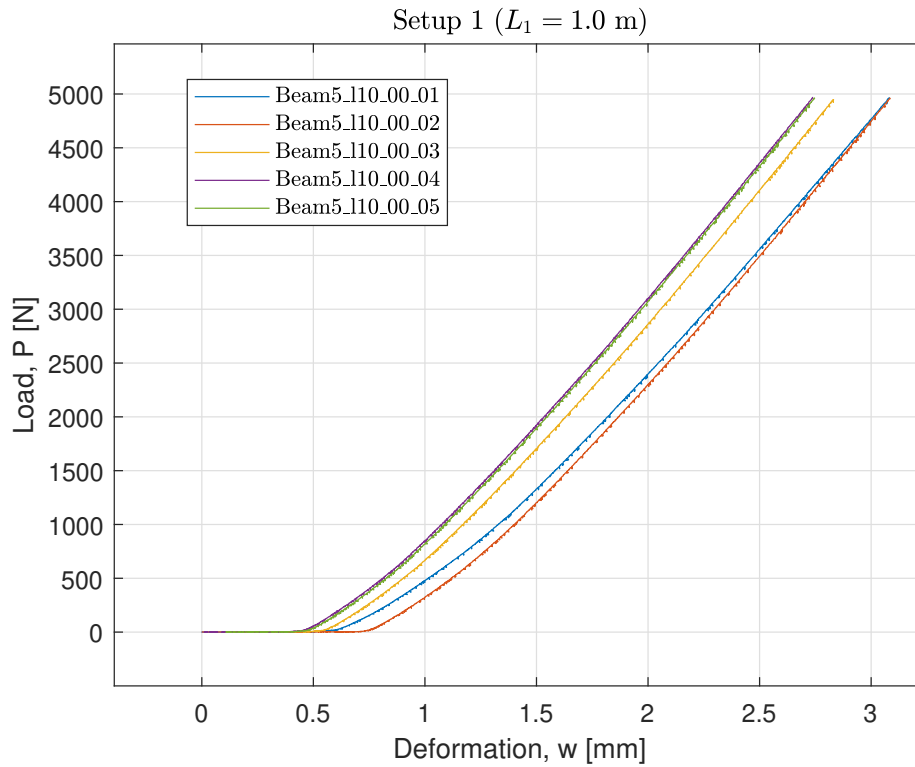


Figure A.3: Load-deformation curves for beam specimen 5 exerted to out-of-plane bending.

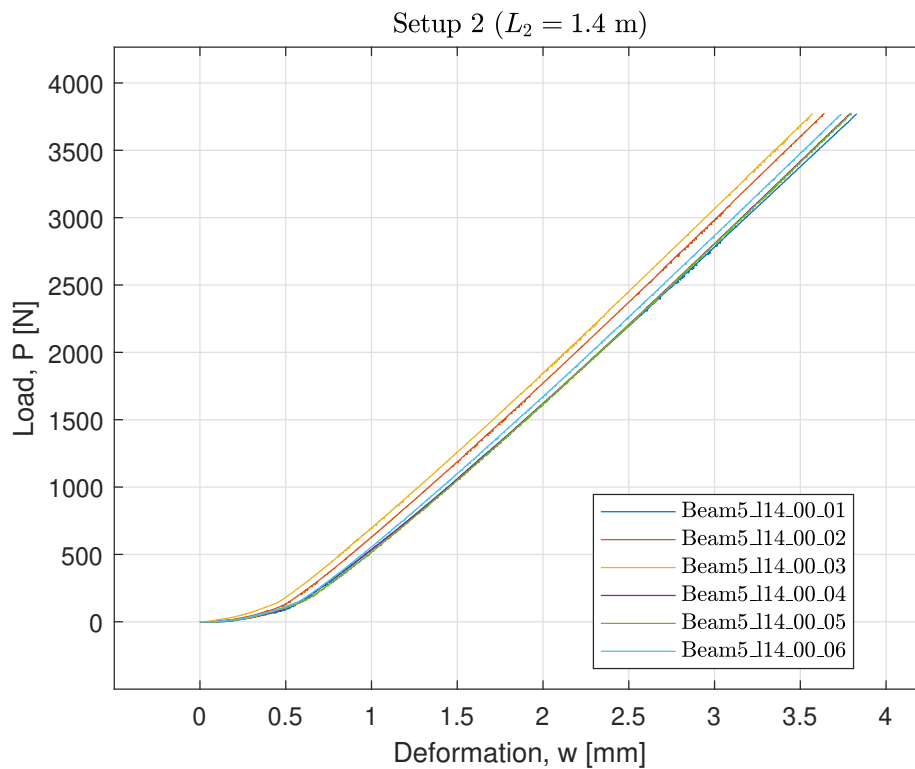


Figure A.4: Load-deformation curves for beam specimen 5 exerted to out-of-plane bending.

A.2 Main tests

Table A.2: Measured data from tests of Specimen 1 beams.

Test	Ellapsed time [s]	Max def. [mm]	Max force [N]	r [-]	q [N]	k [N]
beam4.l10_00_01	362	2.9	4971	0.9999	-1808	2343
beam5.l10_00_01	349	2.8	4980	0.9999	-2036	2509
beam6.l10_00_01	358	2.9	4956	1.0000	-1365	2205
beam7.l10_00_01	401	3.2	4963	0.9999	-1500	2012
beam8.l10_00_01	337	2.7	4976	0.9999	-1208	2293
beam9.l10_00_01	421	3.4	4969	0.9999	-1373	1883
beam4.l10_90_01	653	2.6	4008	0.9997	-2868	2620
beam5.l10_90_01	466	1.9	4014	0.9998	-1429	2910
beam6.l10_90_01	577	2.3	4011	0.9998	-1789	2506
beam7.l10_90_01	549	2.2	4007	0.9998	-1012	2280
beam8.l10_90_01	563	2.3	4032	0.9998	-1882	2623
beam9.l10_90_01	689	2.8	4146	0.9999	-1377	2001
beam4.l14_00_01	432	4.3	3775	1.0000	-1092	1127
beam5.l14_00_01	376	3.8	3768	0.9999	-795	1212
beam6.l14_00_01	433	4.3	3776	1.0000	-668	1025
beam7.l14_00_01	482	4.8	3772	1.0000	-607	909
beam8.l14_00_01	421	4.2	3777	1.0000	-658	1053
beam9.l14_00_01	521	5.2	3776	1.0000	-624	844
beam4.l14_90_01	397	3.6	2862	0.9999	-1151	1120
beam5.l14_90_01	316	2.8	2862	0.9999	-595	1216
beam6.l14_90_01	410	3.7	2865	1.0000	-887	1018
beam7.l14_90_01	397	3.6	2865	1.0000	-449	927
beam8.l14_90_01	367	3.3	2868	1.0000	-726	1087
beam9.l14_90_01	501	4.5	2868	1.0000	-809	814

Table A.3: Measured data from tests of Specimen 2 beams.

Test	Ellapsed time [s]	Max def. [mm]	Max force [N]	r [-]	q [N]	k [N]
beam1_l060_00_01	340	1.7	2608	0.9996	-1372	2336
beam2_l060_00_01	277	1.4	2615	0.9995	-1318	2833
beam3_l060_00_01	296	1.5	2625	0.9994	-1576	2828
beam1_l060_90_01	379	1.5	4457	0.9995	-3124	5001
beam2_l060_90_01	289	1.2	4472	0.9992	-3100	6518
beam3_l060_90_01	406	1.6	4504	0.9991	-5750	6295
beam1_l084_00_01	436	3.1	2611	0.9999	-647	1066
beam2_l084_00_01	365	2.6	2608	0.9999	-857	1356
beam3_l084_00_01	346	2.4	2609	0.9999	-973	1479
beam1_l084_90_01	342	2.4	3334	0.9998	-1852	2165
beam2_l084_90_01	232	1.6	3177	0.9997	-1612	2954
beam3_l084_90_01	256	1.8	3190	0.9997	-2325	3070

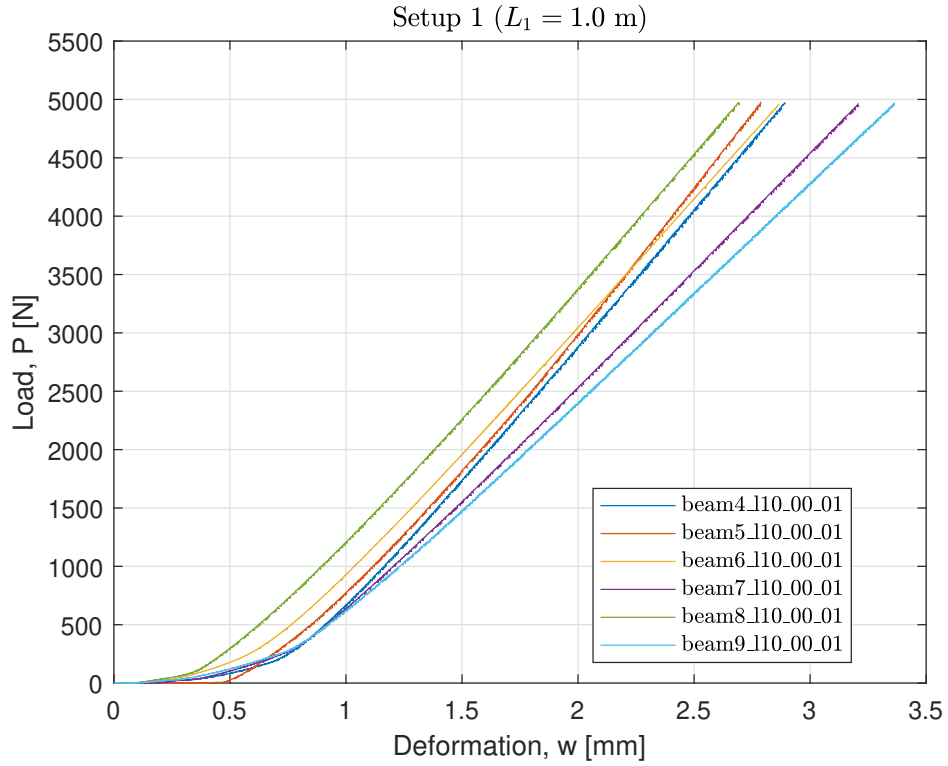


Figure A.5: Load-deformation curves for in-plane loading of Specimen 1 beams.

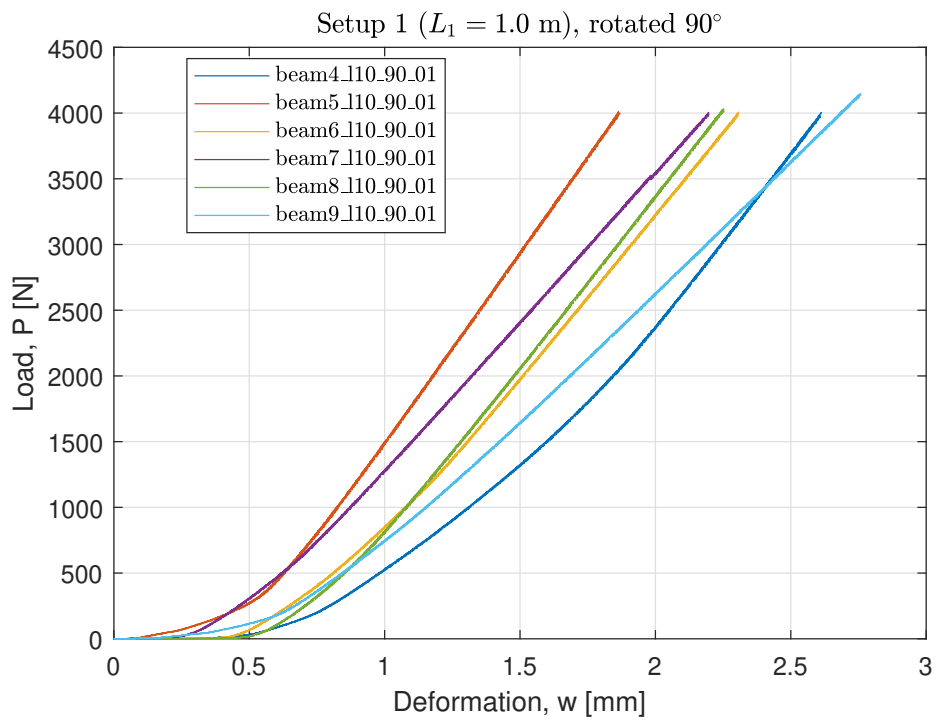


Figure A.6: Load-deformation curves for out-of-plane loading of Specimen 1 beams.

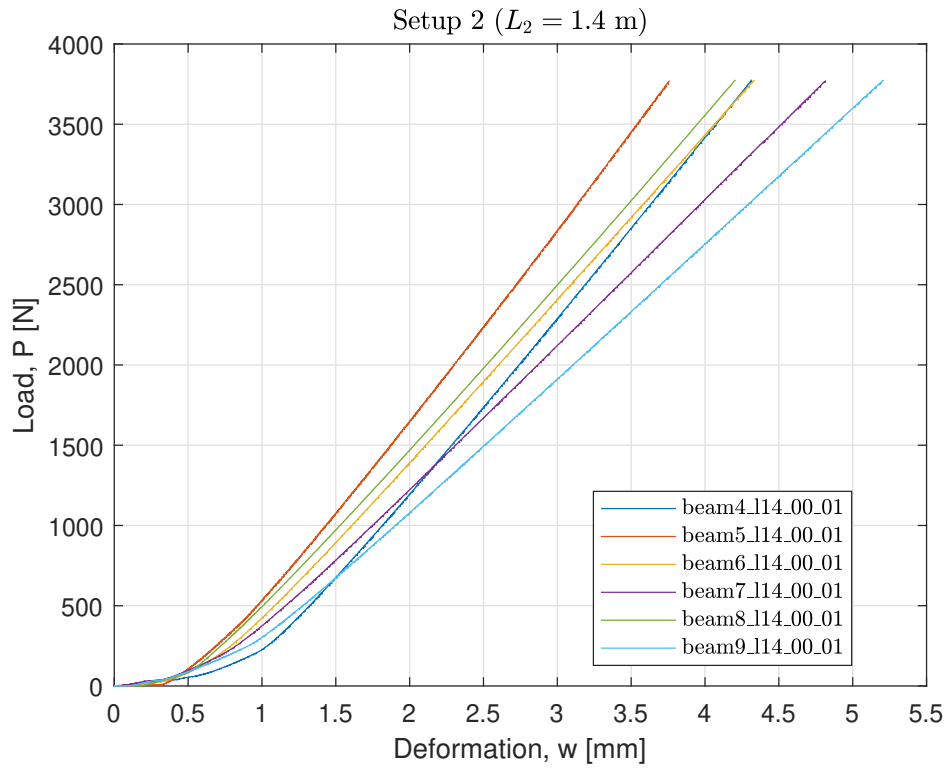


Figure A.7: Load-deformation curves for in-plane loading of Specimen 1 beams.

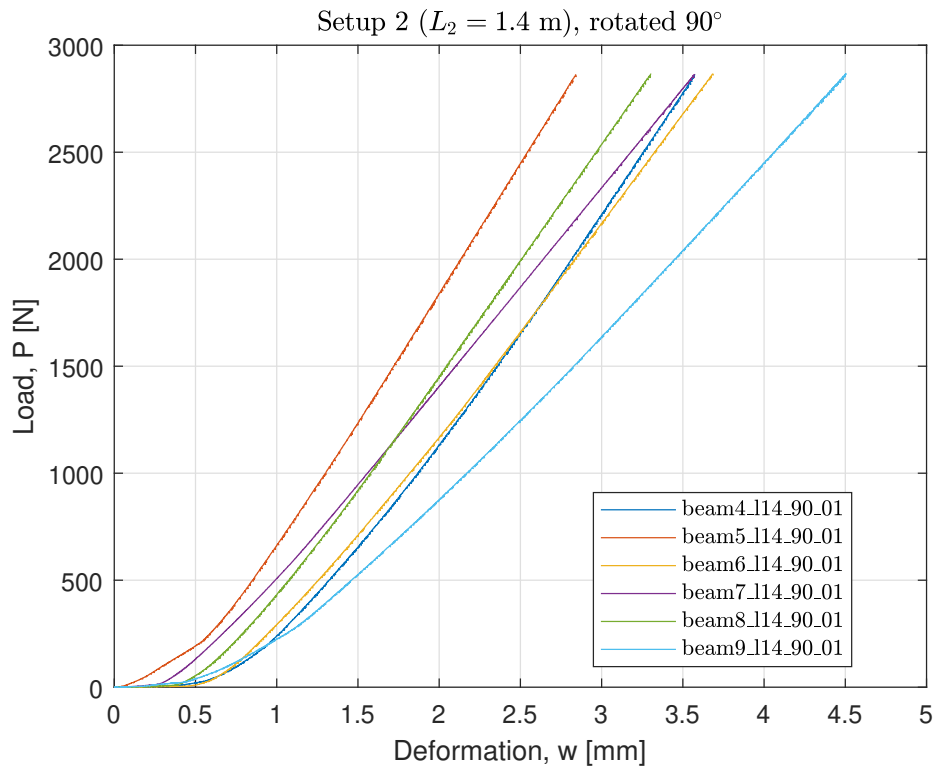


Figure A.8: Load-deformation curves for out-of-plane loading of Specimen 1 beams.

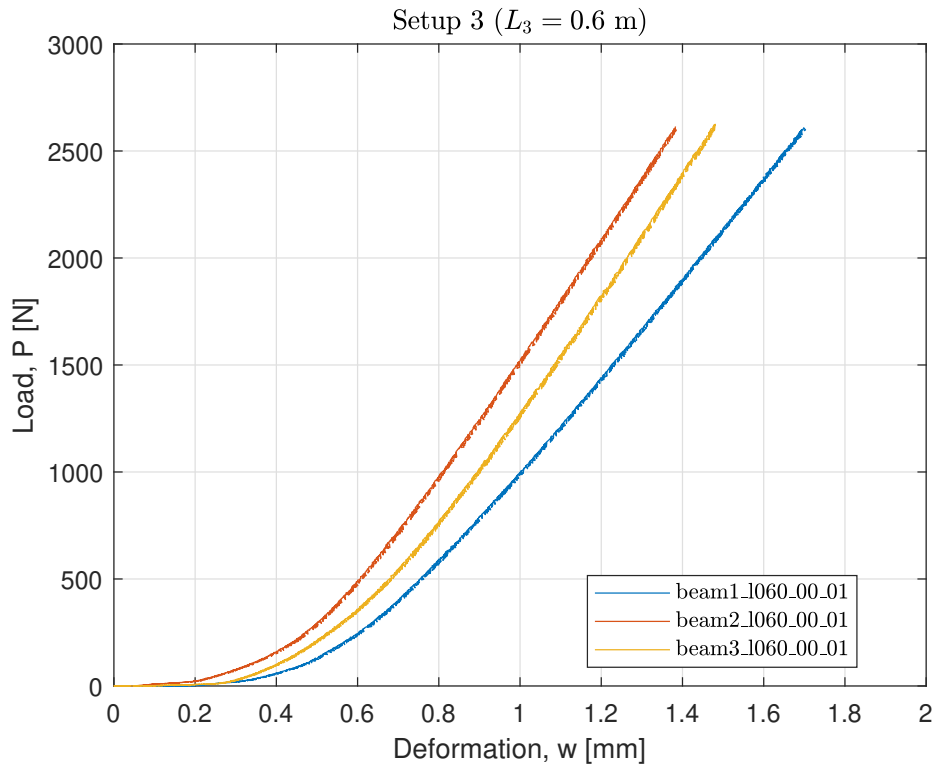


Figure A.9: Load-deformation curves for in-plane loading of Specimen 2 beams.

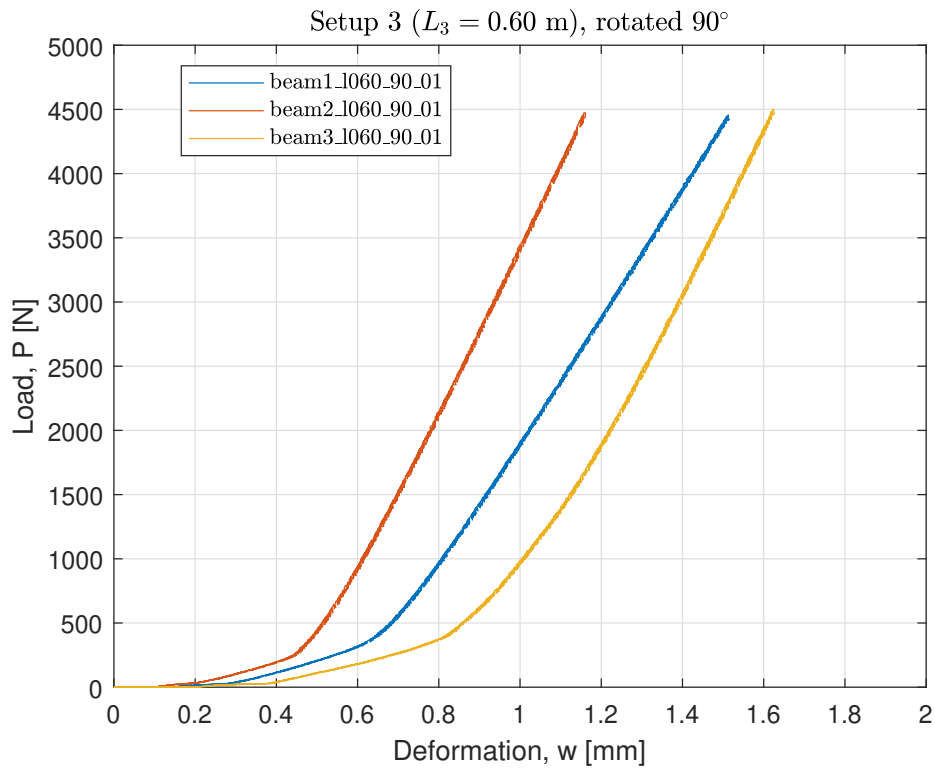


Figure A.10: Load-deformation curves for out-of-plane loading of Specimen 2 beams.

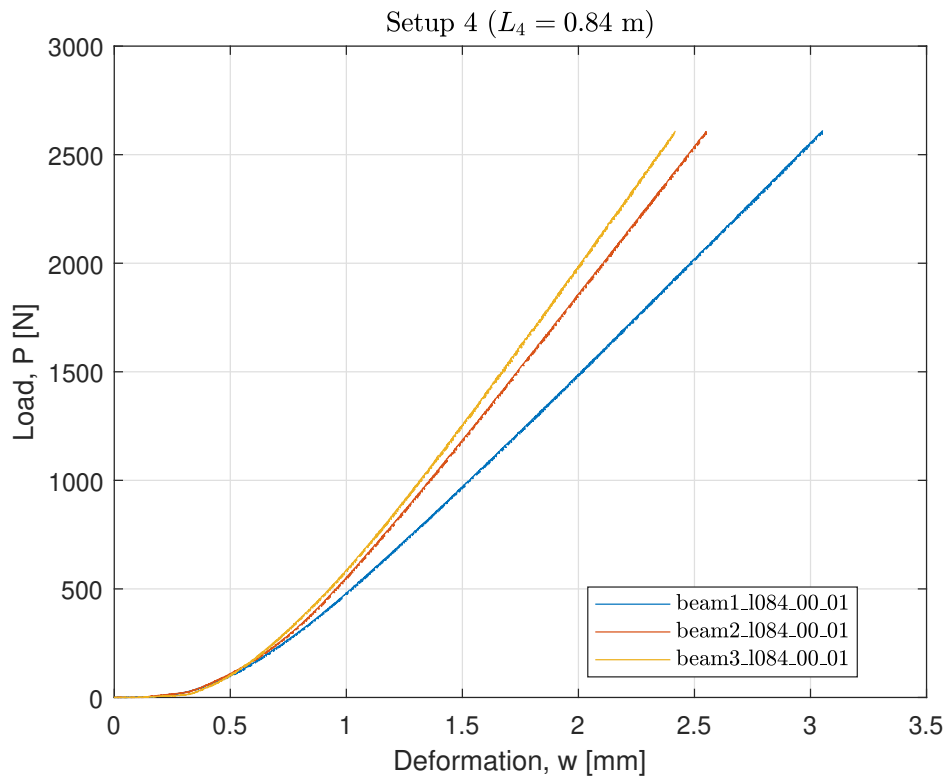


Figure A.11: Load-deformation curves for in-plane loading of Specimen 2 beams.

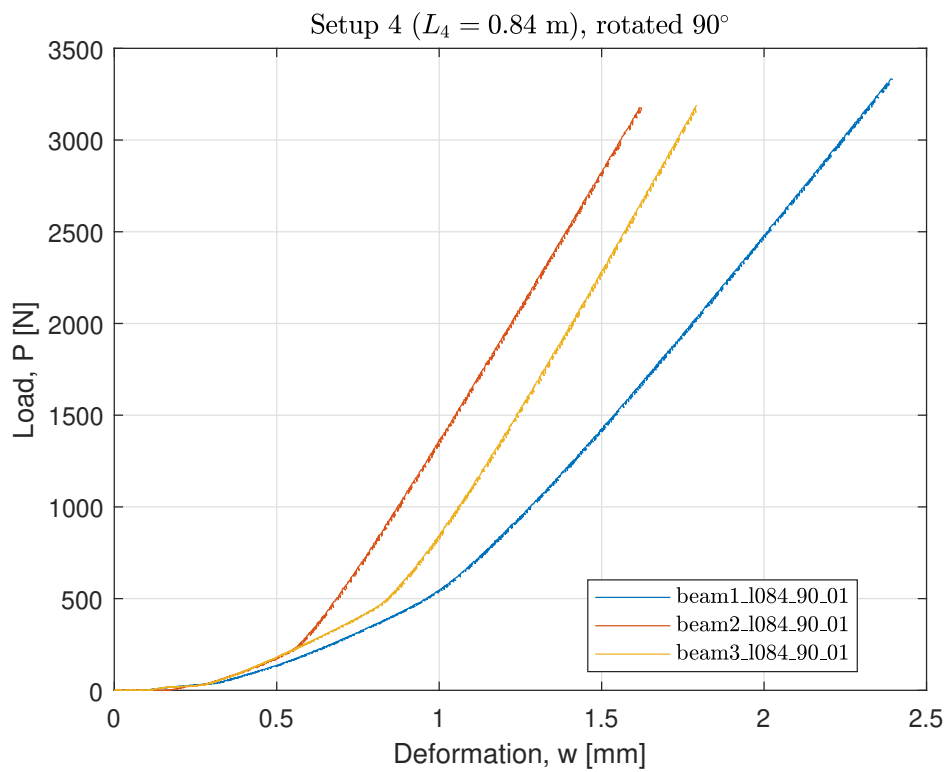


Figure A.12: Load-deformation curves for out-of-plane loading of specimen 2 beams.

Appendix B

Experimental setups

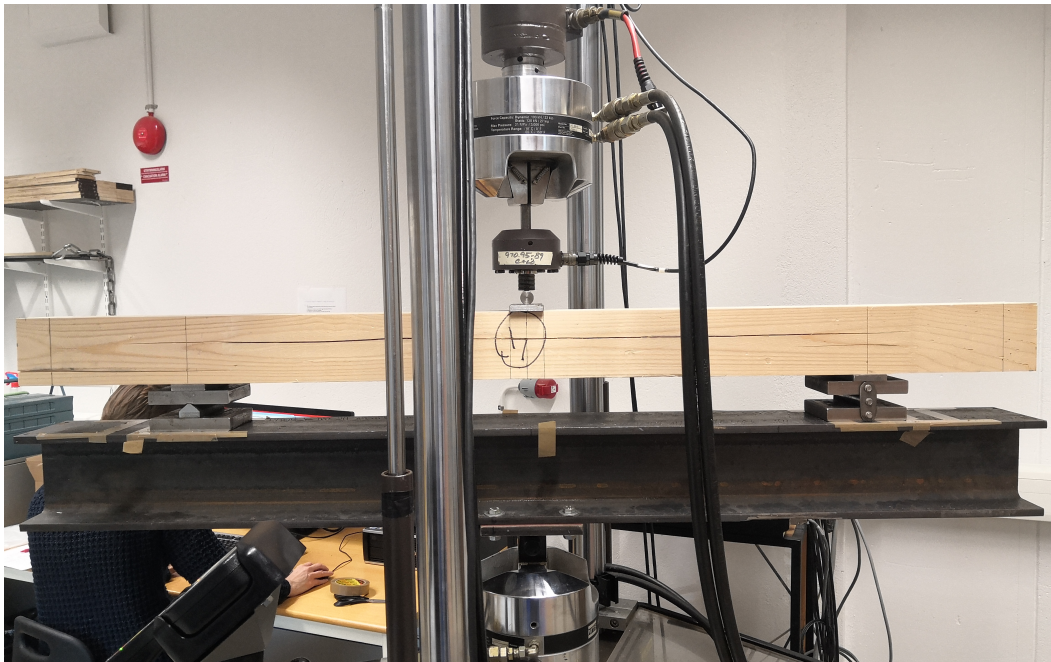


Figure B.1: Test setup for in-plane loaded Specimen 1 beam.



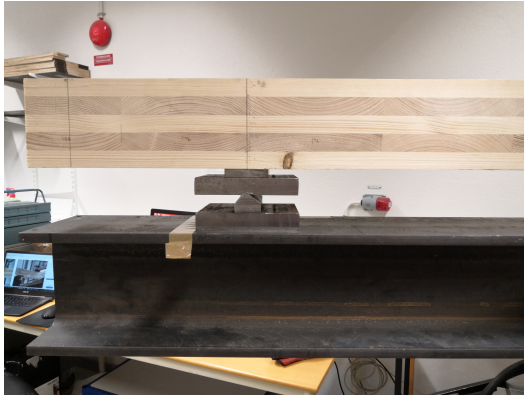
Figure B.2: Test setup for out-of-plane loaded Specimen 1 beam.



Figure B.3: Test setup for in-plane loaded Specimen 2 beam.



Figure B.4: Test setup for out-of-plane loaded Specimen 2 beam.



(a) Fix support with a steel plate mounted on top.



(b) Roller support with a steel plate mounted on top.

Figure B.5: Support conditions for the test setups.



(a) Slope of I-beam test rig.



(b) Example of slope of a CLT-beam.

Figure B.6: Example of slopes due to both CLT-beam imperfections, and test rig imperfections.



Figure B.7: Initial load application conditions due to slope of test rig and CLT-beam, see Figure B.5.

Appendix C

Shear stress distribution

C.1 Specimen 1 beam

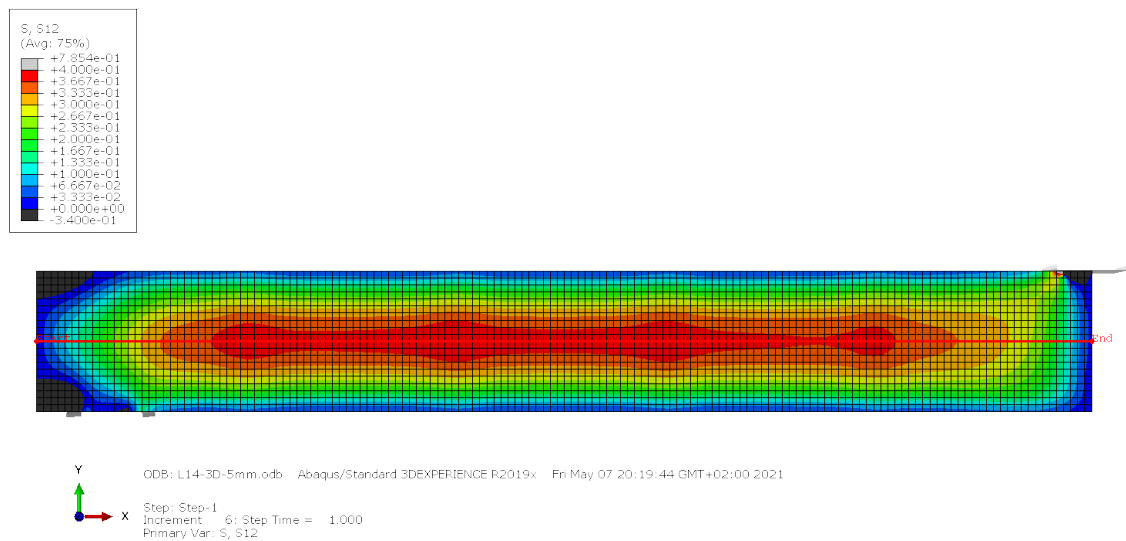


Figure C.1: Path 1 illustrated in a cut of the xy -plane showing the outermost longitudinal layer.

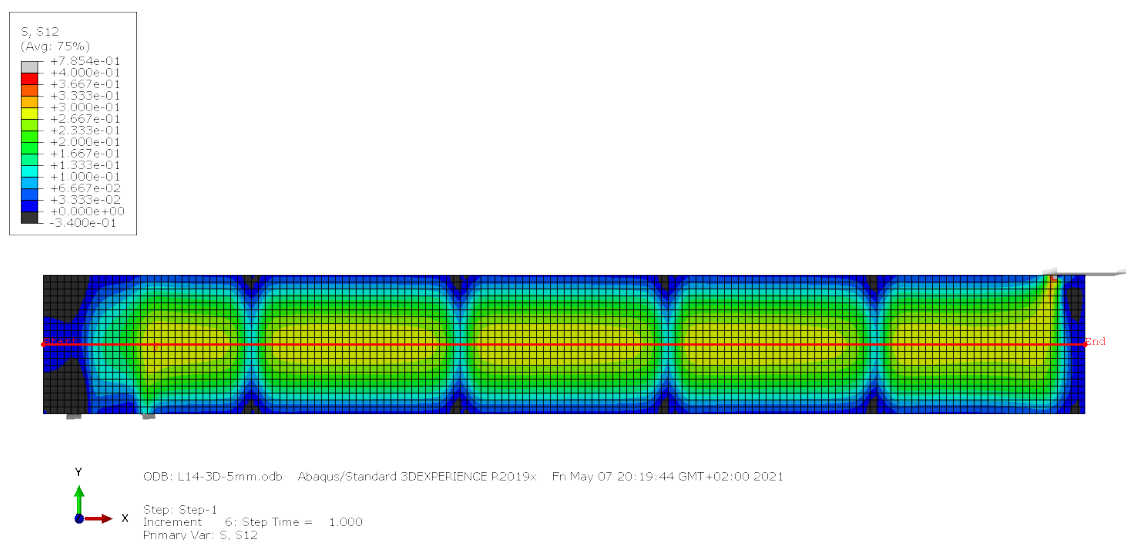


Figure C.2: Path 2 illustrated in a cut of the xy -plane showing the outermost transverse layer.

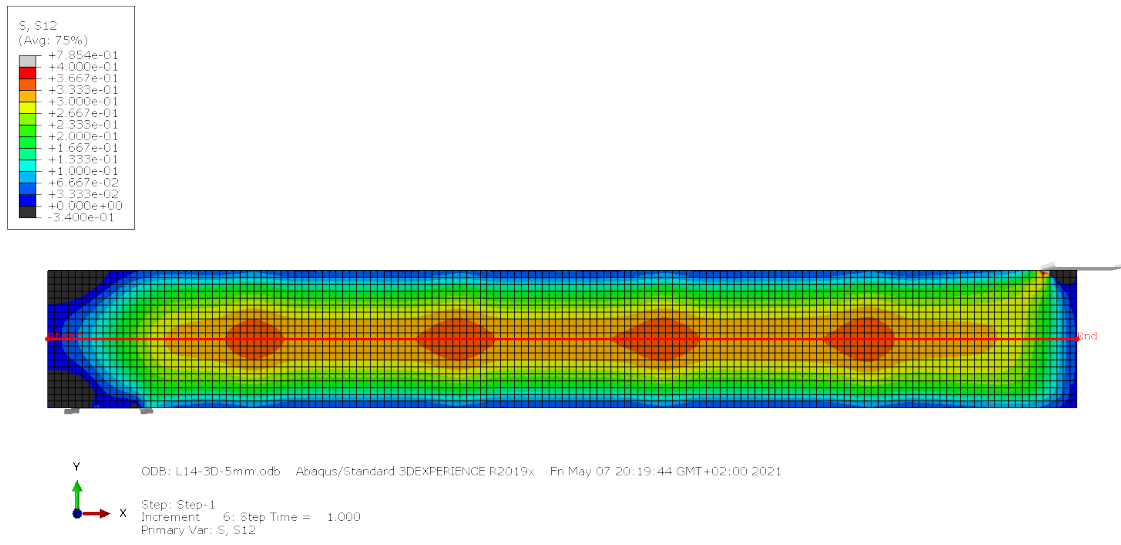


Figure C.3: Path 3 illustrated in a cut of the xy -plane showing the centre longitudinal layer.

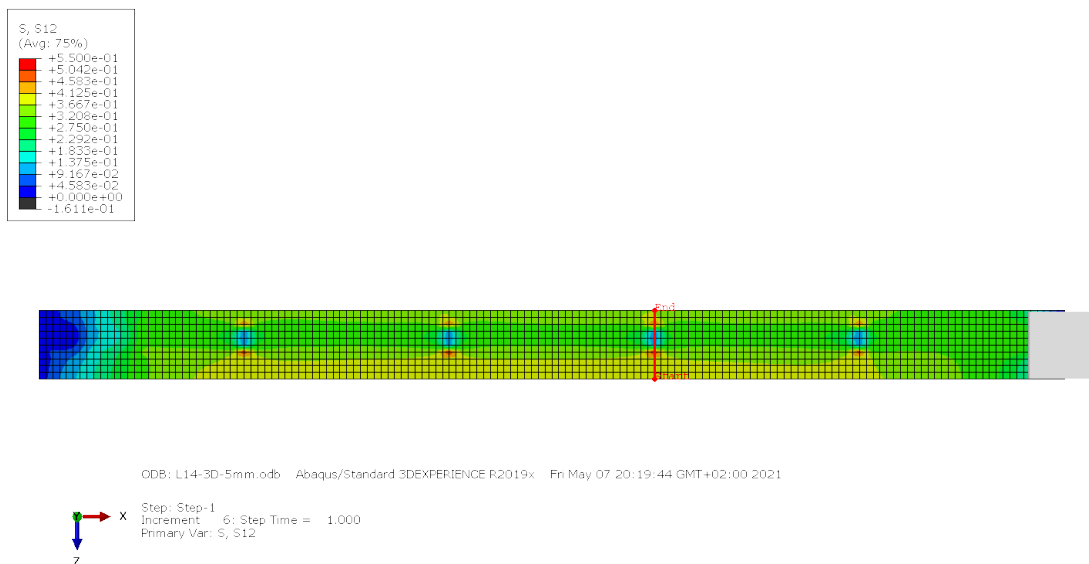
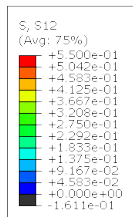


Figure C.4: Path 4 illustrated in a cut of the xz -plane showing the mid section of the beam.



ODB: L14-3D-5mm.odb - Abaqus/Standard 3DEXPERIENCE R2019x - Fri May 07 20:19:44 GMT+02:00 2021



Figure C.5: Path 5 illustrated in a cut of the xz -plane showing the mid section of the beam.

C.2 Specimen 2 beam

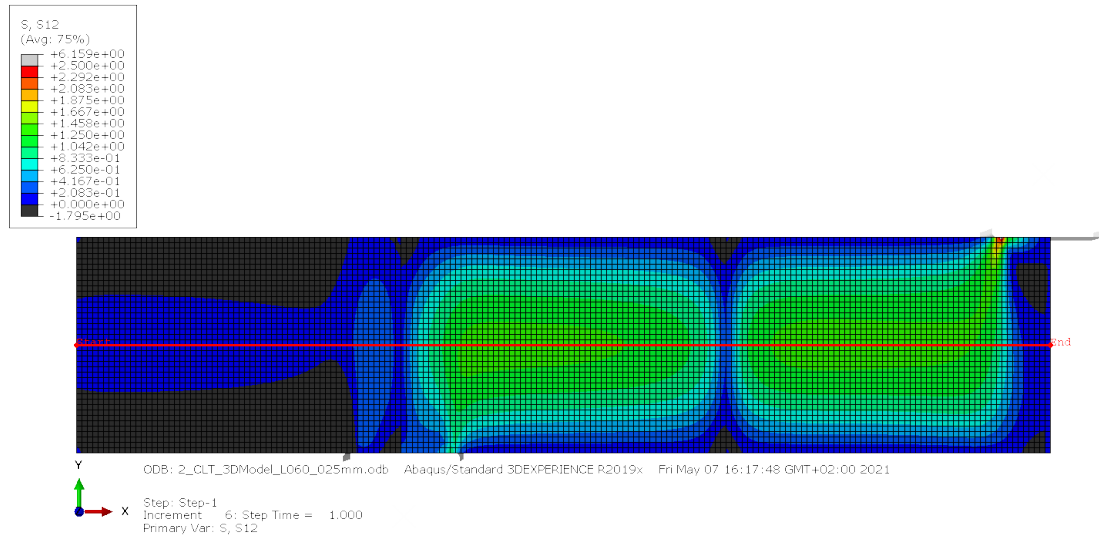


Figure C.6: Path 1 illustrated in a cut of the xy -plane showing the outermost transverse layer.

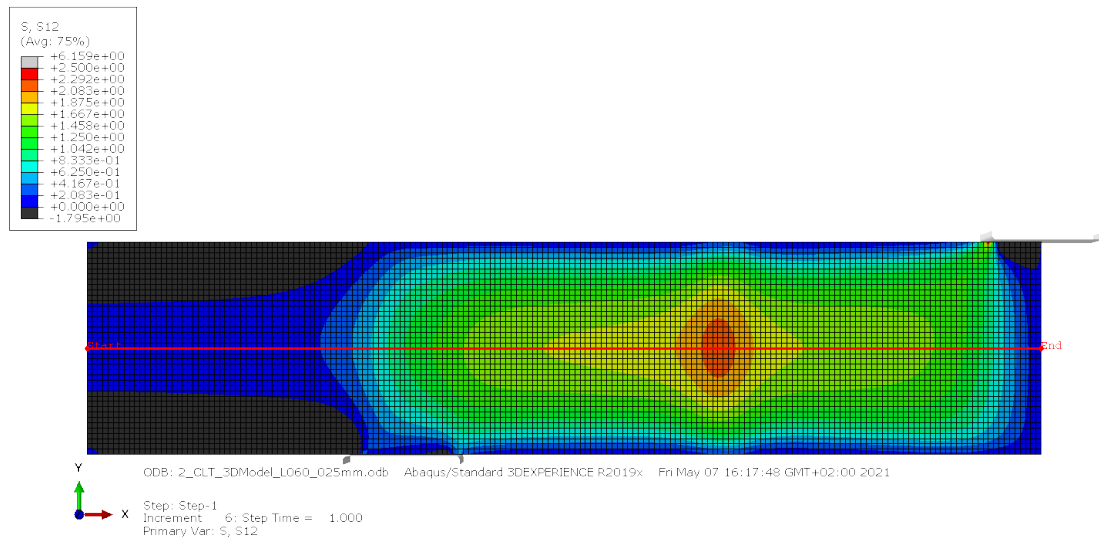


Figure C.7: Path 2 illustrated in a cut of the xy -plane showing the outermost longitudinal layer.

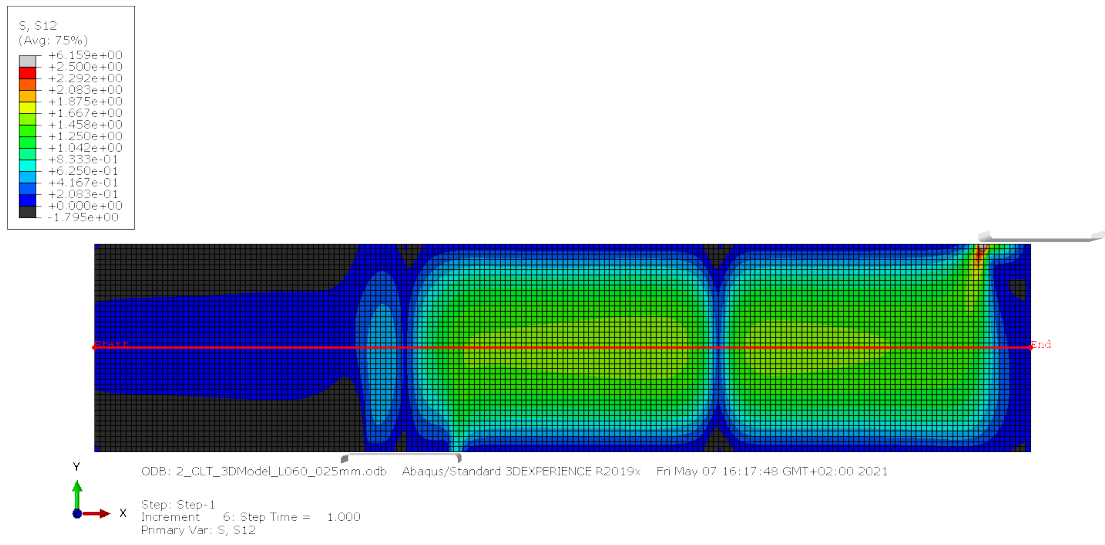


Figure C.8: Path 3 illustrated in a cut of the xy -plane showing the centre transverse layer.

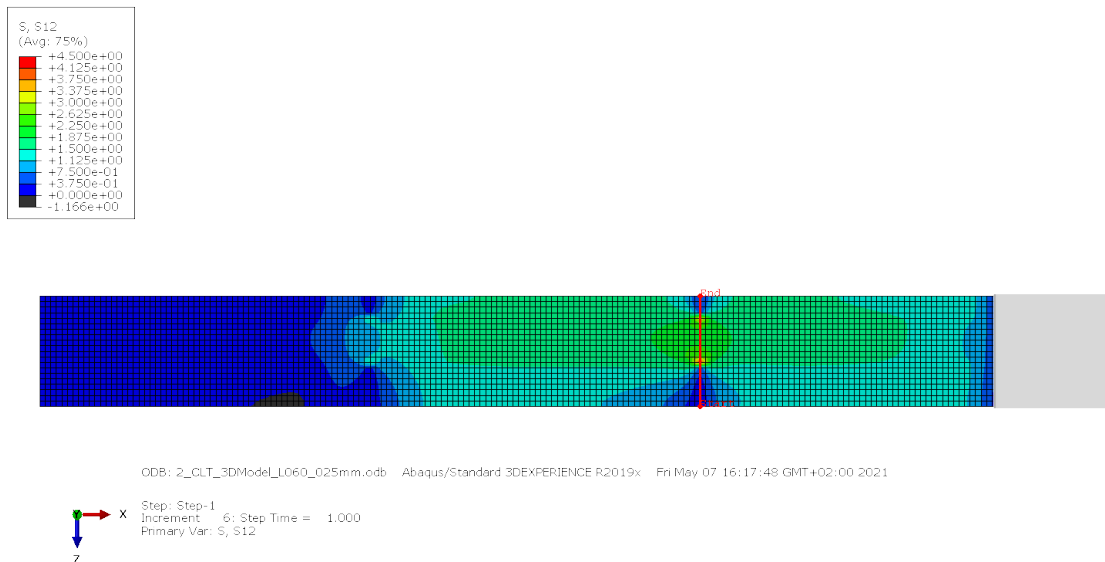
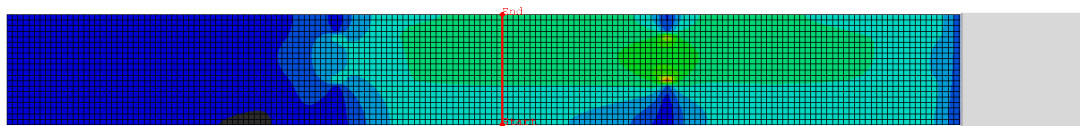
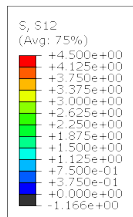


Figure C.9: Path 4 illustrated in a cut of the xz -plane showing the mid section of the beam.



ODB: 2_CLT_3DModel_LL060_025mm.odb Abaqus/Standard 3DEXPERIENCE R2019x Fri May 07 16:17:48 GMT+02:00 2021

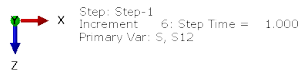


Figure C.10: Path 5 illustrated in a cut of the xz -plane showing the mid section of the beam.

Appendix D

Matlab code

D.1 Script for calculating shear correction factor

```
1 function [I,G,Kappa]=Stiffness_timo(n,d,MOE)
2 % [I,G,Kappa]=Stiffness_timo(n,d,MOE)
3 %-----
4 % PURPOSE
5 % Compute CLT element stiffness using Timoshenko theory with shear
6 % correction factor
7 %
8 % Equation nomenclature and references are made to
9 % pro:holz Cross-Laminated Timber structural design, Annex 2. (p. 184)
10 %
11 % INPUT: (SI units)
12 % n = [n]; number of layers (n=3,5,7,9)
13 % d = [d]; thickness of each layer
14 % (d=scalar -> same thickness throughout)
15 % (d=vector -> individual layer thicknesses,
16 % first scalar is top layer)
17 %
18 % MOE = [EL ET GLT GRT]; timber stiffnesses
19 % EL: Long. stiffness
20 % ET: Trans. stiffness
21 % GLT: shear stiff. LT/LR
22 % GRT: shear stiff. RT
23 %
24 % OUTPUT:
25 % I = [IL IT] Eff. stiffness / meter width, long. and transv. dir
26 % G = [GL GT] Eff. shear stiffness / meter width, long. and ...
    transv. dir
27 % Kappa = [KappaL KappaT]
28 %
29 %-----
30 % Copyright (c) Division of Structural Mechanics and
31 % Division of Structural Engineering.
32 % Lund University
33 %
34 % Modified by Henrik Danielsson, 2020-02-03
35 %-----
36
37 if isscalar(d)==1
38     d=d*ones(1,n);
39 end
40 w = 1; %Stiffnesses / meter width
41
42 for k=1:2
```

```

43 % Position of CoG in each layer (from upper edge)
44 for i=1:n
45     if i==1
46         zBar(i) = d(i)/2;
47     else
48         zBar(i) = sum(d(1:(i-1)))+d(i)/2;
49     end
50 end
51
52 % Position of global CoG (from upper edge)
53 if k==1
54     modi = 1;
55 else
56     modi = 0;
57 end
58 for i=1:n
59     if mod(i,2)==modi %Longitudinal layers
60         E(i) = MOE(1);
61         G(i) = MOE(3);
62     else %Transverse layers
63         E(i) = MOE(2);
64         G(i) = MOE(4);
65     end
66 end
67 zBars = sum(E.*d.*zBar) / sum(E.*d);
68
69 % Distance of individual layer CoG to the global CoG
70 z = zBar-zBars;
71
72 % Distance of individual layer top to the global CoG
73 zo = z-d/2;
74
75 % Distance of individual layer bottom to the global CoG
76 zu = z-d/2+d;
77
78 % Index of the layer containing the CoG
79 m = median(d);
80
81 % Moment of inertia
82 A = w.*d;
83 I_k = sum(E/MOE(1).*w.*d.^3/12) + sum(E/MOE(1).*A.*z.^2);
84
85 % Shear correction coefficient
86 ESi = E.*w.*(zu.^2/2-zo.^2/2); %(eqn 19)
87 for i=1:n %Tabular calculation of the double integral (eqn 17,18)
88     Poly(i) = E(i)^2*w^2/60 * ...
89         (3*zu(i)^5-10*zo(i)^2*zu(i)^3+15*zo(i)^4*zu(i)-8*zo(i)^5) ...
90         +sum(ESi(1:(i-1)))*w*E(i)/60*(20*zu(i)^3-60*zo(i)^2*...
91         zu(i)+40*zo(i)^3) ...
92         +sum(ESi(1:(i-1)))^2*(zu(i)-zo(i));
93     Poly(i) = Poly(i)/(G(i)*w);
94 end
95 IntPoly = sum(Poly);
96
97 KappaZ = sum(G.*A)/(MOE(1)*I_k)^2 * IntPoly;
98
99 % Shear correction factor
100 Kappa_temp = 1/KappaZ;

```

```

101
102 % Shear stiffnes of the CLT panel
103 Sclt = Kappa_temp * sum(G.*w.*d); %Total shear stiffness GA
104 G_k = Kappa_temp .* G; %Eff shear stiff of ...
      individual layer
105 Kappa(k) = Kappa_temp;
106
107 % Generate output results
108 I(k) = I_k; %Second moment of inertia
109 Geff(k) = Sclt/w/sum(d); %Avg shear stiffness of the panel
110 G = Geff;
111 end
112 %----- end ...
      -----

```

D.2 Script for performing linear interpolation

```
1 %           Master's thesis - 30 hp           %
2 % ----- %
3 %           5-Layer CLT-beam           %
4 %           Linear Interpolation           %
5 % ----- %
6 %           Purpose:           %
7 %           %
8 %           Script that imports test data   %
9 %           from CSV-files and cuts away the %
10 %          testdata outside of the interval %
11 %          | 0.5 * Fmax - Fmax |           %
12 %          Afterwards a linear interpolation is %
13 %          performed within this interval and the %
14 %          values are saved as output parameters %
15 %           %
16 %          Created by: Emil Nilsson         %
17 %          2020-03-31                       %
18 % ----- %
19
20 function [output] = Linear-Interpolation(input1, input2, input3)
21
22 format shortG
23 % Separating the data values into three vectors
24 time = input1;
25 deformation = input2;
26 force = input3;
27
28 % Flagging for different lengths of vectors
29 ctrlvar = isequal(size(deformation), size(force)) || ...
    (isvector(deformation) && isvector(force) && ...
    numel(deformation) == numel(force));
30 if ctrlvar ≠ 1
31     disp('***** ERROR - Measurement data sets have ...
    different lengths *****')
32     return
33 end
34
35 % Maximum values
36 ellapsedtime = max(time);
37 maxdeform = max(deformation);
38 maxforce = max(force);
39
40 % Creating new vectors within the prescribed intervals
41 forcelim = 0.5 * maxforce;
42 separator = force ≥ forcelim;
43 deformation = deformation(separator);
44 force = force(separator);
45
46 % Performing a linear interpolation using built in function fitlm
47 mdl = fitlm(deformation, force);
48
49 % Plotting the linear interpolation (uncomment to visualize)
50 % figure(1)
51 % plot(deformation, force); hold on
```

```
52 % x1 = linspace(deformation(1), deformation(end), ...  
    length(deformation));  
53 % y = -2417 + 2392 * x1;  
54 % plot(x1, y)  
55  
56 % Extracting statistical data from mdl struct (Tables)  
57 r = corrcoef(deformation, force); r = r(1,2);  
58 Rsquared = mdl.Rsquared.Ordinary;  
59 Intercept = mdl.Coefficients(1,1); Intercept = table2array(Intercept);  
60 x1 = mdl.Coefficients(2,1); x1 = table2array(x1);  
61  
62 % Creating output vector  
63 % [output] = Linear.Interpolation(input1, input2, input3)  
64 output = [elapsedtime, maxdeform, maxforce, r, Rsquared, ...  
    Intercept, x1];
```